Quantum Gravity and Quantum Information

On Systems of Enhanced Microstate Entropy

Marco Michel

München 2021

Quantum Gravity and Quantum Information

On Systems of Enhanced Microstate Entropy

Marco Michel

Dissertation
der Fakultät für Physik
der Ludwig-Maximilians-Universität
München

vorgelegt von
Marco Michel
aus Memmingen

München, den 8. Juni 2021

Erstgutachter: Prof. Dr. Georgi Dvali
Zweitgutachter: Prof. Dr. Goran Senjanović
Tag der mündlichen Prüfung: 7. September 2021

Contents

List of Figures

List of Tables

Zusammenfassung

Schwarze Löcher sind äußerst effiziente Speicher von Quanteninformationen. In dieser Arbeit untersuchen wir einen universellen Mechanismus, der dem mikroskopischen Ursprung dieser erhöhten Mikrozustandsentropie zugrunde liegt. Darüber hinaus wollen wir allgemeine Phänomene in Systemen untersuchen, die diesen Mechanismus implementieren, und daraus folgende Implikationen für die Evolution schwarzer Löcher und die Kosmologie diskutieren.

Viele Fragen der Quantengravitation haben ihren Ursprung in der Physik Schwarzer Löcher. Eine bekannte und faszinierende Eigenschaft von Schwarzen Löchern ist, dass ihre Entropie die sogenannte Bekenstein-Grenze sättigt. Im Quanten-N-Portrait von Dvali und Gomez wurde die hohe Entropie S eines Schwarzen Lochs mit der Entstehung von S (fast) masselosen Freiheitsgraden in Verbindung gebracht.

Die Kernidee des Quanten-N-Porträts ist, dass makroskopische Schwarze Löcher oder die de Sitter-Raumzeit eine grundlegende Beschreibung als Vielteilchensysteme besitzen. Sie repräsentieren Zustände weicher Gravitonen mit einer sehr hoher Besetzungszahl. Dies ermöglicht es, Eigenschaften, von denen man annahm, dass sie ausschließlich in der Gravitation zu finden sind, wie die hohe Entropie großer Schwarzer Löcher, als universelle Phänomene zu identifizieren, die auch in nicht-gravitativen Systemen wie atomaren Bose-Einstein-Kondensaten implementiert werden können. Dies eröffnet eine neue Forschungsrichtung, weil wir nun verstehen, dass Schwarze Löcher nicht einzigartig in diesen Eigenschaften sind. Es gibt andere Systeme, die ähnliche Quanteninformationseigenschaften aufweisen und sogar im Labor hergestellt werden können. Erstens entmystifiziert dies Schwarze Löcher, da wir diese Eigenschaften in analogen Modellen tatsächlich untersuchen können. Darüber hinaus können wir etwas über die Physik schwarzer Löcher lernen, indem wir diese Art von Systemen studieren. Daher eröffnet diese Forschungsrichtung die Möglichkeit, wertvolles interdisziplinäres Wissen zu gewinnen.

Im ersten Teil dieser Arbeit identifizieren wir universelle Mechanismen in allgemeinen Vielkörpersystemen, welche die gleiche Entropieeigenschaften wie Schwarze Löcher besitzen. Generische bosonische Systeme mit schwacher und anziehender Wechselwirkung besitzen Zustände mit einer stark erhöhten Speicherfähigkeit. Dies wird ermöglicht durch einen Mechanismus welcher für nahezu masselosen Freiheitsgrade im Spektrum verantwortlich ist und *assistierte Masselosigkeit* genannt wird. Wir argumentieren, dass solche Systeme mit erhöhter Speicherfähigkeit dem universellen Effekt von *Speicherbürde* unterliegen, der sie an einen kritischen Zustand bindet und ihren Zerfall unterdrückt. Wir untersuchen ein Prototypmodell, um zu zeigen, dass die Speicherbürde durch *Umschreiben* gespeicherter Quanteninformationen von einem Satz von Freiheitsgraden zu einem an-

deren überwunden werden kann. Dieser Prozess erfordert jedoch eine Feinabstimmung der Parameter. Wir führen daher numerische Studien durch, um den Parameterraum für mögliche *Umschreibe*-Werte abzubilden.

Aufgrund der universellen Natur von Systemen mit erhöhter Speicherfähigkeit wenden wir unsere Ergebnisse im zweiten Teil auf Schwarze Löcher und die de Sitter-Raumzeit an. Im Fall von de Sitter Raumzeit, welche durch Gibbons-Hawking-Strahlung zerfällt, führt die *Speicherbürde* zu einem Quantenbruch Effekt. Dies hat wichtige Konsequenzen für inflationäre Observablen und steht in voller Übereinstimmung mit früheren Ergebnissen aus der Literatur. Desweiteren eröffnet es die Möglichkeit, dass das Universum seine Quantenerinnerungen aus einer Epoche viel früher als 60 e-Faltungen vor dem Ende der Inflation bewahrt hat.

Als nächstes untersuchen wir Schwarze Löcher als System mit erhöhter Speicherfähigkeit. Wenn wir die Parameter unseres Prototypmodells so auswählen, dass sie mit den Gravitationsskalierungen übereinstimmen, beobachten wir, dass die Entwicklung aufgrund einer unterdrückten Rate von *Umschreiben* im Vergleich zum Anfangsstadium der Verdampfung von Schwarzen Löchern extrem langsam wird. Dies impliziert eine Metamorphose, einschließlich einer drastischen Abweichung von der Hawking-Verdampfungsrate, spätestens nachdem das Schwarze Loch die Hälfte seiner ursprünglichen Masse verloren hat.

Ein weiteres Beispiel für eine ungewöhnlich große Skalenteilung findet sich im Elektroschwachen Hierarchieproblem. Die beobachtete Higgs Masse bleibt angesichts ihrer quadratischen Sensitivität gegenüber einer Ausschlussgrenze, welche so groß wie die Planck-Skala sein könnte, rätselhaft. Im dritten Teil untersuchen wir numerisch das von Dvali und Vilenkin vorgeschlagene kosmologische Relaxationsmodell der Higgs-Masse zur Erklärung des elektroschwachen Hierarchieproblems. Dieses Szenario führt einen neuen Begriff von Natürlichkeit ein, wonach das Vakuum mit einem kleinen Erwartungswert des Higgs-Feldes einem unendlich erhöhten Entropiepunkt der Vakuumlandschaft entspricht, welcher zu einem Attraktor der kosmologischen inflationären Evolution wird. In diesem Rahmen untersuchen wir numerisch die Entwicklung des Higgs-Vakuum-Erwartungswerts. Wir modellieren die inflationären Vakuum-zu-Vakuum-Übergänge, die durch die Nukleation von unter 3-Formfeldern geladenen Membranen ausgelöst werden, als zufällige Irrfahrt. Insbesondere untersuchen wir den Einfluss der Anzahl gekoppelter 3-Formfelder auf die Konvergenzrate des Higgs-Vakuum-Erwartungswerts. Wir entdecken eine erhöhte Rate mit zunehmender Anzahl von Membranladungen. Darüber hinaus zeigen wir, dass für späte Zeiten die Einführung von mehr Ladungen äquivalent zu zusätzlichen Membran-Keimbildungen ist.

Abstract

Black holes are extremely efficient storer of quantum information. In this thesis, we investigate a universal mechanism underlying the microscopic origin of this enhanced microstate entropy. Moreover, we seek to study general phenomena in systems implementing this mechanism and discuss implications to black hole evolution and cosmology.

Many questions of quantum gravity have revolved around black holes. One intriguing and well known property of black holes is that their entropy saturates the so-called Bekenstein bound. In Dvali and Gomez's quantum N-Portrait, the high entropy S of a black holes was linked to the emergence of order S (nearly) gapless degrees of freedom.

The key idea of the quantum N-Portrait is that black holes or de Sitter spacetime actually possess a fundamental description as many-body systems. Namely, they represent states of soft gravitons with very high occupation number. This allows us to interpret properties, that were thought to be exclusive to gravity, like the large black hole entropy, in terms of universal phenomena, which can also be implemented in non-gravitational systems like atomic Bose-Einstein condensates. This opens up a new direction of research because we understand that black holes are not unique. There are other systems that exhibit similar quantum informational properties and that can even be manufactured in a laboratory. First, this demystifies black holes since we can actually probe these properties in analogue models. Moreover, we can learn about black hole physics by studying this type of systems and mapping corresponding findings back to quantum gravity. Therefore, this research direction opens up the possibility of gaining valuable interdisciplinary knowledge.

In the first part of this thesis we identify a universal mechanism in general many-body systems, that can result in a similar degeneracy of microstates as is found in gravity. This results in a large level splitting between the typical energy gap of the system compared to the excitation levels of the aforementioned microstates. Generic bosonic systems with weak and attractive interaction possess states that exhibit a sharply enhanced memory capacity due to emergent nearly-gapless degrees of freedom by a mechanism we call *assisted gaplessness*. We further argue that such systems of enhanced memory capacity are subjected to the universal effect of *memory burden*, which ties them to a critical state and suppresses their decay. We study a prototype model to show that memory burden can be overcome by *rewriting* stored quantum information from one set of degrees of freedom to another one, which becomes increasingly more gapless while at the same time the original set acquires a gap. However, this process requires a fine-tuning of parameters. We therefore perform numerical studies to map the parameter space for possible *rewriting* values.

Due to the universal nature of systems of enhanced memory capacity we apply our

findings to black holes and de Sitter spacetime in the second part. In case of de Sitter, which decays due to Gibbons-Hawking evaporation, the *memory burden* results in a quantum breaking effect. This has important consequences for inflationary observables and is in full agreement with previous results from the literature. It opens up the possibility, that the Universe kept its quantum memories from an epoch much earlier than 60 e-foldings before the end of inflation. Next, we study black holes as a system of enhanced memory capacity. Choosing the parameters of our prototype model to match gravitational scalings, we discover that, due to a suppressed rate of *rewriting*, the evolution becomes extremely slow compared to the initial stage of black hole evaporation. This implies a metamorphosis, including a drastic deviation from Hawking evaporation, at the latest after the black hole has lost half of its initial mass.

Another example for a unusual large splitting of scales can be found in the Electroweak Hierarchy Problem. The observed Higgs mass in light of its quadratic sensitivity to a cutoff that might be as large as the Planck scale remains puzzling. In the third part we numerically study the cosmological relaxation model of the Higgs mass proposed by Dvali and Vilenkin to explain the Electroweak Hierarchy Problem. This scenario introduces a different notion of naturalness according to which the vacuum with a small expectation value of the Higgs field corresponds to an infinitely enhanced entropy point of the vacuum landscape, that becomes an attractor of cosmological inflationary evolution. In this framework we study numerically the evolution of the Higgs vacuum expectation value. We model the inflationary vacuum-to-vacuum transitions, that are triggered by nucleation of branes charged under three-form fields as a random walk. In particular, we investigate the influence of the number of coupled three-forms on the convergence rate of the Higgs vacuum expectation value. We discover an enhanced rate with increasing number of brane charges. Moreover, we show that for late times the inclusion of more charges is equivalent to additional brane nucleations.

Publications

This work is based on a series of project, that are still ongoing or have already been published [1]–[4]. A substantial part of the results presented in this work is based on collaborations with Gia Dvali, Lukas Eisemann and Sebastian Zell. As it is custom in particle physics, all authors share first authorship and are sorted alphabetically. This thesis is intended to embed these works in a wider context, provide adequate background and a unified picture. Therefore, the present thesis is to a large extent an ad verbatim reproduction (with respect to text, equations and figures) of the papers:

1. G. Dvali, M. Michel, and S. Zell, "Finding Critical States of Enhanced Memory Capacity in Attractive Cold Bosons," *EPJ Quant. Technol.*, vol. 6, p. 1, 2019. DOI: 10.1140/epjqt/s40507-019-0071-1. arXiv: 1805.10292 [quant-ph]

2. G. Dvali, L. Eisemann, M. Michel, and S. Zell, "Universe's Primordial Quantum Memories," *JCAP*, vol. 03, p. 010, 2019. DOI: 10.1088/1475-7516/2019/03/010. arXiv: 1812.08749 [hep-th]

3. M. Michel, "Numerical study of a cosmological relaxation model of the Higgs boson mass," *Phys. Rev. D*, vol. 101, no. 11, p. 115 007, 2020. DOI: 10.1103/PhysRevD.101.115007. arXiv: 1910.10940 [hep-ph]

4. G. Dvali, L. Eisemann, M. Michel, and S. Zell, "Black hole metamorphosis and stabilization by memory burden," *Phys. Rev. D*, vol. 102, no. 10, p. 103 523, 2020. DOI: 10.1103/PhysRevD.102.103523. arXiv: 2006.00011 [hep-th]

Further parts of this thesis are based on ongoing projects [5], [6], which are carried out in different collaborations and address the following topics:

5. A numerical program for computing time evolution in a generic quantum system. In collaboration with Sebastian Zell.

6. The time evolution of systems with states of enhanced microstate entropy. In collaboration with Gia Dvali, Lukas Eisemann and Sebastian Zell.

We provide more details on where material from the papers [1]–[4] and ongoing projects is used at the beginning of each chapter.

Chapter 1

Introduction

1.1 Invitation

Black holes are mysterious objects from the point of view of quantum information. One well-established fact about them is that they saturate the Bekenstein bound on information capacity [7], [8]. It was realized that in order to account for such a high entropy, a black hole must deliver qubits with extremely small energy gaps. For a black hole of mass M and corresponding Schwarzschild radius r_g (measured in Planck scale units) these gaps have to be at least suppressed by a factor $\sim 1/M^2$ compared to a quantum level-spacing in any ordinary system of the same size [9]–[11].

It was postulated that the emergence of such approximately gapless qubits, which are responsible for the large microstate degeneracy of a black hole, is in its bare essence the same phenomenon as the appearance of gapless modes around a quantum critical point in a system of attractive bosons [9], [11].

The realization that the microscopic origin of the Bekenstein entropy is not exclusive to gravity opens up several exciting research directions. One is the development of a microscopic theory describing a black hole as a bound state of soft gravitons, a so-called quantum N-portrait [11]. The second direction is to use this universal mechanism and implement it in other systems outside of gravity. For example it was shown that the emergence of gapless modes could be a mechanism to enhance the memory capacity in neural networks [12], [13]. Moreover, it can in principle be implemented in cold bosonic systems, which might have important application to quantum computing and quantum information storage [9], [14], [15]. The above connection can also give an interesting prospect of simulating in table top quantum experiments the key mechanism of information storage in such seemingly-remote systems as black holes and quantum neural networks.

This thesis seeks to continue this line of research by developing and studying many-body systems that share the black hole property of enhanced microstate entropy. The main novelty to previous work in this direction will be the focus on the dynamics of states of enhanced memory capacity. This will allow us to draw conclusions on systems with a large degeneracy of microstates in general and, moreover, novel implications to the dynamics of black holes and de Sitter spacetime, which lie in the gravitational sector of this class of systems.

1.2 Conventions

We shall apply the following conventions in this work. We set $c = k_B = 1$ throughout the thesis. We will keep Planck's constant $\hbar$ explicit in this introductory chapter, but we will set it to one afterwards. The metric signature is set by $\eta_{\mu\nu} = (-1, 1, 1, 1)$.

Newton's constant shall be denoted by G_N. We write the Planck mass as $M_p = \sqrt{\hbar/G_N}$ and the Planck length as $L_p = \sqrt{\hbar G_N}$. The numerical value of the (reduced) Planck mass is given by $M_P = 2.48 \times 10^{18}$ GeV.

1.3 Black Holes

Since black holes play a major part in this work, we shall briefly review some of their intriguing properties. From the point of view of general relativity, a Schwarzschild black hole is described as a manifold with the following metric

$$ds^2 = g_{\mu\nu} dx^\mu dx^\nu = -\left(1 - \frac{r_g}{r}\right) dt^2 + \left(1 - \frac{r_g}{r}\right)^{-1} dr^2 + r^2 d\Omega^2, \tag{1.1}$$

where the Schwarzschild radius is given by $r_g = 2G_N M$. M denotes the ADM-mass and $d\Omega^2$ is the metric on the two-sphere. Its most prominent feature is the sign change of the factors $(1 - r_g/r)$ precisely at the radius r_g. This switched role of the coordinates r and t has important physical consequences. The fact that r becomes time-like after $r = r_g$ marks a sphere, called the event horizon, which no light-like worldline can escape after entering. In particular, this means that any information about the interior of a black hole remains inaccessible for any outside observer. On top of that, the metric of an uncharged black hole is completely fixed by the mass. This property is condensed in so called no-hair theorems (see for example [16]). These extraordinary properties made black holes an arena of theoretical gedankenexperiments for many branches of physics.

In this thesis we are especially interested in the quantum informational properties of black holes. An important thermodynamical implication of the existence of a horizon has been pointed out by Bekenstein. In order to maintain the second law of thermodynamics in the universe a black hole has to carry an entropy, which scales with its area A [7]. After demonstrating a deep connection between thermodynamics and black hole physics in [17], the precise numerical value of the entropy, as well as the temperature, have later been determined in [8] by Hawking:

$$T = \frac{\hbar\kappa}{2\pi} = \frac{1}{8\pi G_N M}, \qquad S = \frac{\pi r_g^2}{\hbar G_N} = \frac{1}{4}\frac{A}{L_p^2}, \tag{1.2}$$

where κ denotes the surface gravity and the horizon area is given by $A = 4\pi r_g^2$. Hawking also showed that black holes radiate with a thermal spectrum and therefore evaporate [8]. The presence of $\hbar$ indicates that this is an inherently quantum process. The typical energy E of one quantum and the rate of particle production Γ in this radiation process is given by

$$E \approx \frac{\hbar}{r_g}, \qquad \Gamma \approx \frac{1}{r_g}. \tag{1.3}$$

We note that this calculation can be carried out in the framework of semi-classical gravity independent of a specific UV-completion. This is possible, since for macroscopic black holes the curvature at the Schwarzschild radius is much smaller than M_p, at which quantum gravitational effects are expected to become important. For black holes of small masses $M \sim M_p$ this treatment breaks down and must be superseded by a full theory of quantum gravity. It is important to reiterate that Hawking's results were obtained by considering quantum fluctuations on top of a rigid Schwarzschild background of infinite mass. Specifically, these calculations do not take backreactions to the metric into account, which therefore remains, strictly speaking, static and eternal. With this assumption the outgoing radiation is perfectly thermal and carries no information about the origin of the black hole. Generalizing these results to black holes with finite mass lead to the so called information paradox. However, this approach was challenged shortly after it was published and it was pointed out that the neglected backreaction in Hawking's calculation would render its results invalid after a period of time after the black hole is still macroscopic [18]. More recently it was pointed out that a finite mass black hole cannot maintain exact thermality of Hawking radiation [19], which renders a possible paradox baseless. The deviation from perfect thermality provides a built-in measure of the validity of the semi-classical treatment since equation (1.2), together with $\dot{M} \sim r_g^{-2}$, leads to $\dot{T}/T^2 \sim 1/S$ (see [19]). This quantity sets the lower bound on the deviation from thermality. It vanishes only in the strict semi-classical limit $G_N \to 0,\ M \to \infty,\ r_g = \text{finite}$. It is important to note that in this limit $S \to \infty$. Only in this limit, the standard Hawking result is exact. However, for finite mass black holes and non-zero G_N, the deviations from the thermal spectrum are set by $1/S$.

1.4 De Sitter Spacetime

In the previous section we reviewed certain aspects of black holes with emphasis on their quantum informational properties. We saw an especially interesting connection between the event horizon area and the Bekenstein entropy in formula (1.2). One of the surprising and impressive features of this formula is its universality. It can be applied to all kinds of black holes including different charges, geometries and rotations. It also applies to cosmological horizons, like the event horizon in de Sitter spacetime [20].

The manifold of de Sitter is classically described by the following metric:

$$ds^2 = -dt^2 + a_0^2 e^{2\sqrt{\frac{\Lambda}{3}}t}\left(d\chi^2 + \chi^2 d\Omega^2\right), \tag{1.4}$$

with a scale parameter a_0 and a positive cosmological constant Λ. This metric can also be regarded as a four-dimensional hyperboloid, which is extrinsically embedded in a 5-dimensional Minkowski spacetime:

$$ds^2 = -z_0^2 + z_1^2 + z_2^2 + z_3^2 + z_4^2 = l_\Lambda^2. \tag{1.5}$$

The quantity $l_\Lambda \equiv 1/H$ is the so called de Sitter radius, where H is the Hubble parameter. It can be shown that this metric is a solution to the vacuum Einstein equation with a

positive cosmological constant Λ and therefore satisfies

$$G_{\mu\nu} + \Lambda g_{\mu\nu} = 0, \tag{1.6}$$

where $G_{\mu\nu}$ is the Einstein tensor. The cosmological constant and the Hubble parameter are related by

$$H^2 = \frac{\Lambda}{3}. \tag{1.7}$$

De Sitter spacetime describes an accelerated expanding universe and is of extreme importance for the inflationary paradigm, which solves many puzzles of the hot Big Bang theory. From the perspective of this thesis the most interesting aspect of this spacetime is that it also exhibits an event horizon. This allows us to characterize it, analogous to the Bekenstein entropy of black holes, by its Gibbons-Hawking entropy [20]

$$S = \frac{3\pi}{\hbar G_N \Lambda} = \frac{1}{4}\frac{A}{L_p^2}, \tag{1.8}$$

with the de Sitter horizon area $A = \pi l_\Lambda^2$. The analogy between black holes and de Sitter extends further. Similar to the Hawking radiation, the de Sitter horizon also produces particles in form of Gibbons-Hawking radiation [20]. Analogue to Eq. (1.3), the typical energy and the rate of this evaporation is given by

$$E \approx \frac{\hbar}{l_\Lambda}, \qquad \Gamma \approx \frac{1}{l_\Lambda}. \tag{1.9}$$

Equivalent to the black hole case the entropy (1.8) becomes infinite in the semi-classical limit.

1.5 Quantum N-Portrait

In this section we review the basics of the multi-particle framework of gravity put forward by Dvali and Gomez in a series of publications [9], [11], [21]–[24], since we will often refer to it in the following parts of this thesis.

Based on the premise that classical solutions in quantum field theory should have a representation in terms of some underlying fundamental quanta, every classically extended object can be interpreted as a bound state of a large number N of constituents. In this framework the classical theory is recovered in the limit $N \to \infty$. For a finite number of constituents quantum corrections appear.

This idea of interpreting classical lumps as bound states[1] was applied to black holes in [9], [11]. In this so called corpuscular picture of gravity Minkowski spacetime is a distinct ground state and black holes, de Sitter and other spacetime manifolds are considered to be excitations on top of this vacuum. Geometry is no longer considered to be a fundamental quantity, but a mean-field consequence arising as an expectation value of an underlying quantum state. A natural candidate for the constituents of spacetime is the graviton.

[1] For an application of this idea to solitons we refer to [25] and [11].

Correspondingly, any geodesic in a curved spacetime is the result of scattering processes with the gravitons constituting the condensate.

Considering a black hole as a condensate also allows for a natural interpretation of Hawking radiation. Completely equivalent to a Bose Einstein condensate in condensed matter physics a black hole loses constituents due to re-scattering. It was calculated in [11] that in this picture the standard Hawking rate can be recovered.

Before we continue, we want to state a few quantitative results of this line of research, that will become useful later on. In particular, the wavelength of gravitons that build up a black hole is set by the typical energy of the system. As we have already reviewed in section 1.3, this scale is set by the geometrical parameter r_g:

$$E_g \sim \frac{\hbar}{r_g}. \tag{1.10}$$

With this the number of constituents of a black hole can easily be estimated to be

$$N \sim \frac{M^2}{M_p^2} \sim \frac{r_g^2}{L_p^2}. \tag{1.11}$$

The dimensional scattering strength α_g is given by

$$\alpha_g = \frac{\hbar G_N}{r_g^2} = \frac{1}{N}. \tag{1.12}$$

The last thing we require for the following analysis is the Hawking radiation rate. As described above, evaporation in the Black Hole N-Portrait is no longer a vacuum process, but is described as a regular scattering, which kicks particles out of the condensate from time to time. Quanta escape whenever their energy exceeds the binding energy [11]

$$E_{\text{escape}} = \frac{\hbar}{\sqrt{N} L_p}. \tag{1.13}$$

The easiest process contributing to this is an ordinary $2 \to 2$ scattering. The corresponding Feynman diagram involves two 3-point interaction vertices. This indicates that the amplitude scales as α_g and the rate therefore with α_g^2. Since the particular gravitons, that scatter, are within a condensate of total occupation N, the scattering amplitude gets enhanced by a combinatorial factor of $\binom{N}{2} \approx N^2$. The last factor contributing to the rate is the characteristic energy of the process. This is given by Eq. (1.13). In summary, the rate for such a process to the leading order in N is,

$$\Gamma \approx \frac{1}{N^2} N^2 \frac{\hbar}{\sqrt{N} L_p} = \frac{1}{r_g}. \tag{1.14}$$

1.6 Quantum Breaking

Since the birth of quantum theory an important question is on which timescale is it possible to approximate a system, that is intrinsically quantum, by a classical equation.

The specific example of a spreading wave packet and the following break down of the Bohr correspondence principle was already studied in [26]. The corresponding timescale is called the Ehrenfest time. It is usually assumed that the bigger and the more macroscopic a system is the less quantum effects are important[2]. In this sense macroscopic objects become increasingly more classical. Motivated by a small coupling strength and small curvatures (much smaller compared to the Planck scale M_p) this paradigm is usually also applied to gravity in such a way that quantum effects are ignored for macroscopically extended spacetimes. For example, this paradigm was applied to black holes physics in the calculation of Hawking radiation, as well as Gibbons-Hawking radiation, in case of de Sitter.

In the special case of de Sitter spacetime this approach was challenged in [31]. Based on the concept of quantum breaking, which is the timescale t_q after which a given system can no longer be approximated as classical and which was first introduced in [32], it was argued that due to internal scattering processes de Sitter spacetime cannot remain static. Based on the Quantum N-Portrait [24] (see also section 1.5 for further references), which models de Sitter spacetime as an excited and coherent state on top of Minkowski vacuum, the authors computed a finite timescale, after which a description in terms of a classical metric breaks down. They identified re-scattering processes of gravitons as the source of both Gibbons-Hawking radiation as well as a build-up of quantum corrections, that lead to a significant deviation after the timescale t_q.

It was also argued in [31], [33] that this would lead to a fundamental inconsistency in case a quasi-de Sitter configuration continues to exist on a timescale that is longer than its quantum break-time. For details we refer to the original papers [24], [31], [33], [34].

This line of research was later extended to cosmic QCD axions [35], [36] and to general discrete symmetries, that are spontaneously broken after inflation [37].

1.7 Enhanced Microstate Entropy

In section 1.3 on black holes and in section 1.4 on de Sitter spacetime we emphasized the extraordinarily large microstate entropy of those two systems. A large entropy means that the system can be in a large number of microstates for a given macrostate. Since one prominent macroscopic parameter is energy, an important question is how many microstates are accessible within a fixed energy gap ΔE. Therefore, a large entropy means that many distinct states have the same energy and consequently fit into the same narrow energy gap. In the following we shall quantify this statement.

Generally speaking, a system with a microstate entropy S has by definition e^S distinct microstates. A system can achieve this by providing of order S lowly occupied[3] and nearly gapless degrees of freedom (d.o.f). Summarized, we have

$$\#microstates = e^S\,, \qquad \#\text{d.o.f} \sim S. \tag{1.15}$$

[2]Note that there are well known examples of systems that exhibit quantum effects on macroscopic scales like superconductivity [27], [28] or Bose Einstein condensation [29], [30]

[3]Note that the maximal occupation number of a single mode only counts logarithmically towards the total microstate entropy.

A natural measure of gaplessness would be to compare the energy difference of distinct microstates with the fundamental energy gap $E_{typical}$ of the system in consideration. Therefore, to account for a entropy S, all S degrees of freedom (or equivalently quantum modes) have to be excitable without exceeding ΔE. This gives the following constraint for a single mode:

$$\Delta E \lesssim \frac{E_{\text{typical}}}{S} \,. \tag{1.16}$$

We remark that in the case, in which the entropy carrying modes have positive or negative energies with equal probability, it is also possible to adopt the following weaker constraint

$$\Delta E \lesssim \frac{E_{\text{typical}}}{\sqrt{S}} \,. \tag{1.17}$$

In this scenario, not all but most microstates fit within ΔE. This is, however, still sufficient to account for the entropy scaling (1.15). Throughout this thesis, the difference between the bounds (1.16) and (1.17) will be inessential.

Next, we apply these considerations to black holes. In this case the typical energy is given by $E_{\text{typical}} = \hbar r_g^{-1}$. This is the average amount of energy a black hole loses by radiating one Hawking quantum. Let us take a closer look at properties (1.16) and (1.17). They mean that the system exhibits energy gaps, that can be arbitrarily smaller than the typical level spacing. Therefore, the existence of many approximately gapless degrees of freedom is a necessity for systems with a large entropy. This implies that systems with an enormous entropy, like black holes or de Sitter spacetime, have to exhibit modes, that have an extremely small energy gap. Concluding we want to note that the existence of many gapless modes is not a property, which is exclusive to gravity, but can also be constructed in simple many body systems as we will demonstrate in later chapters.

1.8 The Electroweak Hierarchy Problem

The seminal discovery of the Higgs field at the LHC has left us with a perfect Standard Model (SM) of particle physics potentially valid up to energies well above the Planck scale $M_P = 2.48 \times 10^{18}$ GeV. At the same time, it left unsolved one of the most mysterious puzzles in particle physics: the so-called Hierarchy Problem. The difference of many orders of magnitude between $M_{W,Z,H} \approx 100$ GeV and $M_p \approx 10^{19}$ GeV is puzzling in light of the sensitivity of the Higgs mass towards anything above the electroweak scale. To understand the nature of the problem better we shall briefly review important concepts of the Hierarchy Problem in the following.

The mass term of the Higgs field H in the SM is given by

$$m^2 H^\dagger H, \tag{1.18}$$

which is invariant under gauge and global symmetries on H. This invariance renders the Higgs mass parameter open to loop corrections. This means that the Higgs mass receives contributions from every scale which it interacts with. Therefore, the huge difference between the Planck and electroweak scale turns out to be problematic, when we

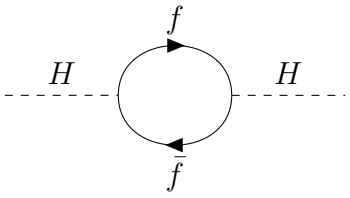

Figure 1.1: Radiative correction to the Higgs boson mass.

compute radiative correction to the Higgs boson mass in form of 1-loop diagrams. For example, a fermion loop as it is shown in Fig. 1.1 with coupling λ_f yields a radiative correction

$$\Delta m_H^2\Big|_{\text{fermion-loop}} = -\frac{\lambda_f^2}{8\pi^2}\cdot\Lambda^2 + \dots\,, \tag{1.19}$$

where we introduced a cutoff Λ to regularize the loop integral. The ellipsis stand for additional terms that are logarithmic in the cutoff, which we shall ignore here. Details on the calculation can be found in any textbooks on quantum field theory, see for example [38]. Similar terms arise from gauge bosons and the Higgs self-coupling. This means that in total the Higgs mass is schematically given by

$$m_H^2 \sim m_{H,\text{bare}}^2 + \underbrace{(\lambda_g^2 + \lambda^2 - \lambda_f^2 + \dots)\cdot\Lambda^2 + \dots}_{\text{SM}} + \underbrace{\dots}_{\text{New Physics}} \simeq (125\,\text{GeV})^2\,, \tag{1.20}$$

where we suppressed numerical factors in each term, λ_g is the coupling constant to gauge bosons and λ is the Higgs self-coupling. The important observation here is that various different contributions from standard model physics share the common quadratic factor[4] Λ^2. At first glance, it is not clear which value Λ should have. Furthermore, its precise meaning in a renormalizable theory, which requires an input scale, is not clear.

However, this no longer holds true in the presence of gravity [39]. The reason for that is that gravity puts a precise bound on masses, above which no elementary particle can exist. To see that no particle exists with a mass larger than M_p we briefly review the reasoning in [39]. For a particle of mass m there are two important associated length scales. Namely, the Compton wavelength L_c, which represents a distance at which quantum fluctuations become important, and the gravitational radius L_g, at which an object would become a black hole if its entire mass is localized within this radius. These are given by

$$L_c = \frac{\hbar}{m}\,, \qquad L_g = \frac{\hbar m}{M_p^2}\,, \qquad L_p = \sqrt{\hbar G_N}\,. \tag{1.21}$$

For comparison we also added the Planck length L_p, which is the scale at which quantum gravitational effects are expected to become strong, for easy comparison. Let us now consider an object of mass $m < M_p$. For this object the Compton scale is much larger than the Planck scale or the gravitational radius, i.e. $L_c > L_p > L_g$. In this regime

[4] These quadratic divergences occur only for scalar particles. As noted above, fermions and vector bosons are protected from them by chiral symmetry and gauge invariance, respectively.

quantum effects are much more important than contributions from gravity. Moreover, gravitational features are completely shielded by quantum effects. Therefore, this object can be interpreted as an elementary particle. On the other hand, for masses $m > M_p$ we get $L_c < L_p < L_g$. This means that this object represents a (macroscopic) black hole and can therefore be considered to be (semi-)classical. Thus, the Planck scale is an upper bound on the mass of any elementary particle. This makes the Hierarchy Problem real, since it implies the existence of a universal regulator scale M_p. However, having $\Lambda^2 = M_p^2$ in Eq. (1.20) combined with the observational fact that $m_H \approx 125\,\mathrm{GeV}^2$ requires a precise cancellation of all those various contributions to a precision $\sim M_H^2/M_P^2 \sim 10^{-34}$. This is the essence of the Hierarchy Problem and challenges our current understanding of high energy physics. This puzzle is also widely considered to be the main motivation[5] for searching for new physics [41]. On top of all contributions from the SM, gravity itself contributes to the Higgs mass in form of quantum black holes. These are objects with mass $m \approx M_p$ and behave in many regards very similarly to elementary particles and would also lead to Planck scale contribution in form of new physics in (1.20).

To address this puzzle many solutions have been proposed in the literature. One approach is to stabilize the Higgs mass due to additional symmetries. For example, in a supersymmetry approach Planckian contributions cancel between partners and superpartners, thus removing the quadratic sensitivity to the cutoff [42], [43]. Another approach is to directly lower the cutoff Λ. One possibility to bring down the gravitational scale is via extra dimensions [44], [45] as well as large number of species [46], [47] (for a similar approach in a cosmological context see for example [48] and [49]). Other approaches are technicolor [50], [51] or warped extra dimensions [45]. However, the predicted stabilizing new physics, which is required around a scale not much larger than the weak scale in these proposals, have not been observed at currently available energy scales at LHC. This observational fact challenges those approaches.

However, an alternative idea, which was already suggested in pre-LHC era, is solving the Hierarchy Problem via cosmological relaxation of the Higgs mass [52], [53]. This scenario does not rely on any low energy physics, as it can push the scale of the onset of new physics up to the Planck scale. It also introduces a notion of naturalness [41], that is fundamentally different from the standard one by 't Hooft [54]. Here, the vacuum with the small value of the Higgs mass has infinite entropy and represents an attractor of cosmological evolution. The non-observation of any new physics at the LHC gives a serious motivation for a detailed study of this scenario. A list of recent references based on the same idea can be found in [41]. We shall focus on this specific approach in this thesis and discuss it in more detail in chapter 4.

[5] For a different philosophical viewpoint see [40]. There, a more practical approach to new physics is advocated by emphasizing observational shortcomings of the SM, like neutrino masses and dark matter. Consequently, the question of the origin of certain numerical values should be considered a secondary task.

1.9 Outline

The outline of this thesis is as follows. In chapter 2 we study systems of enhanced memory capacity. Motivated by black holes and condensed matter physics we identify a possible mechanism, called *assisted gaplessness*, that can dynamically generate an abundance of gapless modes, which result in an enhanced microstate entropy. Next, we shall discuss a robust procedure to identify states of enhanced memory capacity in the spectrum of a generic bosonic system which additionally exhibits at least some attractive interactions. We refer to this procedure as *c-number method*, because it relies on replacing quantum operators by c-number valued expectation variables in the presence of large occupation numbers. We demonstrate our method on a simple three-mode system, which is derived from a weakly and attractively interacting Bose gas with Dirichlet boundary conditions. The finding that cold atom systems can exhibit a similar entropy scaling as a black hole opens up an exciting perspective of simulating quantum informational properties of gravity in simple prototype systems. Moreover, it could lead to the realization of black hole type information processing and storage in table-top experiments and may even be applied to quantum devices. Next, we explore implications to the overall dynamics, if a system exhibits states, that are accompanied with nearly gapless degrees of freedom in the spectrum. First, we explore if a system naturally evolves towards such a state if such is dynamically accessible. Afterwards, we discuss possible implications to the scenario of UV-completing of classicalization. Concluding, we study the generic phenomenon of *memory burden*, which is naturally linked to systems, that implement *assisted gaplessness*. We shall see that the stored quantum information in the gapless degrees of freedom generically backreacts and resists any deviation away from a critical configuration. We also discuss possible scenarios to delay or avoid this *memory burden* effect. We put special focus on the mechanism of *rewriting*, which tries to alleviate the *memory burden* by transferring information from one set of quantum modes to another. To quantify this behavior we perform numerical simulations on a prototype system.

We apply the general concepts and properties of states of enhanced memory capacity to gravitational systems in chapter 3. First, we study the implications of *assisted gaplessness* to de Sitter spacetime. Next, we argue that because of its enormous entropy de Sitter also has to experience the phenomenon of *memory burden*. This back reaction of the quantum information stored in the Gibbons Hawking entropy results in a quantum breaking effect similar to the one discussed in section 1.6. Further, we discuss possible implications on inflationary observables. We conclude by commenting on a possible inconsistency of de Sitter spacetime in case that de Sitter quantum breaks, before it gracefully exits this state. Additionally, we apply our findings of chapter 2 to black holes. We argue that, because of its similarities to de Sitter spacetime with regards to quantum information, the same reasoning applies also to black holes. Similarly, the *memory burden* results in a quantum breaking effect, which leads to deviation from the semiclassical Hawking rate at the latest after half of the mass has evaporated. Our numerical studies indicate a significant slow down of evolution after this sets in. We furthermore provide a preliminary analysis on possible implications to observational bounds on primordial black holes as dark matter candidate.

We turn to the Hierarchy Problem in chapter 4. First, we briefly review the scenario of a Higgs vacuum expectation value relaxation in the cosmic attractor model introduced by Dvali and Vilenkin. We then confirm the relaxation of the Higgs VEV to the attractor value by numerical simulations. Furthermore, we extend the analysis to additional three-form fields and study their effect on the convergence rate. This study is motivated by embedding the attractor scenario into various fundamental theories that contain multiple forms.

For transparency purposes we point out that some of the results obtained and published together with collaborators have subsequently been reported in their respective dissertations. Explicitly, results form [1] and [2] were reported by Sebastian Zell [55]. Results from [2] and [4] will also be reported independently by Lukas Eisemann (in preparation). Furthermore, parts of [1] which are the basis of section 2.2.3, were already reported in my Master thesis [56]. Specific references will be given in the corresponding chapters.

Chapter 2

Enhancement of Memory Storage Capacity

Systems of enhanced memory capacity, which exhibit states with an abundance of microstates, pose a very interesting topic. For one, they are realized in nature in the form of black holes and de Sitter spacetime. Since the quantum aspects in gravity are not fully understood yet, studying generic properties of analogue systems might shed more light on their gravitational realizations. Secondly, these systems are equally interesting from the perspective of condensed matter physics and might even have applications in quantum devices for storage or computing.

In this chapter we first introduce a general mechanism that leads to states of enhanced memory capacity in section 2.1. This mechanism relies on large occupation numbers and weakly attractive interaction between at least some of the degrees of freedom in the system. We coined this mechanism *assisted gaplessness*. We shall demonstrate it on a simple prototype system.

In the following section 2.2 we introduce the *c-number method* which helps to identify such states of enhanced memory capacity in the spectrum of such system. Especially in systems, which achieve an abundance of microstates by the means of *assisted gaplessness* and therefore exhibit large occupation numbers, this method is significantly easier than a full diagonalization. The procedure will be demonstrated on a concrete prototype system consisting of 3 quantum modes.

In section 2.3 we study the time evolution of systems that are initially prepared in a non-critical state, but possess such a state accessible in their spectrum. We confirm that such states are indeed attractors of dynamical evolution. We furthermore quantify this behavior and also discuss possible applications of our findings to the concept of UV-completion by classicalization.

In section 2.4 we introduce a general property of states with enhanced memory capacity, which we call *memory burden*. The quantum information that is stored in the emerged gapless degrees of freedom in such a state backreact to any evolution that would evolve the system away from the critical configuration and in that sense stabilize it. We then study possible scenarios to avoid such a strong backreaction due to the quantum effect of *memory burden*. However, we shall see that this universal phenomenon can not

be avoided on long enough timescales and even in fine-tuned cases, where the burden can be reduced, it is not efficient enough to avoid backreaction altogether.

This chapter is based on the paper [1], which is joint work with Gia Dvali and Sebastian Zell, as well as the papers [2] and [4], which is joint work with Gia Dvali, Lukas Eisemann and Sebastian Sell. Section 2.1 follows [1]. The next section 2.2 is also based on [1] where preliminary results including Figs. 2.5, 2.4, 2.3, 2.2 and 2.1 were already reported in [56]. Exact references are given in the text. Section 2.3 is based on yet unpublished work [5] in collaboration with Gia Dvali, Lukas Eisemann and Sebastian Sell. For the most part section 2.4 is based on [4] and to a smaller extend on [2].

2.1 Assisted Gaplessness

In the following we shall discuss a mechanism to produce dynamically a large number of nearly degenerate states in a bosonic system contributing to a large microstate entropy.

A generic bosonic system is described by a set of K degrees of freedom in the form of quantum oscillators. The corresponding creation and annihilation operators $\hat{a}_k$ and $\hat{a}_k^\dagger$, where $k = 1, \ldots, K$ satisfy the standard canonical commutation relations (CCR):

$$[\hat{a}_j, \hat{a}_k^\dagger] = \delta_{jk}\,, \qquad [\hat{a}_j, \hat{a}_k] = [\hat{a}_j^\dagger, \hat{a}_k^\dagger] = 0\,. \tag{2.1}$$

The number operator of a k-mode is defined by $\hat{n}_k \equiv \hat{a}_k^\dagger \hat{a}_k$. Eigenstates of this operator, which we denote by $|n_k\rangle$, where n_k is the corresponding eigenvalue, form a complete basis of the Hilbert space. Inspired by bit-registers in information theory we will mostly be interested in states of the form

$$|n_1, \ldots, n_K\rangle \equiv |n_1\rangle \otimes |n_2\rangle \otimes \ldots \otimes |n_K\rangle\ , \tag{2.2}$$

where we interpret a specific set of occupation numbers $n_1, \ldots, n_K$ as a distinct *memory pattern*. Information can then be encoded in these types of patterns. An important quantity of a specific memory pattern is its associated energy cost and more specifically the amount of energy required to rewrite a memory register from one pattern to another. In general, for a given Hamiltonian $\hat{H}$ the energy for a specific pattern is given by

$$E_{n_0,n_1,\ldots} \equiv \langle n_1, \ldots, n_K | \hat{H} | n_1, \ldots, n_K \rangle\,. \tag{2.3}$$

In case of free oscillators the energy level-spacing between states of different occupation for a specific mode $\hat{a}_k$, i.e. $|n_k\rangle$ and $|n_k \pm 1\rangle$ is given by a constant which we shall denote by the energy gap ϵ_k. The energy cost for a fixed memory pattern is then given by

$$E_{n_0,n_1,\ldots} = \sum_k \epsilon_k n_k. \tag{2.4}$$

Similarly, the energy difference between two states $|n_1, \ldots, n_K\rangle$ and $|n_1', \ldots, n_K'\rangle$ is simply $\Delta E = \sum_k \epsilon_k (n_k - n_k')$.

To acquire a large microstate entropy a system has to fit a large number of these $|n_1, \ldots, n_K\rangle$ in a small energy gap ΔE. However, unless ϵ_k are extremely small numbers,

generic states are usually separated by a large energy difference and therefore do not count towards a large microstate entropy. In the following, we will adjust the situation by introducing a specific type of interaction between the *memory modes* $\hat{a}_k$ and another degree of freedom which we denote by $\hat{a}_0$. The corresponding annihilation and creation operators shall again satisfy the bosonic commutation relations (2.1) and we denote its number operator with $\hat{n}_0 \equiv \hat{a}_0^\dagger \hat{a}_0$. When we apply this to concrete examples in later chapters we will see that this mode $\hat{a}_0$ is usually the one with the smallest energy gap ϵ_0 and can therefore be highly occupied, which we will assume from now on. The important property of the interaction between $\hat{a}_0$ and the $\hat{a}_k$ modes is that it is attractive. An particularly easy choice is:

$$\hat{H} = \epsilon_0 \hat{n}_0 + \left(1 - \frac{\hat{n}_0}{N_c}\right) \sum_{k=1}^{K} \epsilon_k \hat{n}_k \,, \tag{2.5}$$

where $1/N_c \ll 1$ is the interaction strength. The reason for this specific structure will become apparent shortly. If the $\hat{a}_0$ mode is unoccupied, the energy cost for a specific pattern reduces again to Eq. (2.4). However, as soon as $\hat{n}_0$ gets populated the effective gap of the $\hat{a}_k$ modes shrinks due to the attractive coupling. In the limit of large occupation of $\hat{n}_0$ we can use a Bogoliubov approximation, replacing the number operator $\hat{n}_0$ with its corresponding expectation value n_0 and this way obtain an easy description of the effective gaps $\mathcal{E}_k$ of the $\hat{n}_k$ modes:

$$\mathcal{E}_k = \left(1 - \frac{n_0}{N_c}\right) \epsilon_k. \tag{2.6}$$

It becomes immediately clear that

$$\mathcal{E}_k \to 0 \qquad \text{for} \qquad n_0 \to N_c, \tag{2.7}$$

and the effective gaps exactly vanish for the critical occupation $n_0 = N_c$. In this case the *memory modes* become gapless and all states of the form

$$|\underbrace{N_c}_{n_0}, n_1, \ldots, n_K\rangle \,, \tag{2.8}$$

become degenerate in energy for arbitrary occupation numbers $n_1, \ldots n_K$. Since the $\hat{a}_0$ mode is assisting the memory modes in becoming gapless we shall call $\hat{a}_0$ the *master mode*. However, this comes with a cost. In order to alleviate the energy cost for storing and rewriting information by making the memory modes gapless, one first has to invest the energy $\epsilon_0 N_c$ to bring the system into its critical state. Only then a sector of the Hilbert space with an enhanced entropy becomes accessible.

Assuming for a moment that each of the memory modes can choose among d different possible states $|n_k\rangle$ with $n_k = 0, 1, \ldots, d-1$, equivalent to a qudit, this system exhibits $(d+1)^K$ distinct microstates with minuscule energy difference around the critical and macroscopic occupation $n_0 = N_c$. This is equivalent to an entropy

$$S = K \ln(d+1). \tag{2.9}$$

So to account for an entropy S a physical system has to provide of order $K \simeq S$ nearly degenerate degrees of freedom.

2.2 C-number Method

2.2.1 The Method

In the introduction 1.7 and the last section 2.1 we discussed the importance and several properties of gapless modes and an actual mechanism that produces dynamically an abundance of those. In this section we shall take a slightly different perspective and argue that the existence of at least a few gapless degrees of freedom is a very generic feature of bosonic systems that are weakly attractive interacting.

As we saw in the last section 2.1 assisted gaplessness can be a robust mechanism to provide for an abundance of gapless modes in the spectrum. However, up until now we only discussed the bare essence on a simplified model in which there is a strict separation between modes that becomes gapless and therefore contribute to the microstate entropy and the mode that assisted them by lowering their effective gap. In more sophisticated systems such clear distinction may not be that easy and multiple modes can be macroscopically occupied and can furthermore contribute to collective excitations, which will carry the information. A specific example for such a system is given by the Lieb-Lininger model with attractive interaction and Dirichlet boundary condition. This behavior can also be found in quantum neural networks which we shall discuss in more detail in section 3.3. In the following we discuss a method for identifying gapless (collective) degrees of freedom in the spectrum of such systems. Our method is by no means exhaustive in the sense that it may not identify all states accompanied with gapless modes. Here we pursue the more modest goal of finding at least some of those.

Let us start with a generic bosonic Hamiltonian

$$\hat{H} = \hat{H}(\hat{a}_1^\dagger, \dots \hat{a}_K^\dagger, \hat{a}_1, \dots, \hat{a}_K, \epsilon_k, \alpha) \tag{2.10}$$

where again $\hat{a}_k^\dagger, \hat{a}_k$ represent the creation and annihilation operators of a set of quantum oscillator degrees of freedom satisfying the CCR (2.1). Furthermore, ϵ_k are the free gaps of the different modes and α is a set of parameters which shall represent the different coupling constants in the theory. For simplicity we shall assume the Hamiltonian written in these operators to be normal ordered. Furthermore we shall restrict ourselves here to a specific subclass of systems that exhibit total particle number conservation. This is equivalent to a global $U(1)$ symmetry. Note that any continuous symmetry of the Hamiltonian automatically leads to a flat direction in the energy landscape transforming states of same energy into each other. To illustrate this we can consider the simple example of a free quantum oscillator:

$$\hat{H} = \hat{a}^\dagger \hat{a}. \tag{2.11}$$

This Hamiltonian also possesses a global $U(1)$ symmetry parameterized by a complex phase that transforms

$$\hat{a} \to e^{i\varphi}\hat{a} \qquad \text{and} \qquad \hat{a}^\dagger \to e^{-\varphi}\hat{a}^\dagger. \tag{2.12}$$

Note that we are only interested in gapless modes that emerges due to assisted gaplessness and our c-number method. However, our procedure is also sensitive to flat direction which

arise from continuous symmetries. For that reason we have to incorporate such symmetries in the method which we shall demonstrate on a specific example. It is straightforward to see that the states $|\Psi(\hat{a})\rangle$ and $|\Psi(e^{i\phi}\hat{a})\rangle$ are degenerate in energy and are therefore connected by a gapless transformation. This, however, is not connected to attractive interaction. Since the c-number method is sensitive to the symmetries of the Hamiltonian we shall demonstrate how to take those into consideration on the example of $U(1)$ in the following.

A particle number conserving incarnation of Hamiltonian (2.10) has the following form

$$\begin{aligned}\hat{H} &= \sum_{k=0}^{K} \epsilon_k \hat{a}_k^\dagger \hat{a}_k + \sum_{k,j,m,n=0}^{K} \alpha^{(4)}_{kjmn} \hat{a}_k^\dagger \hat{a}_j^\dagger \hat{a}_m \hat{a}_n \\ &+ \sum_{k,j,m,n,o,p=0}^{K} \alpha^{(6)}_{kjmnop} \hat{a}_k^\dagger \hat{a}_j^\dagger \hat{a}_m^\dagger \hat{a}_n \hat{a}_o \hat{a}_p \\ &+ \sum_{k,j,m,n,o,p,q,r=0}^{K} \alpha^{(8)}_{kjmnopqr} \hat{a}_k^\dagger \hat{a}_j^\dagger \hat{a}_m^\dagger \hat{a}_n^\dagger \hat{a}_o \hat{a}_p \hat{a}_q \hat{a}_r + \dots ,\end{aligned} \tag{2.13}$$

It is again easy to see that this Hamiltonian is invariant under the transformation (2.12). We shall also assume that the full Hamiltonian is bounded from below to be consistent.

To reiterate, the sole requirements for the existence of states with enhanced microstate entropy are

1. The system consists of bosonic degrees of freedom allowing for high occupation numbers

2. Some of the interactions are attractive to form a non-trivial energy landscape

Usually identifying gapless modes reduces to the task of finding eigenvectors of the Hamiltonian with an eigenvalue that is close to or equal zero. However, even though there exist approximation schemes to avoid a computational intense diagonalization of the complete Hamiltonian this task usually gets harder the greater the Hilbert space grows. In the following on the other hand we want to show that larger systems in form of higher occupation numbers can actually help identifying gapless modes more easily. The crux of our method will be that a high occupation enables us to replace operators by their expectation values in form of a Bogoliubov approximation simplifying calculations enormously. This replacement for the specific case of a total particle number conserving symmetry has the following form

$$\hat{\vec{a}} \to \vec{a}\,, \qquad \hat{\vec{a}}^\dagger \to \vec{a}^*\,, \tag{2.14a}$$

$$\hat{a}_0 \to \sqrt{N - \sum_{k=1}^{K} |a_k|^2}\,, \qquad \hat{a}_0^\dagger \to \sqrt{N - \sum_{k=1}^{K} |a_k|^2}\,, \tag{2.14b}$$

where a_k are complex numbers and we introduced the abbreviation

$$\vec{a} = (a_1, \dots, a_K)\,, \qquad \vec{a}^* = (a_1^*, \dots, a_K^*)\,. \tag{2.15}$$

Note that due to particle number conservation we expressed the *master mode* $\hat{a}_0$ in terms of the total particle number and the sum of the remaining modes. This reduces $K+1$ quantum operators to only K complex variables. However, this only fixes the modulus of the replaced mode. Additionally we have to fix a global phase later on. We want to emphasize again that we shall *construct* a state which comes with at least one gapless degree of freedom. So we are especially not limited to the ground state or similar outstanding choices. Therefore, motivated by the indicated scaling in the conservation law Eq. (2.14) we shall assume that the complex valued expectation values of the operators scale with the total particle number of the system, i.e. $a_i \sim \sqrt{N}$. In summary, we obtain the replacement

$$\hat{H}(\hat{\vec{a}}^\dagger, \hat{\vec{a}}, \hat{a}_0^\dagger, \hat{a}_0) \to H_{\mathrm{bog}}(\vec{a}, \vec{a}^*)\,, \tag{2.16}$$

where $H_{\mathrm{bog}}(\vec{a}, \vec{a}^*)$ is an algebraic c-number function, which depends on K complex variables. Naturally, replacing operators with expectation values introduces an error. Usually this error in the Bogoliubov approximation scales as $1/N$. Consequently, the approximation becomes exact in the limit of infinite occupation number. In order to keep the collective coupling constant we will apply the following limit procedure

$$N \to \infty\,, \qquad \alpha^{(i)} \to 0\,, \qquad \text{with } \lambda^{(i)} \equiv \alpha^{(i)} N^{i/2-1} = \text{const.}\,, \tag{2.17}$$

where we suppressed the indices of the coupling constants. Throughout the remainder of this section the limit $N \to \infty$ will always correspond to the procedure (2.17) with an implicit interaction strength scaling $\alpha^{(i)} \to 0$. In this limit the Bogoliubov approximation and therefore the c-number method are exact. For a finite number of particles N there are corrections that scale as a power of $1/N$.

After finding a simplified approximate representation of the system (2.13) in case of large occupation numbers we will now discuss the conditions for the Bogoliubov Hamiltonian H_{bog} that lead to the existence of gapless excitation. For this purpose we introduce the notion of a *critical point* of a c-number representation of a Hamiltonian. It is defined as a value $\vec{a}_\circ$ such that its first derivative as a function of the complex numbers a_k vanishes,

$$\left.\frac{\partial H_{\mathrm{bog}}}{\partial \vec{a}}\right|_{\vec{a}=\vec{a}_\circ} = 0\,, \tag{2.18}$$

and moreover the determinant of the second derivative matrix is zero,

$$\det \mathcal{M}\Big|_{\vec{a}=\vec{a}_\circ} = 0\,, \qquad \text{where } \mathcal{M} \equiv \begin{pmatrix} \mathcal{B}^* & \mathcal{A} \\ \mathcal{A}^T & \mathcal{B} \end{pmatrix}. \tag{2.19}$$

Here the matrices $\mathcal{A}$ and $\mathcal{B}$ denote $\mathcal{A}_{kj} \equiv \frac{\partial^2 H_{\mathrm{bog}}}{\partial a_k^* \partial a_j}$ and $\mathcal{B}_{kj} \equiv \frac{\partial^2 H_{\mathrm{bog}}}{\partial a_k \partial a_j}$, which implies $B^T = B$ and $A^\dagger = A$. So we deal with a *stationary inflection* point of the function $H_{\mathrm{bog}}(\vec{a}, \vec{a}^*)$, i.e., a point at which the curvature vanishes in some directions.

If the complex valued function H_{bog} exhibits such a *critical point* then this implies (within $1/N$ corrections) the existence of a state with emergent gapless degrees of freedom. This statement holds in the full quantum theory. In other words, any critical point in the Bogoliubov Hamiltonian corresponds to a state of enhanced memory capacity. To

show this we expand the Hamiltonian around the expectation value of a macroscopic background state with total occupation number N and corresponding to Eq. (2.14) replace the $\hat{a}_0$ mode with

$$\langle \hat{a}_0 \rangle \approx \langle \hat{a}_0^\dagger \rangle \approx \sqrt{N - \sum_{k=1}^{K} \langle \hat{a}_k^\dagger \hat{a}_k \rangle} \,. \tag{2.20}$$

Again, this introduces an error of order $1/N$ which vanishes in the double scaling limit (2.17). This replacement incorporates particle number conservation, removes the unwanted symmetry and reduces the Hamiltonian to a K-mode system. Next, we consider quantum fluctuation around this background field by shifting the operators by the stationary inflection point of the c-number Hamiltonian H_{bog},

$$\hat{\vec{a}} \to \vec{a}_\circ + \hat{\vec{\alpha}} \,, \qquad \hat{\vec{a}}^\dagger \to \vec{a}_\circ^{\,*} + \hat{\vec{\alpha}}^\dagger \,. \tag{2.21}$$

Note that a simple constant translation of the operators does not change their algebraic structure. So the shifted operators $\hat{\alpha}_k$ and $\hat{\alpha}_k^\dagger$ still satisfy the same canonical commutation relations (2.1). Such a replacement is always possible and is exact on the level of the full quantum Hamiltonian. However, the Hamiltonian is in general not diagonal in these new modes.

Next we shall study the spectrum around critical background state at which gapless modes emerge in more detail. For our purposes it is enough to only consider terms up to quadratic order in the Hamiltonian. Note that there are no linear terms around this specific state $\vec{a}_\circ$ since it extremizes the Bogoliubov Hamiltonian and therefore all first order derivatives vanish. Also note that we choose a macroscopic state in which the background modes scale as $a_k \sim \sqrt{N}$. In contrast to that the fluctuations around this *critical point* remain independent of N. This leads to an effective suppression of $1/\sqrt{N}$ for each factor of $\hat{\alpha}_k$ in each term of the Hamiltonian. So in the limit (2.17) of large N, the second-order term dominates and the effective Hamiltonian takes the following form:

$$\langle \hat{\mathcal{H}} \rangle \;=\; H_0 + \langle \hat{\vec{\alpha}}^\dagger \mathcal{A} \hat{\vec{\alpha}} \rangle \;+\; \frac{1}{2} \Big(\langle \hat{\vec{\alpha}} \mathcal{B} \hat{\vec{\alpha}} \rangle \;+\; \langle \hat{\vec{\alpha}}^\dagger \mathcal{B}^* \hat{\vec{\alpha}}^\dagger \rangle \Big) \,, \tag{2.22}$$

where the constant $H_0 \equiv H_{\text{bog}}(\vec{a}_\circ, \vec{a}_\circ^{\,*})$ denotes the value of the c-number function at the extremal point. In the following we will drop this irrelevant constant in the Hamiltonian and write in block-matrix form:

$$\langle \hat{\mathcal{H}} \rangle \;=\; \frac{1}{2} \langle \begin{pmatrix} \hat{\vec{\alpha}}^\dagger & \hat{\vec{\alpha}} \end{pmatrix} \begin{pmatrix} \mathcal{B}^* & \mathcal{A} \\ \mathcal{A}^T & \mathcal{B} \end{pmatrix} \begin{pmatrix} \hat{\vec{\alpha}}^\dagger \\ \hat{\vec{\alpha}} \end{pmatrix} \rangle + \text{const.} \tag{2.23}$$

Now we can diagonalize the Hamiltonian by following Bogoliubov transformation:

$$\begin{pmatrix} \hat{\vec{\alpha}}^\dagger \\ \hat{\vec{\alpha}} \end{pmatrix} = \mathcal{T} \begin{pmatrix} \hat{\vec{\beta}}^\dagger \\ \hat{\vec{\beta}} \end{pmatrix} \,, \qquad \text{with } \mathcal{T} = \begin{pmatrix} V^* & U \\ U^* & V \end{pmatrix} \,, \tag{2.24}$$

or written in the entry level and equivalent form,

$$\hat{\alpha}_k = U_{kj}^* \hat{\beta}_j^\dagger + V_{kj} \hat{\beta}_j \,, \tag{2.25}$$

where U and V are the transformation matrices and $\hat{\beta}_j^\dagger, \hat{\beta}_j$ are the new modes that form a diagonal canonical basis. These should still represent bosonic quantum oscillators. Therefore, the canonical commutation relations imply the conditions:

$$VV^\dagger - U^*U^T = \mathbb{1}\,, \qquad VU^\dagger - U^*V^T = 0\,. \tag{2.26}$$

To ensure we end up with a diagonal matrix we choose the matrices U and V such that off-diagonal terms, of the type $\hat{\beta}_j\hat{\beta}_k$ and $\hat{\beta}_j^\dagger\hat{\beta}_k^\dagger$, are absent from the Hamiltonian. This implies that U, V satisfy

$$U^\dagger\mathcal{A}^TV^* + V^\dagger\mathcal{A}U^* + V^\dagger\mathcal{B}^*V^* + U^\dagger\mathcal{B}U^* = 0\,. \tag{2.27}$$

In this way, we bring the Hamiltonian to the form

$$\langle\hat{\mathcal{H}}\rangle \;=\; \langle\hat{\beta}_k^\dagger\mathcal{E}_{kj}\hat{\beta}_j\rangle \;+\; \text{const.}\,, \tag{2.28}$$

where the matrix $\mathcal{E}$ is given by

$$\mathcal{E} \equiv U^\dagger\mathcal{A}^TU + V^\dagger\mathcal{A}V + V^\dagger\mathcal{B}^*U + U^\dagger\mathcal{B}V\,. \tag{2.29}$$

Note that the conditions (2.26) and (2.27) remain unaffected if U and V are rotated under a unitary matrix. We can use this freedom to find a unitary transformation that brings $\mathcal{E}$ to diagonal form. Therefore we assume $\mathcal{E}$ to be diagonal in the following.

To determine the existence of gapless modes in the Hamiltonian $\mathcal{E}$ written in the new operators $\hat{\beta}_k$ we have to know if it contains zero eigenvalues. A sufficient condition for this is if its determinant vanishes. However, we already assumed that we are at a critical point $a_\circ$ around which the Hamiltonian (2.28) was expanded. We therefore know that the second derivative matrix $\mathcal{M}$ contains a zero eigenvalue. Note that $\mathcal{M}$ and $\mathcal{E}$ are related via the transformation matrix $\mathcal{T}$. Because the transformation matrix $\mathcal{T}$ is regular and therefore the dimension of the kernel (and number of zero eigenvalues) is invariant under such transformation we can consider $\det\mathcal{E} = 0$ equivalently to $\det\mathcal{M}$. Moreover the determinant of the matrix $\mathcal{T}$ can be determined with the help of following relation

$$\mathcal{T}\mathcal{J}\mathcal{T}^\dagger = \mathcal{J}\,, \tag{2.30}$$

where $\mathcal{J} = \text{diag}(\mathbb{1}, -\mathbb{1})$ and $\mathbb{1}$ is a unit matrix of dimension K. Consequently, we can compute $\det\mathcal{T} = 1$. For details on these transformation properties and more general diagonalization methods for bilinear Hamiltonians we refer to [57]. In short, our assumption $\det\mathcal{M} = 0$ implies $\det\mathcal{E} = 0$. Therefore, gapless degrees of freedom exist among the quantum modes $\hat{b}_k$. Moreover, due to the previously mentioned invariance of the dimension of the kernel under the regular transformation $\mathcal{T}$ the number of zero eigenvalues in $\mathcal{M}$ and the corresponding number of gapless degrees of freedom among the $\hat{\beta}_k$ modes is the same.

We want to reiterate that above results are exact in the double scaling limit (2.17) in case for infinite particle number N. For finite occupation numbers there will emerge correction that scale as a power of $1/N$. They originate from higher order terms which we dropped earlier and corrections to the replacement (2.20). So similar to a quantum

phase transition which can only occur for infinite particle numbers [58] those modes are only nearly-gapless, with a gap that vanishes as $1/N$ for $N \to \infty$. Note that also the exact position in state space of $\vec{a}_\circ$ will receive $1/N$ corrections. However, we can always make those contributions arbitrarily small by choosing a large enough N. Concluding, also for finite N the energy efficiency for storing quantum information in these nearly gapless modes is severely enhanced. Therefore we conclude that a critical point in the complex number valued Bogoliubov Hamiltonian H_{bog} corresponds to the appearance of nearly-gapless modes in the full quantum theory. In summary, each zero eigenvalue of the second derivative matrix $\mathcal{M}$ leads to a nearly-gapless mode.

Note that our c-number method is in spirit equivalent to the study of the Gross-Pitaevskii equation [59], [60], which corresponds to working in position space rather than in momentum operators. Also in this paradigm the field operator $\hat{\psi}$ is expanded around a classical background value: $\hat{\psi} = \psi_{\text{cl}} + \delta\hat{\psi}$. Here studying the spectrum of fluctuation $\delta\hat{\psi}$ allows to determine gapless modes. Our method is conceptually the momentum space analogue of this technique. The c-number method first relies on a transition to momentum space by expanding the field operator $\hat{\psi}$ in mode operators $\hat{a}$. After that we expand the operators around their classical expectation value: $\hat{\vec{a}} = \vec{a}_\circ + \hat{\vec{\alpha}}$.

Coherent State Basis

Before we actually apply the c-number method to an exemplary system we first want to mention another point of view on our procedure to determine states of enhanced memory capacity. Instead of using number eigenstates, we can also take advantage of coherent states. These represent states that most closely resemble the oscillatory behavior of a classical harmonic oscillator and are another kind of template state that can be used to determine critical configurations. Before we start, note that coherent states $|\vec{a}\rangle$ are the eigenstates of the destruction operators:

$$\hat{a}_k \, |\vec{a}\rangle = a_k \, |\vec{a}\rangle \, , \tag{2.31}$$

where a_k is a complex eigenvalue. This eigenvalue can also be computed with the help of expectation value of the number operator

$$|a_k|^2 = \langle \vec{a}| \, \hat{n}_k \, |\vec{a}\rangle \, . \tag{2.32}$$

Using this it becomes clear that taking an expectation value of the Hamiltonian (2.13) over a coherent state $|\vec{a}\rangle$ simply amounts to the Bogoliubov approximation (2.14). This is an equivalent procedure to the replacement of operators by their expectation value c-numbers. Therefore, we can write

$$\langle \vec{a}| \, \hat{H} \, |\vec{a}\rangle = H_{\text{bog}} \, . \tag{2.33}$$

This means that coherent states explicitly realize the replacement (2.16). An immediate upside of this point of view is that this procedure is exact also for finite N. The Bogoliubov Hamiltonian H_{bog} can therefore be understood as the expectation value of a coherent state. In particular, this construction is relevant when the Bogoliubov Hamiltonian possesses a

stationary inflection point $\vec{a}_\circ$. If in this case the eigenvector with vanishing eigenvalue is given by $\vec{\delta a}$, then we can consider the state $|\vec{a}_\circ + \epsilon\vec{\delta a}\rangle$. For small values of ϵ, it fulfills

$$\langle \vec{a}_\circ + \epsilon\vec{\delta a}|\, \hat{H}\, |\vec{a}_\circ + \epsilon\vec{\delta a}\rangle = \langle \vec{a}_\circ|\, \hat{H}\, |\vec{a}_\circ\rangle \ . \tag{2.34}$$

This corresponds to a whole family $|\vec{a}_\circ + \epsilon\vec{\delta a}\rangle$ of states with approximately the same energy. Therefore information can be stored in this set of states exceptionally efficiently. Note, however, that coherent states do not form an orthonormal basis. So not every state in this family counts towards the microstate entropy and only those that differ enough in the operators $\hat{a}_k$ can be sufficiently distinct. This can me made explicit by considering the scalar product of two coherent states $|\vec{a}\rangle$ and $|\vec{a}'\rangle$:

$$|\, \langle \vec{a}|\vec{a}'\rangle\, |^2 = \mathrm{e}^{-\sum_k |a_k - a_k'|^2} \ . \tag{2.35}$$

To make the overlap sufficiently small we have to demand that we only count states that satisfy

$$\sum_k |a_k - a_k'|^2 \gg 1 \, . \tag{2.36}$$

Naturally, regardless in which basis the memory states are represented, their number and therefore the entropy is the same. So the information storage capacity is the same in the coherent state basis as well as in the basis of number eigenstates of the Bogoliubov modes $\hat{\beta}_k$. Explicitly, this can be seen by using relation (2.36). It is clear from this that coherent states can be counted as different as soon as

$$|n_k - n_k'| \gg \sqrt{n_k} \, , \tag{2.37}$$

where $n_k = |a_k|^2$ and $n_k' = |a_k'|^2$. Using this to count states we get of order $\sqrt{n_k}$ different possible expectation values of the particle number. On top of this we have additional distinct states by varying the phases φ_k. Taking into account the uncertainty, $\Delta n_k \Delta\varphi_k \gtrsim 1$, this gives $\sqrt{n_k}$ different phases for each modulus n_k. Combining those two this gives n_k different states, the same result as in the basis of number eigenstates. Although computationally there is no obvious advantage of using coherent states rather than number eigenstates in the c-number method, their usefulness lies in the ability of taking a smooth classical limit. This convenience will come in handy when generalizing the concept of enhanced memory capacity to classical systems like neural networks [12]

We next shall apply our c-number method first to an easy example which was already solved in the literature as an easy crosscheck since all equations can be solved analytically and the Bogoliubov transformation can be carried out explicitly. After that we apply our procedure to the more difficult analogue system with Dirichlet boundary condition rather than periodic one.

Comparison with Goldstone Phenomenon

On a side note we want to discuss the fundamental difference of the appearance of gapless modes due to assisted gaplessness, namely an attractive interaction among the quantum modes to the the well-known phenomenon of appearance of gapless excitations in the form

of Goldstone bosons. These emerge as a result of a phase transition accompanied by a spontaneous breaking of a global symmetry. One crucial difference is that gapless modes originating from Goldstone phenomenon exist in a domain past the critical configuration of phase transition. This is not the case in the model studied above. In this model gapless degrees of freedom only emerge exactly at the critical point and appear due to a cancellation between the positive kinetic energy and a negative collective interaction energy. This makes it hard to interpret the phenomenon of assisted gaplessness in terms of a Goldstone mode originating from a spontaneous breakdown of a global symmetry. This difference in particular makes the phenomenon of assisted gaplessness interesting since there is no *a priori* symmetry reason for the emergence of any gapless modes. However, even though the phenomenon has a priori no connection to a symmetry, additional symmetries can greatly enhance the number of gapless modes once assisted gaplessness takes place. One specific example in case of a spherical symmetry is discussed in [61].

2.2.2 Application to a Bose Gas with Periodic Boundary Conditions

As an easy entry point to our method we shall apply it first to the well understood system of a weakly attractively interacting cold and dilute Bose gas with periodic boundary conditions. In this model the interaction can be approximated by a four-point function. Based on the results of [62] this system was subject of extensive studies in a series of papers [9], [10], [14], [15], [32], [63], [64], which focused primarily on its quantum informational properties. In particular, a similar procedure in which an operator valued Hamiltonian was replaced by a c-number function was already used in [10]. Since the spectrum of this theory is already known and all calculations can be carried out analytically it is a great example to understand the application of the c-number method. The Hamiltonian of the periodic system is given by

$$\hat{H} = \int_0^L \mathrm{d}z \left[\frac{\hbar^2}{2m} \partial_z \hat{\psi}^\dagger \partial_z \hat{\psi} - \frac{\hbar^2}{2m} \frac{\pi^2 \alpha}{L} \hat{\psi}^\dagger \hat{\psi}^\dagger \hat{\psi} \hat{\psi} \right], \tag{2.38}$$

with α being a dimensionless and positive coupling strength. The mass of the atoms is given by m and L is the size of the system. We can write this Hamiltonian in momentum space by expanding the field operators $\hat{\psi}$

$$\hat{\psi} = \sqrt{\frac{1}{L}} \sum_{k=-\infty}^{\infty} \hat{a}_k e^{ikz}, \tag{2.39}$$

and plug it in the Hamiltonian (2.38). This yields

$$\sum_{k=-\infty}^{\infty} k^2 \hat{a}_k^\dagger \hat{a}_k - \frac{\alpha}{4} \sum_{k,m,n=-\infty}^{\infty} \hat{a}_k^\dagger \hat{a}_m^\dagger \hat{a}_{n+k} \hat{a}_{m-n}\,, \tag{2.40}$$

with a coupling constant α. Note that we set $\hbar = 1$ and consider for simplicity a specific choice of parameters where we put $m = 1/2$ and the length of the system $L = 2\pi$. The total particle number is given by N. In case of repulsive interaction this system is

also known as Lieb-Liniger model [65], [66]. As it was demonstrated e.g. in [63], higher momentum modes only get marginally occupied for small coupling strength. Therefore, we truncate the Hamiltonian (2.40) and only keep momentum modes with $|k| \leq 1$.

First we have to take care of the symmetries of the system since we are not interested in gapless transformation arising from those. One is again particle number conservation. We have seen that this can be incorporated naturally by replacing the number operator of one quantum mode with the sum of the remaining ones minus the total particle number in the system. Since we consider small couplings we expect the lowest momentum mode $k = 0$ to be occupied the most so shall choose to replace $\hat{a}_0$. This system also exhibits an additional symmetry due to momentum conservation. This symmetry imposes a superselection sector in which the total momentum of the system is fixed. Therefore we can remove this symmetry by fixing a value and consequently choosing a superselection sector. We choose a total momentum of zero which implies that the expectation values of the number operators $\hat{n}_{-1} \equiv \hat{a}_{-1}^\dagger \hat{a}_{-1}$ and $\hat{n}_1 \equiv \hat{a}_1^\dagger \hat{a}_1$ remain equal. So $\langle \hat{n}_{-1} \rangle = \langle \hat{n}_1 \rangle$ has to hold for all times t. Last but not least there is one additional phase symmetry which transform $\hat{a}_{-1} \to e^{-i\phi} \hat{a}_{-1}$ and $\hat{a}_1 \to e^{i\phi} \hat{a}_1$. In summary, we still have to eliminate one modulus and one phase. To achieve that we use the replacement (2.14b) due to particle number conservation and moreover we replace $\hat{a}_{-1} \to \hat{a}$ to get rid of the phase. In summary we have the following replacement rules

$$\hat{\vec{a}} = \begin{pmatrix} \hat{a}_{-1} \\ \hat{a}_1 \end{pmatrix} \to \begin{pmatrix} a_1 \\ a_1 \end{pmatrix}, \qquad \hat{\vec{a}}^\dagger = \begin{pmatrix} \hat{a}_{-1}^\dagger \\ \hat{a}_1^\dagger \end{pmatrix} \to \begin{pmatrix} a_1^* \\ a_1^* \end{pmatrix}, \tag{2.41}$$

and

$$\hat{a}_0 \to \sqrt{N - 2|a_1|^2}\,, \qquad \hat{a}_0^\dagger \to \sqrt{N - 2|a_1|^2}\,. \tag{2.42}$$

This gives the following Bogoliubov Hamiltonian:

$$H_{\text{bog}} = 2|a_1|^2 - \frac{\alpha}{4}\left(N^2 + 2N(a_1 + a_1^*)^2 - 2|a_1|^2(3|a_1|^2 + 2a_1^2 + 2a_1^{*2}) \right). \tag{2.43}$$

After having arrived at a complex valued approximation of the original Hamiltonian we can search for flat directions. According to our description we first have to find an extreme point, see (2.18). So we set the first derivative of (2.43) equal to zero:

$$\frac{\partial H_{\text{bog}}}{\partial a_1} = 2a_1^* - \alpha \left(N(a_1 + a_1^*) - 3a_1^2 a_1^* - 3a_1 a_1^{*2} - a_1^{*3} \right) = 0\,. \tag{2.44}$$

An obvious solution is $a_1 = 0$ on which we shall focus in the following. However, there are also two additional solutions given by $a_1 \approx \pm 0.5345 \sqrt{\frac{\alpha N - 1}{\alpha}}$. At those points our second requirement is fulfilled. They therefore represent turning points but are not associated to a flat direction. So let us return to the solution $a_1 = 0$. The second step is to check under which conditions the determinant of the second derivative matrix $\mathcal{M}$ vanishes at this point. According to (2.19) we check

$$\det \mathcal{M} = -4 + 4\alpha N = 0\,. \tag{2.45}$$

This is obviously true in the case for a collective coupling $\lambda = \alpha N = 1$. This implies the existence of a flat direction and consequently the emergence of a gapless degree of freedom for a collective coupling of $\lambda = 1$ and a state in which all particles occupy the 0-mode. This is in accordance (including corrections of $1/N$) with previous findings, see for example [63].

2.2.3 Application to a Bose Gas with Dirichlet Boundary Conditions

We saw in the previous subsection that finding gapless modes using the c-number method is straightforward in case of periodic boundary conditions. However, in this case also a full numerical diagonalization is available to analyze the system and the benefit of our methods are not apparent. Therefore we shall apply it to the Dirichlet boundary case which is much more involved and is no longer as easily accessible both to numerical as well as analytical methods. However, the choice of different boundary condition is not only motivated by being a harder test for our method but also from a experimental point of view. An experimental realization of a system of enhanced memory capacity would be extremely interesting. This is not only true from a standpoint of quantum informational properties of black holes and quantum gravity in general, but it may also of interest in general for quantum information science and may lead to important technical applications. This study is therefore motivated by a presumed simpler experimental realization of Dirichlet boundary conditions rather than periodic ones. Additionally, it is also interesting how sensitive the emergence of gapless degrees of freedom is to the boundary conditions.

The starting point is again Hamiltonian (2.38). However, this time we impose Dirichlet boundary conditions which can be incorporated by expanding the field operators in the following eigenfunctions

$$\hat{\psi} = \sqrt{\frac{2}{L}} \sum_{k=1}^{\infty} \hat{a}_k \sin\left(\frac{k\pi z}{L}\right). \tag{2.46}$$

This leads to the following momentum space representation of the Hamiltonian:

$$\begin{aligned}\hat{H}^{\text{full}} =& \frac{4\pi^2\hbar^2}{2mL^2}\Bigg[\sum_{k=1}^{\infty}\frac{k^2}{4}\hat{a}_k^\dagger\hat{a}_k - \frac{\alpha}{8}\sum_{k,l,m=1}^{\infty}\Big[(\hat{a}_k^\dagger\hat{a}_l^\dagger\hat{a}_m\hat{a}_{k+l-m} + 2\hat{a}_k^\dagger\hat{a}_l^\dagger\hat{a}_m\hat{a}_{k-l+m}) \\ & - 2(\hat{a}_{l+m+k}^\dagger\hat{a}_l^\dagger\hat{a}_m\hat{a}_k + \hat{a}_k^\dagger\hat{a}_l^\dagger\hat{a}_m\hat{a}_{k+l+m})\Big]\Bigg].\end{aligned}$$

We note that the ground state structure and a possible phase transition resulting in the appearance of gapless modes similar to the periodic case of this theory in the mean field limit was already studied in [56]. However there it was not possible to extract any conclusive information about the precise quantum states in the mean field limit.

Continuing, we further note that Hamiltonian (2.47) is neither analytically nor numerically easy to access. We therefore restrict ourselves to the simpler case where we again truncate the momentum modes. However, in contrast to the periodic case these higher momentum modes are no longer negligible even for small couplings and therefore represent a completely different system which has not necessarily much in common with

the original one. For low particle numbers a numerical diagonalization was carried out in [56] for different truncations $k_{\max} \leq 5$. Here we shall focus on $k_{\max} = 3$ which already shows a rich abundance of different quantum phases. This is also the smallest number if modes for which the non-periodic system behaves qualitatively differently compared to its periodic counterpart. Carrying out the truncation yields

$$\hat{H} = \frac{1}{4}\sum_{k=1}^{3} k^2 \hat{a}_k^\dagger \hat{a}_k - \frac{\alpha}{8}\Big[3\hat{a}_1^{\dagger\,2}\hat{a}_1^2 + 8\hat{a}_1^\dagger \hat{a}_2^\dagger \hat{a}_1 \hat{a}_2 + 2\hat{a}_1^{\dagger\,2}\hat{a}_2^2 + 2\hat{a}_2^{\dagger\,2}\hat{a}_1^2 \tag{2.47}$$

$$+ 8\hat{a}_1^\dagger \hat{a}_3^\dagger \hat{a}_1 \hat{a}_3 + 2\hat{a}_1^{\dagger\,2}\hat{a}_3^2 + 2\hat{a}_3^{\dagger\,2}\hat{a}_1^2 - 2\hat{a}_1^{\dagger\,2}\hat{a}_1\hat{a}_3 - 2\hat{a}_1^\dagger \hat{a}_3^\dagger \hat{a}_1^2 \tag{2.48}$$

$$+ 4\hat{a}_1^\dagger \hat{a}_2^\dagger \hat{a}_2 \hat{a}_3 + 4\hat{a}_2^\dagger \hat{a}_3^\dagger \hat{a}_1 \hat{a}_2 + 2\hat{a}_1^\dagger \hat{a}_3^\dagger \hat{a}_2^2 + 2\hat{a}_2^{\dagger\,2}\hat{a}_1\hat{a}_3 \tag{2.49}$$

$$+ 3\hat{a}_2^{\dagger\,2}\hat{a}_2^2 + 8\hat{a}_2^\dagger \hat{a}_3^\dagger \hat{a}_2 \hat{a}_3 + 2\hat{a}_2^{\dagger\,2}\hat{a}_3^2 + 2\hat{a}_3^{\dagger\,2}\hat{a}_2^2 + 3\hat{a}_3^{\dagger\,2}\hat{a}_3^2\Big]. \tag{2.50}$$

where we again have set for convenience $L = 2\pi$ and $\hbar = 2m = 1$. Our subsequent task is to understand the phase portrait of the Hamiltonian (2.50) with the aim of identifying an emergent gapless mode that leads to enhanced entropy states with long decoherence time and large information storage capacity. For this purpose we shall first introduce the Bogoliubov approximation of this Hamiltonian and study the ground state as a function of the collective coupling λ. This analysis has also been carried out in [56] and shall be repeated for consistency and also to correct a few minor errors in the numerical analysis.

The first step is to perform the Bogoliubov approximation according to our prescription. That means that we have to take into account all symmetries of the Hamiltonian. Note that the conditions of the c-number method for finding states of enhanced memory capacity does clearly not depend on the specific parametrization of the complex variables $\vec{a}$ and $\vec{a}^*$. Therefore we can always reparametrize to find the most useful form [1] . A specifically useful parametrization which already incorporates particle number conservation is given by

$$\hat{a}_1 \to \sqrt{N(1-x)}\cos(\theta)\,, \qquad \hat{a}_2 \to \sqrt{Nx}\mathrm{e}^{i\Delta_2}\,, \qquad \hat{a}_3 \to \sqrt{N(1-x)}\sin(\theta)\mathrm{e}^{i\Delta_3}\,. \tag{2.51}$$

Note that since we already took care of the symmetry emerging from particle number conservation with this specific choice of parameters, we reduced the number of complex variables already by one. In other words, we replaced the initial three modes with two complex numbers that can be written as two moduli and two phases.

The parameter x describes the relative occupation of the 2-mode and is restricted to the interval $0 \leq x \leq 1$. On top of that the angle $\theta \in [0, \pi/2]$ specifies how the remaining particles are distributed among the 1- and 3-mode. Beside those two we have two relative phases Δ_2 and Δ_3. The Bogoliubov Hamiltonian can then be computed by plugging in

[1] The equivalence of the vanishing of the second derivatives in $\vec{a}$ and x is non-trivial and only holds if there are no unoccupied modes, $a_k \neq 0$. Schematically, the reason is that $\frac{\partial H_{\mathrm{bog}}}{\partial a} = a\frac{\partial H_{\mathrm{bog}}}{\partial x}$ and therefore $\frac{\partial^2 H_{\mathrm{bog}}}{\partial^2 a} = a^2\frac{\partial^2 H_{\mathrm{bog}}}{\partial^2 x} + \frac{\partial H_{\mathrm{bog}}}{\partial x}$.

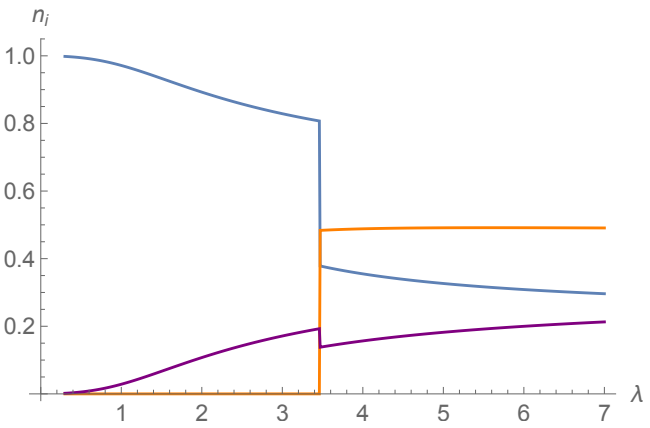

Figure 2.1: Relative occupation numbers of the ground state of the Bogoliubov Hamiltonian as functions of λ. The 1-mode is displayed in blue, the 2-mode in orange and the 3-mode in purple. There is a discontinuous change in the occupation numbers at $\lambda_{gs} \approx 3.5$.

the replacement rules (2.51) into Hamiltonian (2.50):

$$\frac{H_{\text{bog}}}{N} = \frac{1}{4}\left(1 + 3x + 8(1-x)\sin^2(\theta)\right) - \frac{\lambda}{8}\Big[\sin^2(2\theta)(1-x)^2\Big(\frac{1}{2} + \cos(2\Delta_3)\Big) \tag{2.52}$$

$$+ 3 + 2x - 2x^2 + 4x(1-x)\Big(\cos(2\Delta_2)\cos^2(\theta) + \cos(2\Delta_2 - 2\Delta_3)\sin^2(\theta)\Big) \tag{2.53}$$

$$+ 2\sin(2\theta)(1-x)\left(x\cos(2\Delta_2 - \Delta_3) + \cos(\Delta_3)\Big(2x - (1-x)\cos^2(\theta)\Big)\right)\Big]. \tag{2.54}$$

To get a feeling for the system let us first analyze the ground state. We can do so by finding the global minimum of the Bogoliubov Hamiltonian (2.54). It is evident that the choices $\Delta_2 = 0$ as well as $\Delta_3 = 0$ or $\Delta_3 = \pi$ are preferred since they minimize each term separately. This is evident from the last line of the Hamiltonian (2.54). For $3n_2 > n_1$, $\Delta_3 = 0$ is preferred and otherwise $\Delta_3 = \pi$. Next, we minimize the energy with respect to Δ_3 and the remaining two continuous parameters x and θ numerically. This procedure can be carried out for different values of the collective coupling λ. In Fig. 2.1 we plot the occupation numbers for the different modes in the ground state as a function of λ. We observe that the occupation numbers change discontinuously at the critical point $\lambda_{gs} \approx 3.5$, where the subscript gs stands for ground state. This corresponds to a first order phase transition. In order to understand the region around the phase transition better we plot the Bogoliubov Hamiltonian as a function of x and θ for the critical value $\lambda = 3.5$ in Fig. 2.2. It is clear from this illustration of the energy landscape that two disconnected generate minima exist. Since they are disconnected, a transition between those two minima is discontinuous in the respective variables. To illustrate how this second minimum develops by increasing the collective coupling we plot the energy of the ground state as a function of x where we minimize the energy with respect to the other parameters θ and Δ_3. This is shown in Fig. 2.3. We conclude that a local minimum exists at $x = 0$ for all values of λ and that another local minimum at $x = x_{\min}(\lambda) \neq 0$

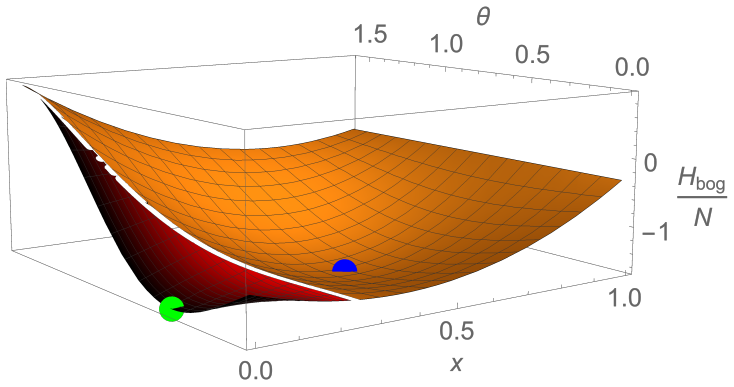

Figure 2.2: Bogoliubov energy (rescaled by the inverse particle number) for $\lambda = 3.5$ as a function of x and θ. The red surface is the region where $\Delta_3 = \pi$ minimizes the energy and in the orange surface, $\Delta_3 = 0$ is preferred. We observe two disconnected, degenerate minima, one for $x = 0$ (green point) and one for $x \neq 0$ (blue point).

starts to exist for $\lambda > \lambda_{lm}$, where

$$\lambda_{lm} \approx 1.8\,. \tag{2.55}$$

We use the subscript lm to indicate light mode and emphasize that due to finite N effects this degree of freedom is not exactly gapless. However, in the context of our method λ_{lm} corresponds to a stationary infliction point and we shall take a close look at this special value in the following. In contrast to that λ_{gs} corresponds to the point where the second minimum and its associated ground state become energetically favorable.

Before continuing by studying in the approximate gapless mode in the spectrum let us summarize our findings about the ground state in the Bogoliubov approximation picture. The ground state changes discontinuously at the critical point $\lambda_{gs} \approx 3.5$ corresponding to a first order phase transition. This can be verified in the full quantum theory by performing a numerical diagonalization of the Hamiltonian (2.50). Already for a moderate particle number of $N \gtrsim 100$ the corresponding plot of the expectation values of the number operators is indistinguishable from Fig. 2.1 reassuring the correctness of our approximation.

This behavior is qualitatively different from the periodic boundary condition case, where a continuous transition, i.e. a second order phase transition, was observed [62]. It is exactly because of this continuous behavior that the slow occupation of higher modes enables one to maintain control by truncating higher momentum modes. The large symmetry and the severely reduced Hilbert space size due to the truncation makes the numerical study of this model feasible and allows for conclusions about the untruncated system. In contrast, the discontinuous behavior of the analog system with Dirichlet boundary

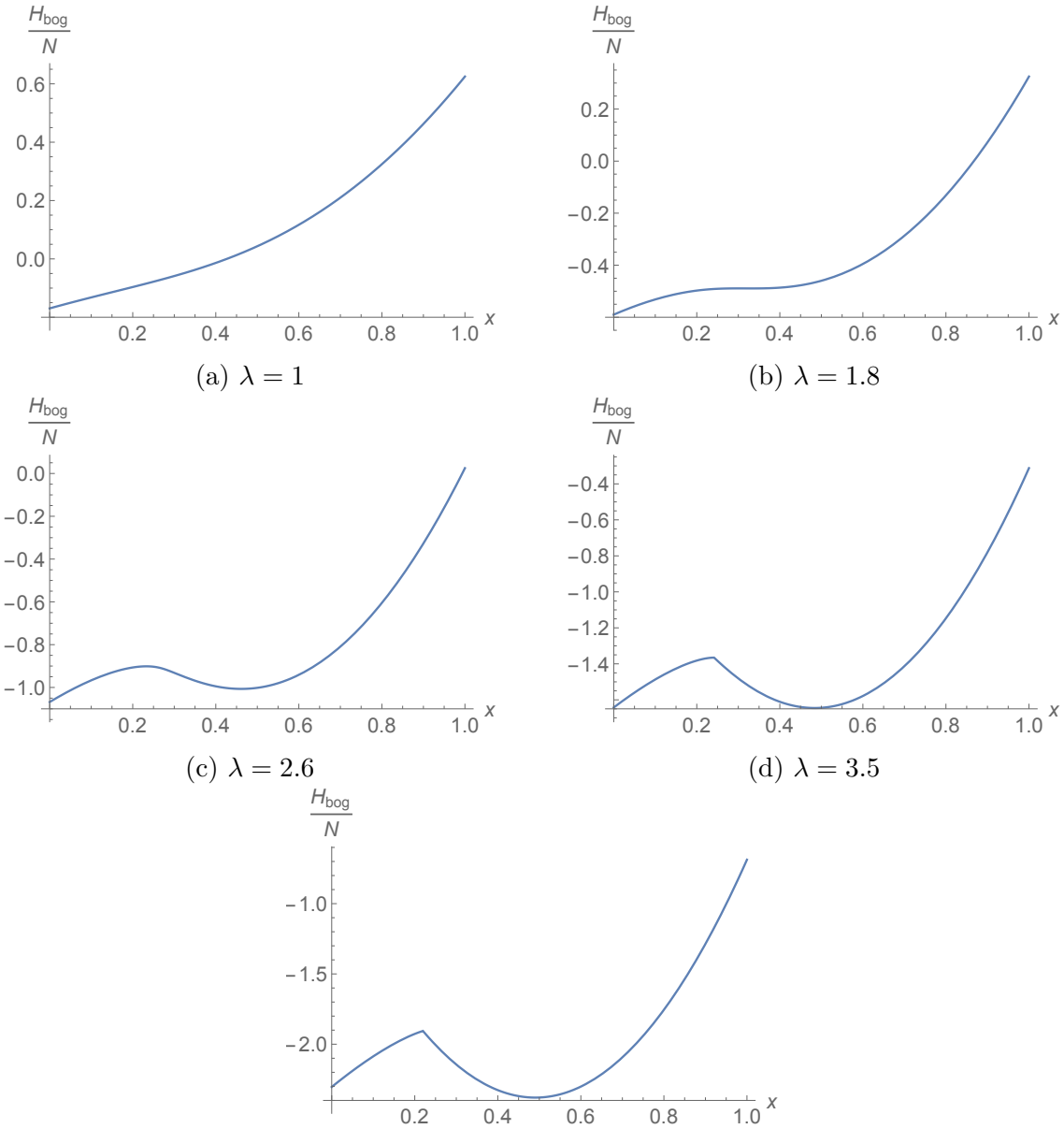

(a) $\lambda = 1$ (b) $\lambda = 1.8$

(c) $\lambda = 2.6$ (d) $\lambda = 3.5$

(e) $\lambda = 4.5$

Figure 2.3: Minimal value of the Bogoliubov Hamiltonian (rescaled by the inverse particle number) subject to the constraint that the relative occupation of the 2-mode is x. At $\lambda_{lm} \approx 1.8$, a stationary inflection point signals the appearance of a second minimum and at $\lambda_{gs} \approx 3.5$, this second minimum becomes energetically favorable.

conditions prevents us from making any reliable statement about the full system (2.47). Therefore, none of our results necessarily have to apply to the full system. For this reason we shall take the system (2.50) as fundamental and do not care about its specific origin from Hamiltonian (2.47). Note that is not a huge drawback, since the truncated system is still evolved enough to be a challenging benchmark for the c-number method and moreover we assume that it is close enough related to the original one to be of experimental significance.

Emergence of a Gapless Mode

After the preliminary study of the ground state of the system (2.50) we shall now focus on the gapless mode emerging around the critical point $\lambda = \lambda_{lm}$. The first task will be to employ the previously developed c-number method at the beginning of this section 2.2. As one of the main motivations of the development of this method this will allow us to skip the involved analysis of the full spectrum. Instead we remain with the much simpler task of showing that the Bogoliubov Hamiltonian (2.43) possesses a stationary inflection point. Since this only involves two complex variables, the problem is reduced to solving a set of analytic equations.

Because of our preliminary work on the groundstate we expect from Fig. 2.3 that a stationary inflection point appears at $\lambda = \lambda_{lm}$. In the following we shall study this special point more closely. According to the c-number method we start by setting the first derivative of the Bogoliubov Hamiltonian equal to zero. This gives us four algebraic equations, which we can solve for the four parameters x, θ, Δ_2 and Δ_3. We find that the latter two parameters behave as in the second minimum, $\Delta_2 = \Delta_3 = 0$. Therefore only the derivatives with respect to x and θ result in non-trivial conditions. Due to their lengthiness and non apparent enlightening structure we display those equation in the appendix A. As we expect from the previous analysis, solutions, i.e., local extrema, only exist for $\lambda > \lambda_{lm}$, which we determine as $\lambda_{lm} = 1.792$. The next task in our method is to ensure that the determinant of the second derivative matrix $\mathcal{M}$ vanishes. Again because of the lengthy expressions and the absence of an apparent easy analytical access we put those in the appendix A. Next we plug in the extreme point and then compute the determinant. The result is displayed in Fig. 2.4a as a function of the collective coupling.

The displayed results confirm that $\det \mathcal{M}$ vanishes as λ approaches λ_{lm} from above. Therefore, both our requirements (2.18) and (2.19) are satisfied and $\lambda = \lambda_{lm}$ corresponds to a stationary inflection point in the Bogoliubov Hamiltonian. Consequently, this critical point correspond to a point of enhanced memory capacity with the emergence of (a) gapless degree(s) of freedom.

As an alternative viewpoint and to ensure the correctness of the c-number method we can also consider the full Bogoliubov transformation. This allows us to obtain the full quantum spectrum in the limit $N \to \infty$. To reiterate the necessary steps, we first have to replace the annihilation (and creation) operators $\hat{a}_1^{(\dagger)} \to \sqrt{N - \hat{a}_2^\dagger \hat{a}_2 - \hat{a}_3^\dagger \hat{a}_3}$ in the full Hamiltonian (2.50) to ensure that we only consider fluctuations that respect particle number conservation in agreement with the full quantum system. After that we expand the Hamiltonian up to second order around the macroscopic background defined

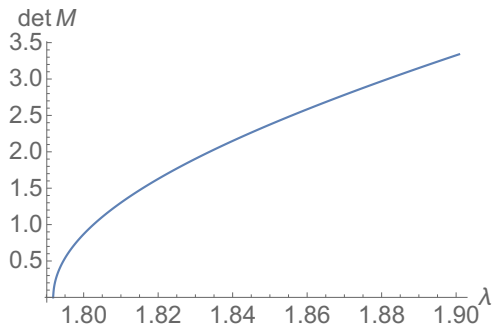

(a) Determinant of the second derivative (A.2) of the Bogoliubov Hamiltonian.

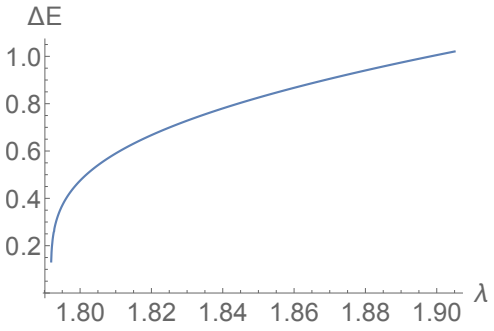

(b) Smallest excitation energy of the second-order quantum Hamiltonian (A.5), obtained after Bogoliubov transforming it.

Figure 2.4: Excitation energy as a function of λ for $N \to \infty$ derived in two different methods. In both cases, we observe a gapless excitation at $\lambda_{lm} \approx 1.792$. Stable excitations only exist for $\lambda \geq \lambda_{lm}$. As is clear from the Hamiltonian (2.47), the energy unit is $\frac{4\pi^2\hbar^2}{2mL^2}$.

by the Bogoliubov approximation (2.51). However, this has been done in the Bogoliubov approximation which is strictly speaking only exact in the limit of infinite N. It remains therefore our task to show that this mode also exists in the full quantum theory with finite total occupation number. We display the result in appendix A in equations (A.4) and (A.5). As before, we subsequently look for pairs (x, θ) where the first derivative (A.4) vanishes and stable fluctuations exist. In accordance with the previous analysis we obtain the same values as above. To calculate the Bogoliubov transformation to diagonalize the corresponding Hamiltonian explicitly we have to rely on numerical methods. Here we shall apply the method described in [57], [67]. From this so diagonalized matrix the energy gaps of the corresponding Bogoliubov modes can be readily read out. The smallest energy eigenvalue as a function of the coupling strengthλ is shown in Fig. 2.4b. This fully matched the previous result obtained by the c-number method displayed in Fig. 2.4a. Thus, this analysis confirms that a gapless mode still exists at λ_{lm} in the limit $N \to \infty$. For finite N, however, we expect deviations to the gaplessness as well as the exact value of λ_{lm} that scale as powers of $1/N$.

Note that this critical state around which an (approximate) gapless mode emerges is not the ground but an excited state. Nevertheless, the present analysis indicated that this point is stable and therefore a viable candidate for efficient quantum information storage. One way to see that is the fact that the energy gaps of all modes are positive and large in the relevant regime $\lambda \geq \lambda_{lm}$, excluding, of course, the flat direction we shall use for information storage. This point is also confirmed by the fact that we did not observe any instabilities in the numerical simulations which we shall discuss later on.

To conclude this paragraph we want to note that to actually write or read out any information this system has to be coupled to an external environment. Such a coupling could destabilize the system in an experimental setting. However, this interaction has to be very small to not disturb the gaplessness in the first place. For a detailed discussion we refer to section 2.4.4. Since this already severely restricts the coupling to external modes

we expect that this is enough to ensure the stability of the critical state. This has to be studied, of course, in a case by case basis for potential experimental realization.

Slow Mode in Full Spectrum

Until now the analysis was based on the Bogoliubov approximation which is only exact in the limit $N \to \infty$. For any finite N we expect corrections that scale with powers of $1/N$. In the following we shall therefore confirm the existence of an approximately gapless mode in the spectrum of the full quantum system in case of a finite number of particles. To this end, we shall use a very general fact, namely that modes with a small energy gap ΔE evolve on the long timescale $\hbar/\Delta E$. In this light we expect a significantly slowed down time evolution for a state close to a critical point. We shall use the appearance of an enlarged timescale as an indicator for gapless modes around a certain state. Note that in case of the periodic system it was explicitly shown that the evolution significantly slows down at the critical point [10]. As already discussed, this memory modes with extremely small gaps also have an experimental signature in form of absorption lines of very low frequency. [2]

The decoherence time of a state also determines how long a state can store information. This is an important property for the use of states of enhanced memory capacity as actual storage of information. As discussed in the beginning of this chapter we chose occupation numbers as an encoding scheme for information. Of course, the specific choice of code is of no physical importance. Therefore we assume that we can experimentally prepare a state in such a way that we can choose its components in a certain basis. If we do a measurement of the state before it has evolved significantly due to the large timescales, we can directly read out the components again and therefore the stored information. However, if the system has already evolved significantly the information gets scrambled and distributed over a large amount of degrees of freedom. A retrieval of information is then only possible with a precise knowledge of the dynamics of the system to reconstruct the spreading of the information. Roughly speaking the timescale of evolution therefore determines a decoherence time. It is the time after which the subset of nearly-gapless modes has been decohered by the rest of the system.

The next step now is to determine the precise quantum state corresponding to the critical configuration. Note that up until now we have only determined macroscopic parameters, namely the collective coupling as well as the relative distribution of particles among the three modes. Therefore we still have to decide on a procedure to associate a quantum state to the specific critical configuration. We then shall verify that this state is indeed connected to a gapless mode by time evolving it. A long timescale (in some measure which we will determine below) would then indicate a gapless mode. This quantum state should in case of $\lambda = \lambda_{lm}$ correspond to a stationary inflection point of the Bogoliubov Hamiltonian. Additionally, we require that we extend this construction also for different values of λ to facilitate comparison and the distinction between states of

[2] As a side remark we want to mention that it is not sufficient to search for eigenstates in the quantum spectrum with nearly the same energy gap. The reason is for example apparent in Fig. 2.3e. Though both groundstates are degenerate in energy the transition is suppressed by a huge barrier. As it was disused above there are no gapless modes associated with such a configuration.

enhanced memory capacity and ordinary states. In the following we shall construct such a quantum state which exists for all $\lambda \gtrsim 1$ and becomes stationary at the critical value $\lambda = \lambda_{lm}$.

Our approach to determine the quantum state $|\Phi_{\text{inf}}\rangle$ is defining a subspace of states close to the inflection point and then selecting the state of minimal energy among them. One requirement is that this subspace should not be too big in order to be sensitive to properties of the stationary inflection point at critical configuration. However, this subset cannot to be small to facilitate the minimization procedure. If the subspace does not contain enough basis states than the energy obtained for these states is too high. Of course this procedure is not unique. However, we shall see that it suffices for our purpose. We note that we expect that many different quantum states exists corresponding to different occupation numbers of the light mode.

Concrete Procedure

In the following we shall outline our concrete procedure. We shall impose two conditions which originate from properties of the inflection point. Firstly, we only consider states for which the expectation value of the relative occupation of the 2-mode matches its critical value $n_2(t)/N = x_{inf}(\lambda)$. Beside that we restrict the set of basis states which we use to form the quantum state $|\Phi_{\text{inf}}\rangle$. We only use those states which do not deviate too much from the critical occupation values. Concretely, we choose an upper bound δn_i on the deviation from the critical value determined from the Bogoliubov Hamiltonian. Assuming additionally that modes with bigger relative occupation should have a bigger spread, we empirically determine $\delta n_1 = 0.4$, $\delta n_2 = 0.375$ and $\delta n_3 = 0.225$ to be a good choice.[3]

After we successfully determined a set of states $|\Phi_{\text{inf}}\rangle$ for different values of the collective coupling we simulate its time evolution numerically on a computer. Here we use the full quantum Hamiltonian with the complete basis of the Hilbert space. We show the expectation value of $n_2(t)$ for a total particle number $N = 60$ for exemplary values of λ in Fig. 2.5. Clearly, a drastic slowdown given by drastically lower frequencies dominate around $\lambda = \lambda_{lm}$.

As a next step we shall quantify this slow down behavior. This will also allow us to estimate the coherence time as a function of λ. For this purpose we extract a typical frequency from the time evolution of $|\Phi_{\text{inf}}\rangle$ by considering its Fourier components. In the discrete Fourier decomposition we only consider frequency up to $n_{\max}$. Thus we obtain so the Fourier coefficients $c_1, c_2, \ldots, c_{n_{\max}}$ corresponding to frequencies $f_1, 2f_1, \ldots, n_{\max} f_1$. Next, we define the mean frequency in the time evolution by

$$\bar{f} := f_1 \frac{\sum_{i=1}^{n_{\max}} i|c_i|^2}{\sum_{i=1}^{n_{\max}} |c_i|^2} \,. \tag{2.56}$$

This timescale associated to the mean frequency can be interpreted as a measure for the

[3] We verified this procedure by comparing the results obtained in this truncation with the ones derived using the full basis in case of small particle numbers where the computation is feasible. For $N \leq 50$, we observed that their qualitative behavior, is identical whereas this no longer seems to be the case for higher N. However, the only important point for us is to come up with some recipe to find the slowly evolving states corresponding to states of enhanced memory capacity.

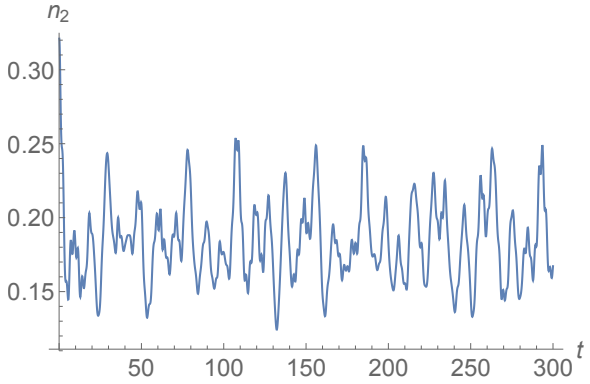

(a) $\lambda = 1.9$

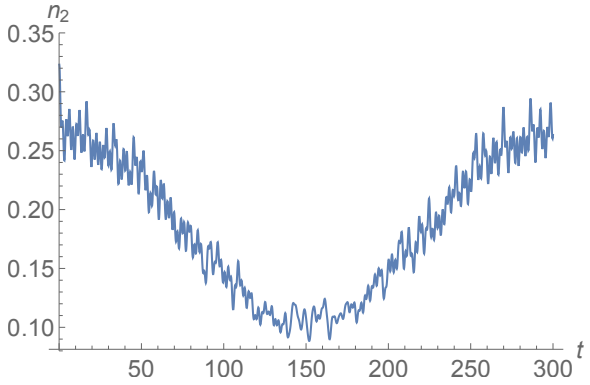

(b) $\lambda = 2.083$

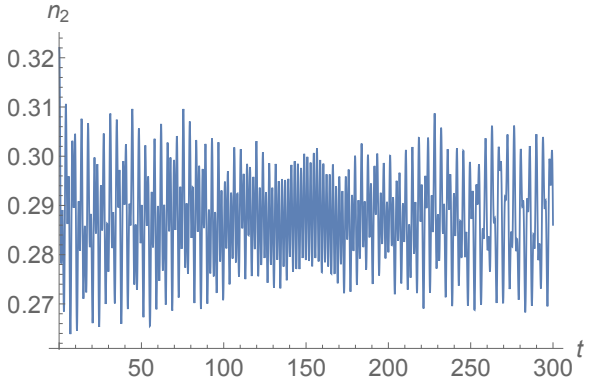

(c) $\lambda = 2.2$

Figure 2.5: Time evolution of the quantum state $|\Phi_{\text{inf}}\rangle$, which corresponds to the inflection point of the Bogoliubov Hamiltonian. The expectation value $n_2(t)$ is plotted for a total particle number of $N = 60$. We observe that lower frequencies dominate around $\lambda \approx 2.083$.

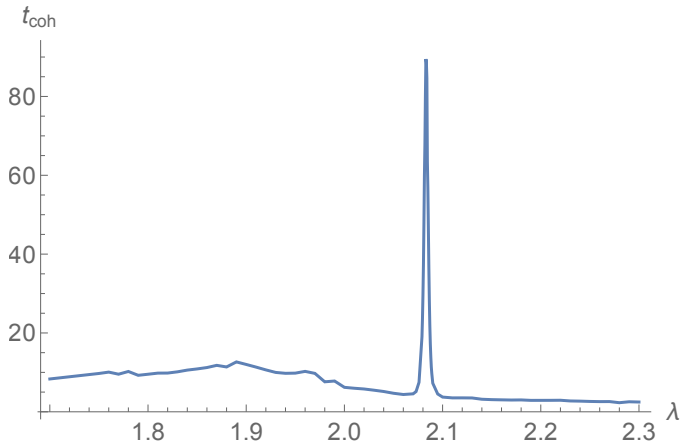

Figure 2.6: Estimate of the decoherence time t_{coh} associated to $|\Phi_{\text{inf}}\rangle$ as a function of λ for a total particle number $N = 60$. We observe that it increases distinctly around the critical value $\lambda \approx 2.083$.

decoherence time. This is the timescale after which the subset of nearly-gapless modes has been decohered by the rest of the quantum modes. In this sense, we get:

$$t_{\text{coh}} = \frac{1}{\bar{f}}\,. \tag{2.57}$$

For the specific choices $f_1 = 1/3000$ and $n_{\max} = 12000$, we show t_{coh} as a function of λ in Fig. 2.6.[4] We observe that the timescale of evolution increases distinctly around the specific value $\lambda \approx 2.083$. This deviation from the critical value $\lambda_{lm} = 1.792$ is expected due to a finite N. As we have discussed previously our reasoning is only exact in the limit $N \to \infty$. We therefore expect deviation from that in our concrete realization with $N = 60$ that scale with $1/N$. In contrast, note that we do not expect t_{coh} to diverge for infinite N because $|\Phi_{\text{inf}}\rangle$ generally contains an admixture of non-gapless modes. Let us quantize these finite N effects:

$$\lambda_{lm}^{(N)} = \lambda_{lm} + a \cdot N^{-b}, \tag{2.58}$$

where $a > 0$ and $b > 0$ are two undetermined fitting parameters. To determine those we repeat this analysis for different particle numbers $40 \leq N \leq 90$. We then again determine the critical value corresponding to the lowest mean frequency $\lambda_{lm}^{(N)}$ and fit to those values the function (2.58). This procedure yields $a = 3.56$ and $b = 0.61$. We note that b is close to $2/3$, which was the result in the periodic system [62]. As can be clearly seen from Fig. 2.7, the numerically determined values $\lambda_{lm}^{(N)}$ are well described by the fitted function (2.58). All these results are a clear indication that the slow evolution we observe in the real time plots is due to emergence of gapless modes near a critical configuration. This

[4]Note that different choices of f_1 and $n_{\max}$ lead to the same result. Therefore, cutting off low and high frequencies to make the considered parameter space finite, which is required in a numerical treatment, has no influence on our findings.

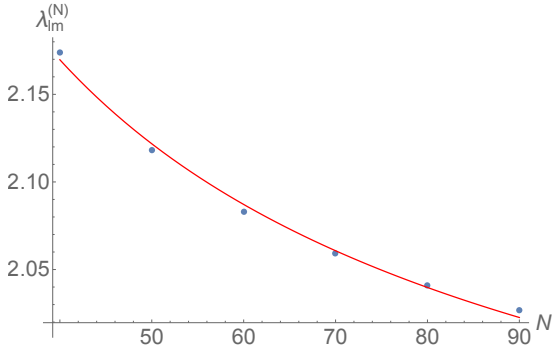

Figure 2.7: Critical value $\lambda_{lm}^{(N)}$ as a function of particle number N. The positions obtained from numerical simulations are plotted in blue. The fitted function (2.58) is shown in red.

fits our prediction with the c-number method in the Bogoliubov treatment. Concluding, we observe the appearance of a nearly-gapless mode around $\lambda = \lambda_{lm}$ for finite values of N as well.

We shall conclude this section by discussing the specific critical state $|\Phi_{\text{inf}}\rangle$ for $N = 60$ and $\lambda = 2.083$ in position space. This might be particularly interesting for a experimental realization of this configuration. The particle density is given by

$$\rho(z) \equiv \langle\Phi_{\text{inf}}|\,|\hat{\psi}|^2\,|\Phi_{\text{inf}}\rangle = \frac{1}{\pi}\sum_{k,l=1}^{3}\langle\Phi_{\text{inf}}|\,\hat{a}_k^\dagger\hat{a}_l\,|\Phi_{\text{inf}}\rangle\,\sin\left(\frac{kz}{2}\right)\sin\left(\frac{lz}{2}\right)\,. \tag{2.59}$$

We plot this so defined particle density for the critical state $|\Phi_{\text{inf}}\rangle$ in Fig. 2.8. Additionally, we illustrate the gapless mode by varying the occupation numbers in the flat direction. For this purpose we fix the value of $\lambda = 2.083$, but slightly vary the value of x used in the minimization procedure that determines the quantum state: $x_i = x_{\text{inf}}(\lambda) + \delta x_i$. We obtain a family of states $|\Phi_{\text{inf, i}}\rangle$, where $|\Phi_{\text{inf, i}}\rangle$ is a state of minimal energy subject to the constraint that its relative occupation of the 2-mode is x_i. The density profiles for these small deviations are also shown in Fig. 2.8.

2.2.4 Encoding Information via Coupling to an External Field

Next we shall discuss another important aspect of using systems of enhanced memory capacity for the storage of quantum information and their realization and probing in a lab environment. We therefore shall discuss how the nearly-gapless mode emerging at the critical value λ_{lm} of the collective coupling can be probed by an external field. For simplicity, we work with the nearly-gapless collective Bogoliubov modes. From the above analysis it is clear that this can always be achieved at a critical point with the help of a Bogoliubov transformation.

We shall denote this Bogoliubov or memory mode again with $\hat{a}$ and its gap with ϵ. Near the critical configuration it is possible to neglect the effect of modes with higher gaps, as long as the energy of the external mode is sufficiently small to not excite them.

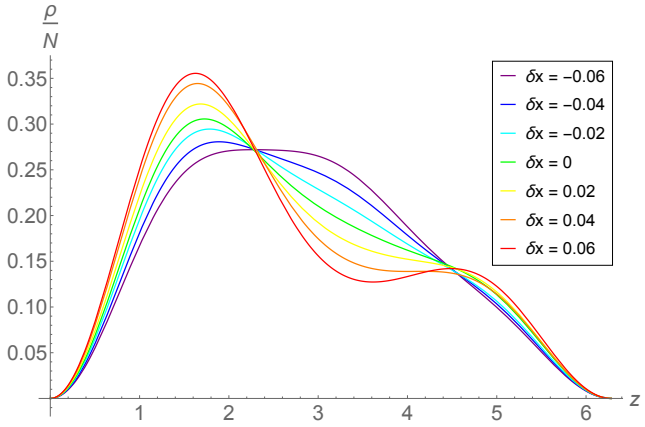

Figure 2.8: Position space representation of the critical state with small variations for $\lambda = 2.083$ and $N = 60$. The relative particle density ρ/N is plotted. The green line corresponds to the critical state $|\Phi_{\text{inf}}\rangle$ itself and the adjacent lines are variations of it, which we obtained by slightly changing the value of x used in the minimization procedure that determines the quantum state: $x_i = x_{\text{inf}}(\lambda) + \delta x_i$. The values of δx_i are indicated in the plot.

Following the discussion in [15], the essential features of the coupling to an external field $\hat{c}$ can already be captured by the simple Hamiltonian

$$\hat{H}_{\text{eff}} = \epsilon \hat{a}^\dagger \hat{a} + \epsilon_\gamma \hat{c}^\dagger \hat{c} + \frac{g}{2}\left(\hat{a}\hat{c}^\dagger + \hat{a}^\dagger \hat{c}\right) , \tag{2.60}$$

where we denote the energy gap of the external mode $\hat{c}$ with ϵ_γ. The index γ indicates that this would most likely correspond to a photon in an experimental setup. Furthermore the parameter g describes the strength of the coupling between the external mode and the memory mode. The structure of this particular Hamiltonian is motivated by following reason. In the expansion of the Hamiltonian around the critical macroscopic background, the coupling in (2.60) is expected to be the leading order term in the interaction term $\hat{a}^\dagger \hat{a}(\hat{c} + \hat{c}^\dagger)$ of the original $\hat{a}$-modes. These interaction conserves total particle number and total momentum. Note that due to its bilinear structure the Hamiltonian can be cast in matrix form again.

As an example let us consider with an initial state, in which the memory mode is empty and the external field is given by a coherent state:

$$|\Phi(t=0)\rangle = |0\rangle_a \otimes |\gamma\rangle_c , \tag{2.61}$$

where γ parameterizes the occupation of the external coherent state. Straightforward calculation gives [15]:

$$\langle \Phi(t)| \hat{c}^\dagger \hat{c} |\Phi(t)\rangle = \gamma^2 \left(1 - \frac{g^2}{\delta_g^2} \sin^2\left(\frac{\delta_g t}{2}\right)\right) , \tag{2.62}$$

where we defined

$$\delta_g = \sqrt{(\epsilon_\gamma - \epsilon)^2 + g^2} . \tag{2.63}$$

It becomes apparent that the interaction between those two subsystems leads to a fluctuation in the occupation number of the external field. To facilitate oscillations between both modes we choose $\epsilon_\gamma \approx \epsilon$. This implies that the coupling has to be small ($g \lessapprox \epsilon$) in order to not disturb the gaplessness of the mode $\hat{a}$ which will be discussed in further detail in section 2.4.4. The time evolution of the expectation value of the occupation numbers of memory modes are given by

$$\langle \Phi(t)| \hat{a}^\dagger \hat{a} |\Phi(t)\rangle = \gamma^2 \frac{g^2}{\delta_g^2} \sin^2\left(\frac{\delta_g t}{2}\right) . \tag{2.64}$$

Therefore we can write any specific memory pattern in the Bogoliubov modes by using soft excitations of an external field. Naturally, this can also used the other way around such that information stored in the $\hat{a}$ modes can be released by emitting soft $\hat{c}$ quanta. Note that equations (2.62) and (2.64) also show why soft external radiation is sensitive to the critical point. It is clear that far away from the critical configuration the lightest mode has a much larger gap such that $\epsilon \gg \epsilon_\gamma$. Consequently, the amplitude of fluctuations gets suppressed as g/ϵ. In other words, due to the large level splitting there is no efficient transfer of occupation possible between the two subsystems. Therefore, soft radiation stops interaction with the system. Thus, a critical point exists, whenever soft radiation, whose energy ϵ_γ is much smaller than the typical energy of the system, i.e., $\epsilon_\gamma \ll \hbar^2/(2mL^2)$, interacts significantly with the particles in the Bose gas. We see therefore that gaplessness is not for free. The energy efficiency of the information storage within the gapless memory mode goes hand in hand with the difficulty of the read-out of the stored quantum information. Because the respective gaps in the memory sector are extremely small, different memory patterns are not easily distinguishable. This results in a long read-out time. This is extremely important in a possible practical application of assisted gaplessness for the storage of quantum information, since the same constraints would apply there as well. Since a system can not be a good storage as well as a read-out device, the best way would be to incorporate a time-dependent interaction term. Since a concrete implementation of the ideas mentioned above reaches beyond our field of expertise, this issue will not be discussed any further within the scopes of this work. Concluding this section we want to also comment on the stability of such critical configuration as it was described above. We saw that such states are typically not identified with a ground state but an excitation above it. However, excited states do not necessarily exhibit an instability in form of a Lyapunov exponent. This can be seen for example in the analysis leading to plot 2.4b. In the limit of large N we have already demonsrated that in the relevant regime $\lambda \geq \lambda_{lm}$ all the gaps are positive and only one becomes zero at criticality. Moreover, we see no signs of any decay in the full numerical analysis of the system, which again confirms the absence of any instability. Correspondingly, we conclude that in the closed system described by the Hamiltonian (2.50) the critical configuration around which a gapless degree of freedom emerges is stable. Of course, the system can be destabilized by coupling it to an external environment just strongly enough. However, in this case we would lose gaplessness and with it the sole reason we have been interested in this system to begin with. We expect that the weakness of the external influence also ensures a sufficient stability of the critical state, although the matter has to be studied on a case by case basis for potential experimental setups.

2.3 States of Enhanced Memory Capacity as Attractors

States of enhanced memory capacity, critical configuration at which gapless modes emerge are a generic feature of weakly and attractively interacting systems with high occupation numbers. In the last section we introduced a robust method of identifying such states in the spectrum. With the c-number methods we are able to determine critical configurations at which gapless degrees of freedom emerge. In case there is not just a single mode, but an abundance of gapless degrees of freedom emerging, these critical points act as attractor states of dynamical evolution.

However, such states are not only interesting from the perspective of condensed matter theory but also have important implications for high energy physics. As an alternative approach to Wilsonian-UV completion the idea of *classicalization* [68]–[70] has been put forward. Its idea is readily described: Instead of exciting new degrees of freedom in the ultra violet, increasingly classical resonances denoted as classicalons are produced. In this sense the theory is self-complete since no new degrees of freedom appear, but already existing low energy degrees of freedom are getting succeedingly excited. An important theory in which *classicalization* might be realized is gravity [68].

2.3.1 Connection to Gravity and Classicalization

Classically, gravity is modeled as the geometry of spacetime. However, an alternative many-body point of view was put forward in [9] which interprets black holes as condensate at the critical point of a quantum phase transition. Shifting the focus on its well-known quantum informational properties it becomes apparent that every quantum mechanical description of a black hole must account for its Bekenstein-Hawking entropy [7]. Consequently, any microscopic description of a black hole must deliver a sufficient number of microstates to be compatible with the Bekenstein-Hawking entropy. As we argued previously this can be accomplished by an adequate number of gapless modes. Therefore, black holes represent a prime example of states of enhanced memory capacity in gravity. By studying such states in non-gravitational systems, which allow for an easier analytic and experimental study, one can therefore try to draw conclusions about the quantum mechanical properties of black holes. Another example sharing a similar abundance in microstate entropy is de Sitter spacetime. In fact also de Sitter with its Gibbons-Hawking entropy [20] saturates the Bekenstein's bound [71] similar to black holes. The transition process to states of enhanced memory capacity is of special interest in case of black holes since this would correspond to a formation process. In high energy particle physics such a formation can be modeled by an $2 \to N$ scattering process, where N represent some large macroscopic number. A detailed computation of this scattering amplitude can be found in [72]. Usually, such processes with a transition to quasi-classical microstates are exponentially suppressed [73]. To overcome this suppression the transition probability has to be sufficiently enhanced due to a high degeneracy of microstates in the final state. Therefore classicalons (or black hole formation in gravity) must be states of enhanced memory capacity. Transitions to states accompanied with a high degeneracy

of microstates is therefore also motivated by applying those findings to the viability of classicalization. Possible applications of classicalization, however, also go beyond gravity. Another classicalizing theory might be found in a Standard Model with a derivative self-coupling of the Higgs. For an easily accessible review on classicalization and references we refer to [39].

2.3.2 The Model

Again we will use *assisted gaplessness* to build a model which exhibits states with an enhanced number of degenerate microstates. We therefore start again with Hamiltonian (2.5). To allow for actual dynamics to move towards or away from the critical configuration we add an additional mode to the system which we denote with $\hat{b}$ and which also fulfills the bosonic commutation relations (2.1). Its number operator is given by $\hat{m} \equiv \hat{b}^\dagger \hat{b}$. This supplementary modes acts as a reservoir which allows for a varying occupation number of the *master mode* $\hat{a}_0$. Before we also introduce interaction of $\hat{a}_0$ and $\hat{b}$ to allow for particle transfer between those modes we shall first focus on the energetics. Let us start with following Hamiltonian

$$\hat{H}_{\text{diag}} = \hat{m}_0 + \hat{n}_0 + \sum_{k=1}^{K} (2 - \alpha\, \hat{n}_0)\, \hat{n}_k \,. \tag{2.65}$$

As will become apparent soon, the non-zero gap of $\hat{b}_0$ is the reason why we replaced $(1 - \alpha\, \hat{n}_0)$ by $(2 - \alpha\, \hat{n}_0)$. Note that only energy differences are physical.

Similar to Eq. (2.6) and assuming the *master mode* to be highly occupied the effective gap of the memory modes are given by

$$\mathcal{E}_k = 2 - \alpha n_0 \,. \tag{2.66}$$

If the occupation of the master mode is zero or low such that $\alpha N_0 \ll 1$ the effective gap is $\mathcal{E}_k \approx 2$. In this case the energy gap between an excitation of a reservoir mode or a memory mode is $\Delta E = 1$ and any transition is energetically strongly suppressed. However, if the *master mode* attains its critical occupation, i.e. $\alpha n_0 = 1$, the effective gap of the memory mode reduces to $\mathcal{E}_k = 1$. This renders the energy difference between $\hat{b}$ mode and the $\hat{a}_k$ modes effectively gapless. In other words, the reservoir and the memory modes can exchange occupation without energy cost. This statement becomes explicit in the Bogoliubov approximation after using $\langle \hat{m}_0 \rangle = N - n_0 - \sum_{k=1}^{K} \langle \hat{n}_k \rangle$, where N is the total particle number in the system and K denotes the number of memory modes in the system:

$$\langle \hat{H} \rangle = N + \sum_{k=1}^{Q} (1 - \alpha n_0) \langle \hat{n}_k \rangle + \mathcal{O}\left(1/n_0\right) \,. \tag{2.67}$$

For the critical occupation $\alpha n_0 = 1$ the expectation value of the energy becomes independent of the occupation of the critical modes. Therefore, we obtain energetically-degenerate microstates whose number is in accordance with Eq. 2.9 given by

$$\mathcal{N}_{\text{cr}} = (d+1)^K \,, \tag{2.68}$$

where d is again the capacity or maximal occupation of each memory mode. Note that the counting Eq. (2.68) assumes that the total particle number of the system is actually high enough to populate all these states, i.e. $N \geq dK + 1/\alpha$. In case of the total particle number N being not sufficient, Eq. (2.68) has to be modified.

Therefore, the system described by the Hamiltonian (2.65) features a critical configuration accompanied by an enhancement of microstate entropy due to the mechanism of *assisted gaplessness*. Next, we shall discuss whether this state is actually dynamically realized in the presence of a reservoir that can potentially source such configuration. So the only missing ingredient is the addition of an interaction term that allows for a transfer of particles between the different modes. We choose following interaction terms

$$\hat{H}_{\text{int}} = \sum_{k=0}^{K} g_k \left(\hat{b}^\dagger \hat{a}_k + \hat{a}_k^\dagger \hat{b} \right) . \tag{2.69}$$

with interaction strength g_k. We impose the following two conditions on the values of the coupling parameters. First, the interaction term should not disturb our energy considerations made above since gaplessness and the resulting enhanced memory state space is the main reason for this study. Since it is bounded as $\langle \hat{b}^\dagger \hat{a}_k \rangle \lesssim g_k N$ in the approximation of large particle numbers, we therefore impose

$$g_k N \ll 1 . \tag{2.70}$$

Secondly, since we want all energetically degenerate microstates, whose number is given by (2.68), are accessible. To ensure this the reservoir has to contain enough particle so the full memory sector of the Hilbert space can actually be explored. Furthermore, we need to ensure that no symmetry renders part of the critical Hilbert space unreachable. In case two or more couplings are identical, e.g. if $g_{k_1} = g_{k_2}$, the operator $\hat{Q} = (\hat{a}_1^\dagger - \hat{a}_2^\dagger)(\hat{a}_1 - \hat{a}_2)$ represents a conserved charge, i.e. the occupation numbers of $\hat{a}_{k_1}$ and $\hat{a}_{k_2}$ are no longer independent. To prevent this all couplings g_k must be sufficiently different to ensure that each memory mode remains distinct. We can satisfy both conditions by choosing[5]

$$g_k = \frac{1}{N^{3/2}} \frac{1}{\sqrt{k+1}} . \tag{2.71}$$

In summary, we obtain the following Hamiltonian:

$$\hat{H} = \hat{m} + \hat{n}_0 + \sum_{k=1}^{K} (2 - \alpha \hat{n}_0) \hat{n}_k + \sum_{k=0}^{K} g_k \left(\hat{b}^\dagger \hat{a}_k + \hat{a}_k^\dagger \hat{b} \right) . \tag{2.72}$$

The free parameters of this model are the number of memory modes K, the maximal distinct occupation states of each memory mode d, the coupling strength α as well as the total particle number N.

[5]This scaling is motivated by the results of [62], where it was shown for a specific system that the energy gap at the critical point scales as $\epsilon_k \sim n_0^{-1/3}$. The choice of g_k should be such that the energy due to the interaction term is smaller than the gap of the critical modes.

2.3.3 Time Evolution

Next we compute the time evolution of this system numerically. The numerical error on the norm of the time evolved state is bounded by 10^{-7}. For the numerical methods and details on the simulation see appendix B and [6].

As an initial state we choose an "empty" state in the sense that all particles of the system are in the reservoir mode $\hat{b}$ and the other modes are empty.

$$|\Psi(t=0)\rangle = |N, 0; 0, ..., 0\rangle \ . \tag{2.73}$$

Moreover, we choose $d = 1$, i.e., the critical modes are qubits and can be either in the state $|0\rangle$ or $|1\rangle$. The motivation of this choice is twofold. First, it facilitates numerical simulations by reducing the size of the Hilbert space. On the other hand it also has a physical effect, since it modifies the ratio of critical vs. non-critical Hilbert space in dependence on the available total particle number. We shall discuss the latter point in more detail below.

Of primary interest will be the effect of the presence of the (gapless) memory modes $\hat{a}_k$. More specifically, we shall study the effect of the existence of a large subspace in the Hilbert space sourced by a large degeneracy of microstates around the critical configuration $\alpha N_0 = 1$ on the dynamics of the system. To this end, we time evolve the state (2.73) for systems with different amount of memory modes K. We simulate the time evolution of the system (2.72) until $t_{\max} = 3000$. For the coupling strength we set $\alpha = 1/6$ and the total particle number $N = 15$. The time dependence of the expectation value of the number operators $\hat{n}_0$ and $\hat{m}$ for exemplary values of K are shown in Fig. 2.9. In the absence of the memory modes (see Fig. 2.9a) the Hamiltonian (2.72) reduces to a two-mode system and can be solved analytically. This analytic solution will become of importance later on in section 2.4. Here we only have to observe that the system simply exchanges particles between the reservoir and the master mode, where the occupations oscillate periodically around the mean $N/2$ with maximal amplitude. The maximal amplitude is facilitated by equal free energy gaps of quanta of the master mode and the reservoir.

However, adding memory modes to the system changes this picture dramatically (see Fig. 2.9b and 2.9c). After a short transition period which can be interpreted as thermalization, the system settles to a stationary regime that differs from the above behavior in two key aspects. First, the mean occupation of the master mode becomes critical ($n_0 = 1/\alpha$) already for relatively small values of K. Secondly, the temporal variance of its occupation number diminishes significantly and the expectation value remains close to its critical value for later times. In this sense, the system is *attracted* towards the critical occupation of the master mode. Therefore, states of enhanced memory capacity become attractors of dynamical evolution. This effect is enhanced by increasing the number of memory modes (see again Fig. 2.9b and 2.9c). However, Fig. 2.9d makes evident that this effect does not continue indefinitely and starts to diminish above a certain value of K. In order to quantify this behavior, we compute for different numbers of memory modes K the temporal mean $\overline{n}_0$ and the temporal variance δn_0^2 of the occupation number of the master mode:

$$\overline{n}_0 = \frac{1}{n}\sum_{j=1}^{n} n_0(t_{\text{cut}} + j\Delta t)\,, \quad \delta n_0^2 = \frac{1}{n-1}\sum_{j=1}^{n}\left(n_0(t_{\text{cut}} + j\Delta t) - \overline{n}_0\right)^2\,, \tag{2.74}$$

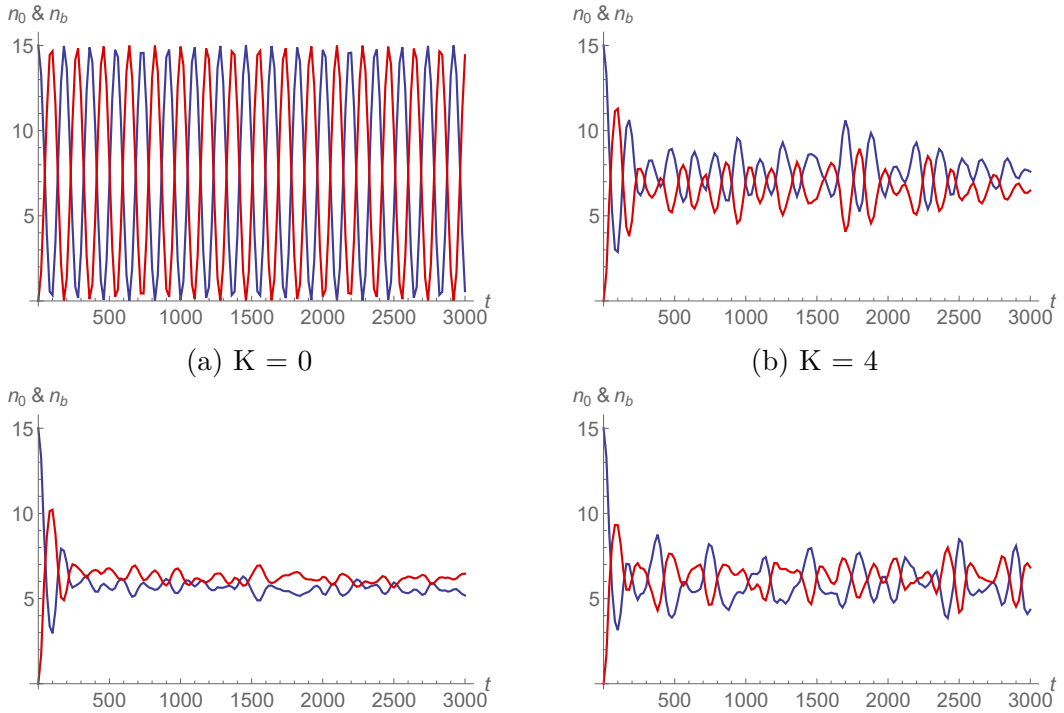

(a) K = 0 (b) K = 4

(c) K = 8 (d) K = 14

Figure 2.9: Real time evolution of the expectation value of the occupation numbers of the master mode $\hat{a}_0$ (red) and the reservoir mode $\hat{b}$ (blue) under the Hamiltonian (2.72) for $N = 15$, $1/\alpha = 6$ and $d = 1$ for various number of memory modes K. Towards $K = 8$, we observe that the mean occupation of the master mode assumes the critical value $n_0 = 1/\alpha$ and that the temporal variance becomes distinctly smaller. A systematic analysis of this behavior can be found in Fig. 2.10.

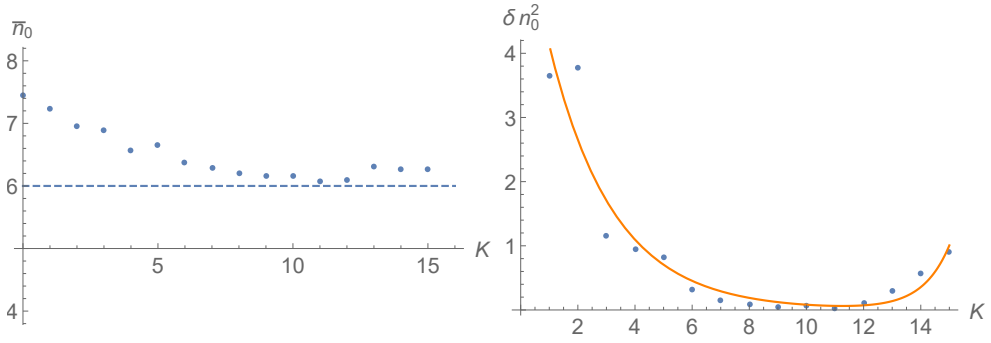

(a) Means (b) Variances

Figure 2.10: Temporal mean and variance (defined in (2.74)) of the occupation number of the master mode $\hat{a}_0$ as a function of the number of memory modes K. We set $N = 15$, $1/\alpha = 6$ and $d = 1$. The means are observed to be closest to the expected value $1/\alpha = 6$ (dashed line) in the range of $8 \lesssim K \lesssim 12$. Likewise, the variance is minimal for $8 \lesssim K \lesssim 12$, which includes $K_* = N - 1/\alpha = 9$, the maximal number of qubits for which the critical Hilbert space is still entirely accessible. The fitted function (2.75) is displayed in orange. The value $\delta n_0^2(K = 0) = 28.2$ is not shown in the plot and also excluded from the fit.

where j labels the taken samples after time step Δt. The number of sampling steps is given by $n = (t_{\max} - t_{\text{cut}})/\Delta t$. To be insensitive to the early thermalization non-stationary regime shortly after $t = 0$ we exclude early times before t_{cut}. In the following we set $\Delta t = 20$ which is sufficient since all relevant frequencies are smaller than $1/20$. Furthermore we chose $t_{\text{cut}} = 500$. In Fig. 2.10 we show the result of this analysis.

In the absence of memory modes the mean value of the occupation number of the master mode is $N/2 = 7.5$. Starting to add $\hat{a}_k$ modes to the system brings this value closer to the critical one $1/\alpha = 6$. For $K \gtrsim 6$ it assumes the critical value up to small deviations that we expect due to corrections to the Bogoliubov approximation that scale as $1/n_0$. Moreover, we observe that the memory modes are not getting highly occupied i.e., the total occupation number in the memory sector is less than 3. In terms of the variance, we see that it naturally assumes its maximal value for $K = 0$ and then decreases significantly for increasing values of $K > 0$. The minimal value of the variance is observed in the range $8 \lesssim K \lesssim 12$ and then increases again for $K > 12$. This result is expected since $K_* = N - 1/\alpha = 9$ is a special value: It is the maximal number of qubits for which the reservoir mode still has enough particles to explore the complete critical Hilbert space, i.e., where N is large enough for all of the critical modes to be occupied while the *master mode* attains its critical value $n_0 = 1/\alpha$ at the same time. These findings suggest an intuitive interpretation. Enlarging the memory pattern space increases the attraction towards the critical point as long as the particle number is big enough to explore the full Hilbert space. Therefore, the temporal variance only decreases if there are enough particles to maintain the critical occupation $n_0 = 1/\alpha$ and in principle simultaneously explore the complete memory space. However, as soon as Hilbert space is added that cannot be fully explored, the effect is reversed. Additional Hilbert space that can not be effectively explored corresponds to

uncritical Hilbert space, i.e. states that are not accessible at the critical point $n_0 = 1/\alpha$. Consequently, the addition of uncritical Hilbert space decreases the attraction towards the critical point and therefore increases the amplitude. In summary, the addition of accessible critical Hilbert space increases criticality whereas non-critical Hilbert space decreases it.

In order to quantify the attractiveness of the critical configuration in this interpretation, we fit the empirically determined variances by a function of the form

$$f\left(\mathcal{N}_{\mathrm{cr}}, \mathcal{N}_{\mathrm{tot}}\right) = A\,\mathcal{N}_{\mathrm{cr}}^{-\tilde{\alpha}} + B\,\mathcal{N}_{\mathrm{tot}}^{\tilde{\beta}}\,, \tag{2.75}$$

where $\mathcal{N}_{\mathrm{tot}}$ is the total size of the Hilbert space and $\mathcal{N}_{\mathrm{cr}}$ is the size of the *accessible* critical Hilbert space. The size of the critical Hilbert space is

$$\mathcal{N}_{\mathrm{cr}} = (d+1)^K \tag{2.76}$$

for $K \leq K_*$, i.e. in the case where the total particle number is sufficient to explore the complete memory space while simultaneously maintaining criticality. However if the particle number is insufficient, i.e. $K > K_*$, $\mathcal{N}_{\mathrm{cr}}$ is smaller and in case of qubits, i.e. $d = 1$, given by

$$\mathcal{N}_{cr}\left(\alpha, N, K\right) = \sum_{n_a=0}^{N-1/\tilde{\alpha}} \binom{K}{n_a}\,, \tag{2.77}$$

where the summation variable n_a is the number of particles that is occupying the memory modes $\hat{a}_k$. In contrast to that the size of the complete Hilbert space $\mathcal{N}_{\mathrm{tot}}$ is given by

$$\mathcal{N}_{tot}\left(N, K\right) = \sum_{j=0}^{N} \sum_{n_a=0}^{j} \binom{K}{n_a}\,. \tag{2.78}$$

Applying the fit function (2.75) to the data in range $1 \leq Q \leq 15$ yields the following values for the parameters[6]: $A = 6.4$, $B = 6.9 \cdot 10^{-10}$, $\tilde{\alpha} = 0.64$ and $\tilde{\beta} = 1.7$. As is evident from Fig. 2.10, the simple function f describes the result well. However, we are not sure if a fit of the form (2.75) is successful in general.

We have concluded that criticality is maximized when K is increased to the maximal value K_* for which the number of particles N still suffices to simultaneously maintain the critical occupation of the *master mode* and all memory modes modes, i.e.,

$$N_* = K_* + 1/\alpha\,. \tag{2.79}$$

This is the minimal value of the total occupation number for which the full critical Hilbert space is still accessible and fully count to the microstate entropy. To isolate the strength of the attraction to a state of enhanced memory capacity from the technicality of a sufficiently large particle reservoir we now study the system in which we increase N and K simultaneously such that Eq. (2.79) is always satisfied. We choose $t_{\mathrm{cut}} = 1500$ for this

[6]Note we restrict ourselves to the range $4 \leq K \leq 15$ since we expect our considerations only to hold if the critical Hilbert space is large enough. For transparency reasons we note that the quality of the fit increases distinctly by excluding smaller values of K.

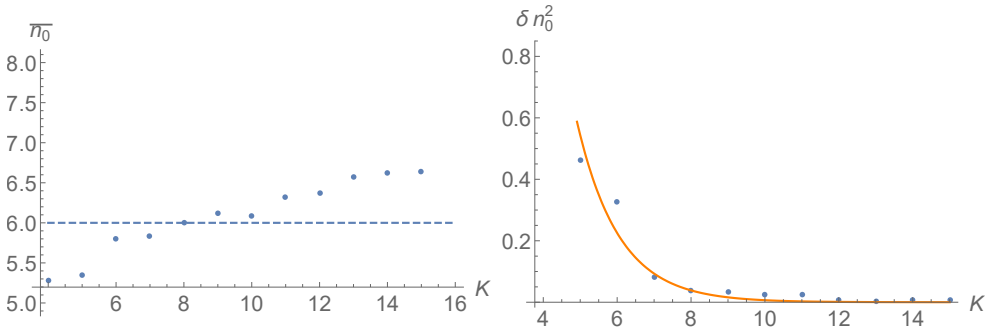

(a) Means (b) Variances

Figure 2.11: Temporal mean and variance (defined in (2.74)) of the occupation number of the master mode $\hat{a}_0$ for the system (2.72) with $1/\alpha = 6$ and $d = 1$ when N and K are varied simultaneously while satisfying $N = K + 1/\alpha$. The means can be observed to be close to the expected value $1/\alpha = 6$ (dashed line) throughout. The variance decreases monotonically. The fitted function (2.80) is displayed in orange. The values for $K \leq 4$ are not shown in the plot and are also excluded from the fit.

analysis. The corresponding results for coupling strength $\alpha = 1/6$ and $d = 1$ are shown in Fig. 2.11.

As expected, we now observe a monotonic increase of the pull to the critical configuration in the sense that the temporal variance decreases as the critical Hilbert space is enlarged. As before, we can try to make this statement quantitative by fitting the function

$$f\left(\mathcal{N}_{\mathrm{cr}}\right) = A\,\mathcal{N}_{\mathrm{cr}}^{-\tilde{\alpha}}\,, \tag{2.80}$$

where we only kept the critical part of the Hilbert space since, we provide a large enough reservoir. This is in accordance with the observation that there is no regime in which the amplitude increases again. Excluding again smaller $K < 4$ and fitting in the range $4 \leq K \leq 20$ yields $A = 13.7$ and $\tilde{\alpha} = 0.96$. We conclude that the simple function (2.80) describes the result well.

We remark that both functions (2.75) and (2.80) describe an exponential dependence of the temporal variance on the number K of memory modes. This observation commensurate with the notion of classicalization. As we have reviewed previously two to many particle scattering amplitudes are exponentially suppressed. However, classicalizing theories overcome this suppression with the help of an exponential enhancement due to a large microstate degeneracy in the final state. Although the amplitude of oscillations and the transition amplitude are different physical quantities, it is conceivable that an exponential suppression of the former is connected to an exponential enhancement of the latter.

In conclusion, we have seen that the system will inevitably move towards this state assuming the critical configuration is physically accessible.

2.4 Memory Burden

Next we shall discus a very generic feature of systems that exhibit a configuration with a sharp enhancement of memory capacity. The universal phenomenon of *memory burden*, which was first introduced in [74], is the result of the collective backreaction of the stored quantum formation in the gapless memory modes to the overall evolution of the system, resisting any deviation from the critical configuration.

2.4.1 General Mechanism

In the last section we discussed how the *master mode* assisted the *memory modes* in becoming gapless. In this section we shall reverse this picture and study how occupation in the $\hat{a}_k$ modes back reacts to the evolution to $\hat{a}_0$. To illustrate this we shall consider first a simple prototype system which we will use as a baseline. Similar to section 2.3 we shall first consider a system consisting of two modes, $\hat{a}_0$ which initial (macroscopically) occupation is N. Additionally, we introduce another mode $\hat{b}_0$ with a number operator $\hat{m}_0 \equiv \hat{b}_0^\dagger \hat{b}_0$ and energy gap ϵ_0. For simplicity and without affecting our point we shall assume the occupation of the $\hat{b}_0$ mode to be initially empty. To facilitate the oscillation between them we set both gaps equal. To allow for transition between those two modes we also introduce a coupling with strength C_0. The Hamiltonian and initial state for this simple 2-mode system is given by

$$\hat{H} = \epsilon_0 \hat{m}_0 + \epsilon_0 \hat{n}_0 + C_0(\hat{a}_0^\dagger \hat{b}_0 + \hat{b}_0^\dagger \hat{a}_0) \tag{2.81}$$

and

$$|\text{in}_1\rangle = |\underbrace{N_c}_{n_0}, \underbrace{0}_{m_0}\rangle\,, \tag{2.82}$$

respectively. This theory can easily be solved analytically and the system performs free oscillations with full amplitude N on a timescale set by the inverse coupling constant. The evolution is described by

$$n_0(t) = N(1 - \sin^2(C_0 t)). \tag{2.83}$$

This solution is illustrated in Fig. 2.12.

Next we shall study how the presence of memory modes can result in a deviation from this. Note, that we will be mostly interested in a setting where $\hat{a}_0$ is macroscopically occupied, roughly speaking, constituting the classical features of the system and an abundance of entropy carrying memory modes where each one only has very low occupation numbers. In other words, we shall study how those quantum mechanically behaving memory degrees of freedom influence the classical evolution (in the mean-field limit).

Therefore, we reintroduce the memory sector and using again assisted gaplessness, similar to Hamiltonian (2.5), add the aforementioned $\hat{b}_0$ to it with the corresponding coupling term:

$$\hat{H} = \epsilon_0 \hat{n}_0 + \epsilon_0 \hat{m}_0 + \left(1 - \frac{\hat{n}_0}{N_c}\right) \sum_{k=1}^{K} \epsilon_k \hat{n}_k + C_0(\hat{a}_0^\dagger \hat{b}_0 + \hat{b}_0^\dagger \hat{a}_0) \tag{2.84}$$

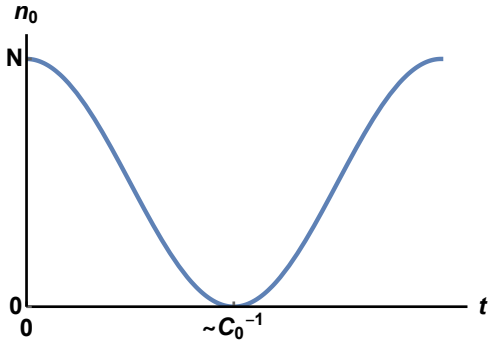

Figure 2.12: Time evolution of Hamiltonian (2.81) (without memory burden).

First note that this system satisfies particle number conservation or equivalently global $U(1)$-symmetries. All $\hat{n}_k$ individually and $\hat{n}_0 + \hat{m}_0$ commute with the Hamilton operator $\hat{H}$ and are therefore conserved in time. So in this system the occupation of each memory mode as well as the sum of $\hat{a}_0$ and $\hat{b}_0$ stay constant for all times.

We shall start with the simplest case. If the memory sector is empty, i.e. all $n_k = 0\,, \forall k$ the system reduces to Hamiltonian (2.81) and the time evolution remains unaltered and is described by plot Fig. 2.12. So let us consider the case with an initial state of the form

$$|\mathrm{in}_2\rangle = |\underbrace{N_c}_{n_0}, \underbrace{0}_{m_0}, n_1, \ldots, n_K\rangle\,, \tag{2.85}$$

with $n_k \neq 0$ for some or all k. It is evident that Fig. 2.12 can no longer depict the evolution accurately. Since the system is in the critical configuration $n_0 = N_c$ the *memory modes* are gapless and regardless of the exact values of the various n_k values all states of the form in Eq. (2.85) are degenerate in energy. However, as soon as $n_0 = \langle \hat{n}_0 \rangle$ moves away from the critical value the $\hat{a}_k$ would reacquire a huge gap. Therefore, due to energy conservation, any deviation from the initial critical state is highly suppressed whenever there is a high load of information in the form of occupation in the *memory sector*. This is the essence of the memory burden phenomenon. In the following we shall quantify this behavior.

Since the *memory burden* μ is intrinsically linked to energy conservation and the change of the effective gaps (2.6) of the *memory modes* we define the *memory burden* [2]

$$\mu \equiv \sum_{k=1}^{K} n_k \frac{\partial \mathcal{E}_k}{\partial n_0} \tag{2.86}$$

as a measure for the backreaction of the stored quantum information. It quantifies the unactualized energy cost of the memory pattern in case the occupation of $\hat{a}_0$ actually changing. For the particular example of (2.84) the *memory burden* is given by

$$\mu = -\sum_{k=1}^{K} \epsilon_k \frac{n_k}{N_c} \tag{2.87}$$

Since the memory sector is not dynamically active, it is still possible to solve the system analytically. The time dependence of the expectation value of $\hat{n}_0$ as a function of

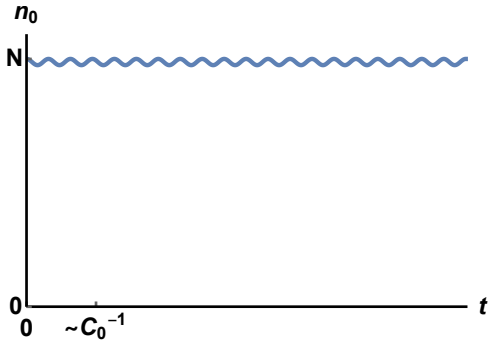

Figure 2.13: Time evolution of Hamiltonian (2.88) (with memory burden).

the coupling strength C_0 and *memory burden* μ is given by [74]

$$n_0(t) = N\left(1 - \frac{4C_0^2}{4C_0^2+\mu^2}\sin^2\left(\sqrt{C_0^2+\frac{\mu^2}{4}}t\right)\right). \tag{2.88}$$

Depending on the value of μ the time evolution of n_0 can drastically differ. For small burden $|\mu| \ll C_0$ the solution (2.88) reduces again to (2.83). However, as soon as either the memory load is high enough of their free gaps ϵ_k are sufficiently big, follows $\frac{C_0}{\mu} \ll 1$. In that case the original relative amplitude $\frac{C_0^2}{C_0^2+\mu^2}$ gets suppressed to $\frac{C_0^2}{\mu^2}$. This is illustrated in Fig. 2.13 for exemplary values of the parameters. Thus, the stored quantum information ties n_0 to its initial and critical value. In other words, the system is stabilized around its point of enhanced memory capacity. This is the essence of memory burden.

2.4.2 Alleviating Memory Burden

It is evident from Fig. 2.13 that memory burden can drastically affect the evolution of a system of enhanced memory capacity. The universality of this phenomenon suggests that every such system should be stabilized in its critical configuration and prevented from decaying or being altered in general. In light of this drastic impact it's natural to ask if memory burden can avoided or at least alleviated to some extent.

Inspecting Eq. (2.86), the two important characteristics of memory burden are the occupation numbers n_k in the memory sector and the dependence of their effective gaps $\mathcal{E}_k$ on n_0. So on first glance reducing occupation numbers by offloading it to other degrees of freedom seems like a valid possibility to reduce the burden of memory. However, as we shall see shortly, this option is severely restricted. To illustrate this point we shall consider the following Hamiltonian

$$\hat{H} = \epsilon_0\hat{n}_0 + \epsilon_0\hat{m}_0 + \sum_{k=1}^{K}\epsilon_k\hat{m}_k + \left(1-\frac{\hat{n}_0}{N_c}\right)\sum_{k=1}^{K}\epsilon_k\hat{n}_k + C_0\sum_{k=0}^{K}(\hat{a}_k^\dagger\hat{b}_k + \hat{b}_k^\dagger\hat{a}_k), \tag{2.89}$$

where we introduced $\hat{b}_k$ as the "free" counterparts of $\hat{a}_k$ modes that are not subjected to mechanism of assisted gaplessness. Their corresponding number operators are give by

$\hat{m}_k \equiv \hat{b}_k^\dagger \hat{b}_k$. For the sake of simplicity, we further couple $\hat{a}_k$ and $\hat{b}_k$ with the same coupling constant[7] C_0 as $\hat{a}_0$ and $\hat{b}_0$. Limiting ourselves to initial times, so we can assume n_0 to be constant, the solution can be obtained equivalently to (2.84) and the expectation value of $\hat{n}_k$ is given by

$$n_k(t) \simeq n_k(0)\left(1 - \frac{4C_0^2}{\epsilon_k^2}\sin^2\left(\frac{\epsilon_k}{4}t\right)\right), \tag{2.90}$$

with $n_k(0)$ being the initial occupation in the k^{th}-memory mode. Here, we additionally assumed $C_0 \ll \epsilon_k$. To ensure that gaplessness of the $\hat{a}_k$ is not disturbed too much we shall restrict ourselves to the case of small couplings. This will be discussed in more detail in section 2.4.4. Similar to Eq. (2.88) the amplitude of oscillation is suppressed by $\left(\frac{C_0}{\epsilon_k}\right)^2$. So similar to the memory burden effect for $\hat{a_0}$ no efficient deviation from the initial occupation is possible. We will come back to this when we apply those findings to gravity in sections 3.1 and 3.2.

In all previous examples we have limited ourselves to systems in which total particle number is conserved. Furthermore, the sum of the occupation in the 0-sector,i.e. $n_0 + m_0$, and in the memory sector,i.e. $\sum_k n_k + \sum_k m_k$ are conserved separately as well. One may wonder if this assumption is too restrictive and memory burden can be alleviated more easily in case of number non-conserving interaction. This, however, is not the case. Broadly speaking, an efficient offloading of the information is again not possible due to the relatively large level splitting. Explicit calculations for the case of number non-conserving interactions can be found in the appendix 2.4.10.

As offloading occupation numbers from the *memory sector* to *external* degrees of freedom is not an efficient process to alleviate *memory burden*, another approach would be to modify the effective gap dependence on the *master mode*. In our prototype example the effective gaps depend linearly on n_0 (see Eq. (2.6)), thus resulting in a relatively steep effective potential. In other words, a slight deviation from the critical occupation $n_0 = N_c$ quickly re-induces the large gap of the *memory modes*. However, depending on the physical system, this effective potential may be more shallow and the dependence may be non-linear. As a simple extension we shall consider a polynomial dependence and take the following Hamiltonian

$$\hat{H} = \epsilon_0 \hat{n}_0 + \epsilon_0 \hat{m}_0 + \left(1 - \frac{\hat{n}_0}{N_c}\right)^p \sum_{k=1}^{K} \epsilon_k \hat{n}_k + C_0(\hat{a}_0^\dagger \hat{b}_0 + \hat{b}_0^\dagger \hat{a}_0) \tag{2.91}$$

where the only difference to Hamiltonian (2.84) is the newly introduced power p of the pre-factor in front of the energy gaps of the *memory modes*. This effectively makes memory burden a higher order process. In this model the effective gaps (2.6) and the *memory burden* (2.86) are

$$\tilde{\mathcal{E}}_k = \left(1 - \frac{n_0}{N_c}\right)^p, \qquad \tilde{\mu} = p\left(\frac{N_c - n_0}{N_c}\right)^{p-1}\mu, \tag{2.92}$$

[7]Note that couplings to the memory modes are severely restricted themselves to not disturb their gaplessness. This is discussed in more detail in section 2.4.4

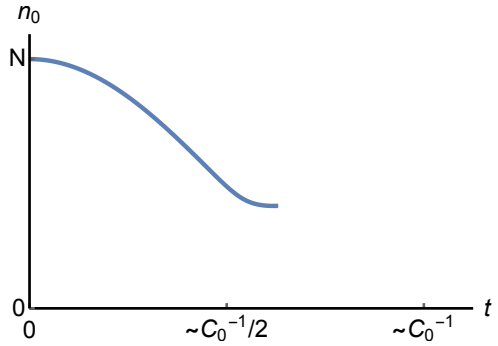

Figure 2.14: Time evolution of Hamiltonian (2.88) (with delayed memory burden).

where we expressed the memory burden in terms of Eq. (2.87). In comparison with the original model (2.87) the memory burden gets suppressed by powers of $((N_c - n_0)/N_c)$. The effective potential is therefore more shallow and slight deviation from the critical occupation results in a slower increase of the effective memory gaps. The larger p is, the more the backreaction gets delayed. However, in this setup it is not possible to avoid memory burden forever. At the critical value $\tilde{\mu} \sim C_0$ backreactions originating from the quantum information set in and memory burden becomes important for the evolution. At this critical value we calculate an upper bound on the deviation from criticality $N_c - n_0$, above which the beack reaction from memory burden cannot be ignored:

$$N_c - n_0 = N_c \left(\frac{C_0}{p|\mu|} \right)^{1/(p-1)} . \tag{2.93}$$

For $\mu > C_0$, it is clear that the backreaction can no longer be avoided, as soon as the deviation from criticality if of order of N_c. At this point the system stabilizes. This behavior is illustrated for specific values of the parameters in Fig. 2.14. At the beginning n_0 follows its free oscillatory evolution, but as soon as memory burden sets in around half-life time, the system gets stabilized.

2.4.3 Avoiding Memory Burden by Rewriting

Since altering the interaction can only delay memory burden until order half decay at the best, the only option remaining is to actually get rid of the occupation altogether. However, as it was discussed at the beginning of this section, a huge level splitting prevents any efficient particle transfer. Consequently, only degrees of freedom with a similar low gap can be efficient occupation number acceptors. As it was already introduced in [74], *assisted gaplessness* can be used to introduce a second memory sector. This second set of memory degrees of freedom, which are not occupied in the beginning, are constructed such that their effective gap vanishes for a smaller value of $n_0 = N_c - \Delta N_c$. So whenever n_0 has lost $\Delta N_c > 0$ particles, the first memory sector will reacquire a gap, whereas this new second sector becomes gapless. We shall introduce this using again an explicit model. The creation and annihilation operators of this second memory sector shall be denoted by $\hat{a}'^{\dagger}_{k'}$ and $a'_{k'}$ respectively. They satisfy the usual commutation relations (2.1).

Their number operator is defined by $\hat{n}'_{k'} \equiv \hat{a}'^{\dagger}_{k'}\hat{a}'_{k'}$ and their free energy gap is given by $\epsilon_{k'}$. The index k' runs from 1 to K'. This can be modeled by the following terms in the Hamiltonian:

$$\hat{H} = \left(1 - \frac{\hat{n}_0}{N_c}\right)\sum_{k=1}^{K}\epsilon_k\hat{n}_k + \left(1 - \frac{\hat{n}_0}{N_c - \Delta N_c}\right)\sum_{k'=1}^{K'}\epsilon_{k'}\hat{n}'_{k'} + \ldots \tag{2.94}$$

where we reverted back to $p = 1$. In this model, a new set of memory modes $\hat{a}'_{k'}$, becomes gapless after n_0 has lost ΔN_c particles. At the same time, the old ones $\hat{a}_k$ acquire nonzero gaps given by $\mathcal{E}_k = \epsilon_k(N_c - \Delta N_c)/N_c$. To facilitate actual transfer of occupation numbers from the first to the second sector we shall consider the following 2-point interaction terms:

$$\hat{H} = \sum_{k=1}^{K}\sum_{k'=1}^{K'} C_{k,k'}(\hat{a}^{\dagger}_k\hat{a}'_{k'} + \text{H.c.}) + \ldots \tag{2.95}$$

with $C_{k,k'}$ a coupling constant. Note that with this type of interaction the total particle number in both sectors combined

$$N_m \equiv \sum_{k=1}^{K} n_k + \sum_{k'=1}^{K'} n'_{k'}, \tag{2.96}$$

is conserved. With all necessary components now introduced we can combine them into a full prototype model:

$$\begin{aligned}
\hat{H} &= \epsilon_0\hat{n}_0 + \epsilon_0\hat{m}_0 + C_0(\hat{a}^{\dagger}_0\hat{b}_0 + \hat{b}^{\dagger}_0\hat{a}_0) && (2.97)\\
&+ \left(1 - \frac{\hat{n}_0}{N_c}\right)\sum_{k=1}^{K}\epsilon_k\hat{n}_k + \left(1 - \frac{\hat{n}_0}{N_c - \Delta N_c}\right)\sum_{k'=1}^{K'}\epsilon_{k'}\hat{n}'_{k'} && (2.98)\\
&+ \sum_{k=1}^{K}\sum_{k'=1}^{K'} C_{k,k'}(\hat{a}^{\dagger}_k\hat{a}'_{k'} + \text{H.c.}) && (2.99)\\
&+ \sum_{k=1}^{K}\sum_{l=1}^{K}\tilde{C}_{k,l}(\hat{a}^{\dagger}_k\hat{a}_l + \text{H.c.}) + \sum_{k'=1}^{K'}\sum_{l'=1}^{K'}\tilde{C}_{k',l'}(\hat{a}'^{\dagger}_{k'}\hat{a}'_{l'} + \text{H.c.}) && (2.100)
\end{aligned}$$

where we additionally introduced intra-sector coupling constants $\tilde{C}_{k,l}$ and $\tilde{C}_{k',l'}$ within each of the two sets of memory modes for the sake of generality. A system described by Hamiltonian (2.97) has two special sets of states. Similar to (2.5), the first set is given by states of the form

$$|\underbrace{N_c}_{n_0}, \underbrace{0}_{m_0}, n_1, \ldots, n_k, \underbrace{0}_{n'_1}, \ldots, \underbrace{0}_{n'_{k'}}\rangle \tag{2.101}$$

in which the *master mode* occupation is such that the first *memory sector* is gapless. As previously explained, all states in (2.101) are degenerate in energy regardless of the exact value of n_k. In addition to that this model features a second set of states characterized by

$$|\underbrace{N_c - \Delta N_c}_{n_0}, \underbrace{\Delta N_c}_{m_0}, \underbrace{0}_{n_1}, \ldots, \underbrace{0}_{n_k}, n'_1, \ldots, n'_{k'}\rangle\,. \tag{2.102}$$

In these states $n_0 = N_c - \Delta N_c$ applies, such that the second sector is gapless, while the first develops a gap. As long as the first sector is empty, those states have the same energy regardless of the specific values of $n'_{k'}$. Note that we further require the initial effective gap of the second memory sector to be greater than the elementary gap of the system

$$|\mathcal{E}'_k| \gg \epsilon_0. \tag{2.103}$$

This serves us to ensure that the $\hat{a}'_{k'}$ modes are not gapless to begin with, since we would have then added them to the $\hat{a}_k$ modes. However, for the following results it is already enough to require the following weaker constraint to hold:

$$|\mathcal{E}'_k| \gg \frac{\epsilon_0}{\sqrt{N_m}}. \tag{2.104}$$

With this it is energetically possible for the system to avoid the memory burden effect during decay by offloading the information from the $\hat{a}_k$ modes to the $\hat{a}'_{k'}$ ones. To be more specific, the system can avoid the backreaction by its memory load by evolving from the initial state (2.101) into the second critical configuration (2.102) under the constraint (2.96) that total particle number in the memory sectors is conserved. However, the absence of energetic restrictions is no guarantee that this transition actually takes place dynamically. Studying this question will be the subject of the next section.

2.4.4 Bounds on Couplings

Before we discuss the actual time evolution we shall investigate another important point. Usually, interactions will offset the gaps of the free theory. Since we introduced couplings to the memory modes within a sector and also to an additional second set of degrees of freedom, these interactions will result in a disturbance of the small gaps. Since approximate gaplessness is the sole reason we are interested in these systems to begin with, we have to make sure that these couplings are small enough to maintain this feature. In other words, we require that the effective mean gap $\mathcal{E}_{\text{eff}}$ stays close to zero also in the presence of interaction. For the sake of the mildest possible bound we assume that interactions between different memory modes contain both attractive, as well as repulsive couplings. In this case distributing N_m particles among the critical memory sector can be interpreted as a 1-d random walk and typically only results in an energy disturbance of $\sqrt{N_m}\mathcal{E}_k$. Imposing that this disturbance is smaller than the elementary gap of the system ϵ_0, we obtain the constraint

$$\mathcal{E}_{\text{eff}} \lesssim \frac{\epsilon_0}{\sqrt{N_m}}. \tag{2.105}$$

Note that dropping the assumptions of equally distributed plus and minus sign contributions to the energy results in the stronger constraint $\mathcal{E}_{\text{eff}} \lesssim \frac{\epsilon_0}{N_m}$. In the following, however, we shall assume that at least the weaker bound (2.105) is satisfied. We shall consider the inter- and intracouplings as distinct cases. We start with the interaction within one memory sector $\tilde{C}_{k,l}$. We assume that all intra-sector coupling are of the same order. For simplicity we start with a two mode system. The Hamiltonian can then be written as a 2×2-matrix:

$$\begin{pmatrix} 0 & \tilde{C}_{k,l} \\ \tilde{C}_{k,l} & 0 \end{pmatrix}, \tag{2.106}$$

where we suppressed the operators for better readability. Since we consider modes within one sector, their gaps on the diagonal should both be zero. Demanding that these gaps are disturbed by at most $\epsilon_0/\sqrt{N_m}$ in the presence of interaction, i.e. $\tilde{C}_{1,2} \neq 0$, implies

$$\tilde{C}_{1,2} \lesssim \frac{\epsilon_0}{\sqrt{N_m}}. \tag{2.107}$$

To generalize this result to more than two modes we can use Wigner's semicircle law. Interpreting the coupling matrices (2.106) as samples of independent and identically distributed random variables with zero mean and unit variance, their generalization to many modes belongs to a Wigner Hermitian matrix ensemble. In this situation, Wigner's semicircle law states that the spectral distribution converges and, in particular, it becomes independent of the dimension K, if the entries of the matrix are rescaled by $1/\sqrt{K}$. For proof and details we refer to other works, e.g. [75]. It is therefore sufficient to suppress the off-diagonal entries of the coupling matrix (2.106) with the appropriate factor

$$\tilde{C}_{k,l} \lesssim \frac{\epsilon_0}{\sqrt{N_m}\sqrt{K}}. \tag{2.108}$$

This ensures approximate gaplessness for the majority of modes even in the presence of interaction. An alternative route to calculate the bounds on the couplings has been shown in [73]. The expectation values of the off-diagonal elements in (2.106) scale as $N_m\tilde{C}_{k,l}$. Note that we also assumed here that couplings with positive and negative signs are equally likely, so that the N_m^2 nonzero entries result in a contribution on the order $\sqrt{N_m^2} = N_m$. Again, demanding that those contributions are smaller than ϵ_0 requires

$$\tilde{C}_{k,l} \lesssim \frac{\epsilon_0}{N_m}. \tag{2.109}$$

In case the total occupation is of the same order as the number of modes ($N_m \sim K$) this bound is identical to the constraint (2.108).

The inter-sector coupling can be treated similarly with the crucial difference that the gaps for different sectors are not the same. Assuming again that all couplings $C_{k,k'}$ are of the same order, we can write the Hamiltonian as

$$\begin{pmatrix} 0 & C_{k,k'} \\ C_{k,k'} & \epsilon_k \Delta N_c/N_c \end{pmatrix}. \tag{2.110}$$

We estimate $\mathcal{E}_{\text{eff}} \sim KC_{k,k'}^2 N/(\epsilon_k \Delta N_c)$. With that we can estimate the bounds on the couplings between different sectors

$$C_{k,k'} \lesssim \frac{\sqrt{\epsilon_0 \epsilon_k \Delta N_c}}{\sqrt{KN_c}(N_m)^{1/4}}, \tag{2.111}$$

which is milder than the bounds (2.108), since $\epsilon_k \geq \epsilon_0$.

2.4.5 Numerical Time Evolution

As we discussed in section (2.4.1) the only viable option to avoid memory burden is to offload the information in the critical sector to another set of degrees of freedom which becomes succeedingly more gapless when the master modes lose constituents. Although this process is energetically allowed, it is a priori not clear that this happens dynamically. Unfortunately, the dynamical system described by Hamiltonian (2.97) is not analytically solvable. Therefore, we shall employ numerical methods to study this system. To simulate this system on a computer we have to specialize to a particular realization, meaning we have to choose specific values for the parameters of the model. In light of the applications of these models to gravity in section 3 we shall apply a few simplifications in accordance with these systems to reduce the parameter space. First, we set the free gaps of all memory modes in both sectors to be equal, $\epsilon_m \equiv \epsilon_k = \epsilon_{k'}$. Additionally, we assume that the couplings between sectors $C_{k,k'}$ and couplings within a sector $\tilde{C}_{k,l}$ are of the same order. This allows us to extract a common factor and write the couplings in the form $C_m f_i(k,k')$, where C_m is a common factor to all couplings and $f_i(k,l)$ takes values of order one and different for every pair of indices k and l. The ladder point is important to break the exchange symmetry $\hat{a}_k \leftrightarrow \hat{a}_l$. Otherwise both modes describe the same degree of freedom and could have been removed from the beginning. In the following we choose $|f_i(k,l)| \in [0.5;1]$. Their exact value is of no importance to our analysis and could in principle be picked randomly. However, for the sake of consistency and ensure that they have different values for distinct pairs (k,l), we use the following procedure to assign them values

$$f_i(k,l) = \begin{cases} F_i(k,l) - 1 & \text{for} \quad F_i < 0.5 \\ F_i(k,l) & \text{for} \quad F_i \geq 0.5 \end{cases} \tag{2.112}$$

where $F_i(k,l) = \left(\sqrt{2}(k+\Delta k_i)^3 + \sqrt{7}(l+\Delta l_i)^5\right) \mod 1$. Moreover, we set $\Delta k_1 = \Delta k_2 = 1$, $\Delta k_3 = K+1$, $\Delta l_1 = \Delta l_3 = K+1$ as well as $\Delta l_2 = 1$. Note that this system still conserves (2.96). Also the total occupation in the master mode $\hat{a}_0$ and its free counter part $\hat{b}_0$ remains constant during evolution. Therefore also $\epsilon_0(\hat{n}_0 + \hat{m}_0)$ corresponds to a conserved quantity. Since as initial state we only consider eigenstates of this operator, it only leads to a trivial global phase and we can omit it. In turn, we will use ϵ_0 as a basic energy unit. We arrive at the Hamiltonian

$$\begin{aligned} \frac{\hat{H}}{\epsilon_0} = & \frac{\epsilon_m}{\epsilon_0}\left(1 - \frac{\hat{n}_0}{N_c}\right)\sum_{k=1}^{K}\hat{n}_k + \frac{C_0}{\epsilon_0}\left(\hat{a}_0^\dagger \hat{b}_0 + \hat{b}_0^\dagger \hat{a}_0\right) \\ & + \frac{\epsilon_m}{\epsilon_0}\left(1 - \frac{\hat{n}_0}{N_c - \Delta N}\right)\sum_{k'=1}^{K'}\hat{n}'_{k'} + \frac{C_{\mathrm{m}}}{\epsilon_0}\Bigg\{\sum_{k=1}^{K}\sum_{k'=1}^{K'} f_1(k,k')\left(\hat{a}_k^\dagger \hat{a}'_{k'} + \mathrm{h.c.}\right) \\ & + \sum_{k=1}^{K}\sum_{\substack{l=1 \\ l\neq k}}^{K} f_2(k,l)\left(\hat{a}_k^\dagger \hat{a}_l + \mathrm{h.c.}\right) + \sum_{k'=1}^{K'}\sum_{\substack{l'=1 \\ l'\neq k'}}^{K'} f_3(k',l')\left(\hat{a}_{k'}^{'\dagger} \hat{a}'_{l'} + \mathrm{h.c.}\right)\Bigg\}, \end{aligned} \tag{2.113}$$

where we set $\epsilon_0 = 1$ from here on.

To end up with a finite dimensional Hilbertspace to facilitate numerical computations we truncate the maximal occupation of each memory mode to one. Every $\hat{a}_k$ then repre-

sents a qubit. In general we shall consider initial states such that the first memory sector $\hat{a}_k$ is critical and N_m of these modes are occupied. The reservoir mode $\hat{b}_0$ as well as the second memory sector will start empty. Correspondingly, an initial state is of the form

$$|\text{in}\rangle = |N_c, 0, \underbrace{1, \ldots, 1}_{N_m}, 0, \ldots, 0\rangle \,, \tag{2.114}$$

where we set the occupation number of the first N_m modes in the first memory sector to 1. In the following we shall study how the behavior changes by varying the parameters of the Hamiltonian (2.113). As a baseline we shall choose the following values

$$\epsilon_m = \sqrt{20}\,, \quad N_c = 20\,, \quad \Delta N = 12\,, \quad K = K' = 4\,, \quad C_0 = 0.01\,, \quad N_m = 2\,. \tag{2.115}$$

Note that the Hilbert space grows exponentially in the number of included modes as it is evident from the microstate entropy consideration (2.9). This severely limits the values of K and K' that can be simulated efficiently on a computer. In this study the highest number of memory modes in the initial sector considered is $K = 8$. Choosing parameters according to (2.115), the only free choice remaining is the overall coupling strength C_m. This parameter will be of major interest in the following.

2.4.6 Possibility of Rewriting

To compute the time evolution we use a software package based on a Krylov subspace method. This package allows us to compute expectation values as a function of time with a rigorous upper bound on the numerical error, i.e. the norm of the difference between the exact time-evolved state and its numerical approximation. This bound is set to 10^{-6}, with exception for the large $K = 8$ system, for which we use 10^{-5} to increase the feasibility of simulating large numbers of sample systems. For details on the numeric and specific implementation we refer to the appendix B or [6]. In this section we consider the system (2.97) with parameters given by (2.115) and with an initial state of the form (2.114). The time evolution of the expectation value of $\hat{n}_0$ and $\sum_k \hat{n}_k$ for different values of the coupling strength C_m is plotted in Fig. 2.15. In case of no interaction between the two memory sectors, i.e. $C_m = 0$, the system simplifies by replacing $\sum_{k=1}^{K} \hat{n}_k \to N_m$ and $\sum_{k'=1}^{K'} \hat{n}'_{k'} \to 0$. The system then has the analytic solution (2.88). This is illustrated in Fig. 2.15a. We observe that the critical sector is frozen and the amplitude of the oscillation of the *master mode* is strongly suppressed due to the *memory burden* effect introduced in section 2.4.1.

This behavior also continues for many non-zero values of the coupling as can be seen for an exemplary value in Fig. 2.15b. Although the time evolution of the system becomes more involved and can no longer be described by the simple solution (2.88), the value of n_0 is basically still tied to its initial value and the critical sectors remain effectively frozen.

There are, however, certain values of the coupling for which the behavior of the systems changes significantly. For those specific and fine-tuned values the amplitude of the oscillation between $\hat{a}_0$ and $\hat{b}_0$ increases distinctly, albeit on a significantly longer timescale compared to the free oscillation without burden. This is illustrated in Fig. 2.15c and 2.15d for two specific example values. As previously described this oscillation of the master mode is facilitated by offloading occupation from the first memory sector to the second

one. We observe that this diminishing of the memory burden by rewriting the information from $\hat{a}_k$ to $\hat{a}'_{k'}$ modes can happen either via an instantaneous jump [as in Fig. 2.15c] or via synchronized oscillations [as in Fig. 2.15d]. Although the exact mechanism behind the two different behaviors is not clear at this point, both are in line with our statement that n_0 can only change significantly, if the memory burden is reduced by offloading information from the memory sector to other degrees of freedom. Also note that the transition from state (2.101) to (2.102) is by no means complete. This can be understood by considering the following aspects. For one, the transition is still suppressed, which we will take a closer look at in section 2.4.9. Secondly, the state-space volume in the Hilbert space of superpositions of classes (2.101) and (2.102) is much higher than the number of states of the individual sets. Roughly speaking, similar to the reasoning in section 2.3, the number of states consisting of a superposition of states in which either the first or the second sector is critical outnumbers obviously the number of states in a single sector individually. We expect that complete rewriting into the second set of memory modes can be facilitated by adding further sectors, to which the $\hat{a}'_{k'}$ modes can transfer information.

In the following we shall refer to values of the overall coupling C_m for which partial rewriting is talking place as *rewriting values*. As we already noted in the beginning of this paragraph these values are rare and fine-tuned. This can be seen in Fig. 2.16a, where we plot the maximal amplitude of the expectation value n_0 as a function of C_m. In fact for small values $C_m < 1$ there exists only a few number of these special values. They become more frequent for stronger coupling strength, however, we loose gaplessness and clear distinction between the two different critical configurations blurs so we shall limit ourselves to the regime $C_m \leq 1$. Note that this plot refers to the specific system (2.97) with parameter choice (2.115). We remark, however, that for other parameter choices, we have observed much more abundant rewriting values. There are also indications that making memory burden a higher order process by setting the exponent in (2.91) to $p > 1$ increases the abundance of *rewriting values*. However, we did not perform enough simulations to make a definite statement about this point.

For the same parameter values we consider the exemplary choice $p = 2$, where we made in (2.97) following replacements:

$$1 - \frac{\hat{n}_0}{N_c} \to \left(1 - \frac{\hat{n}_0}{N_c}\right)^2, \qquad 1 - \frac{\hat{n}_0}{N_c - \Delta N_c} \to \left(1 - \frac{\hat{n}_0}{N_c - \Delta N_c}\right)^2 . \tag{2.116}$$

According to Eq. (2.92) this reduces the memory burden by a factor of approximately 0.03. For this estimate we use that $N_c - n_0$ can get as large as 0.3 for $p = 1$; see Fig. 2.16a. In order to make both cases comparable we keep the free amplitude of n_0 in case of zero coupling between the memory sectors on the same order of magnitude as for the $p = 1$ case. This can be achieved by reducing C_0 by the same factor,i.e. set $C_0 = 0.0003$. The corresponding maximal amplitude plot can be seen in Fig. 2.16b. Apart from the aforementioned increase in frequency of *rewriting values*, we observe the same qualitative behavior as for $p = 1$.

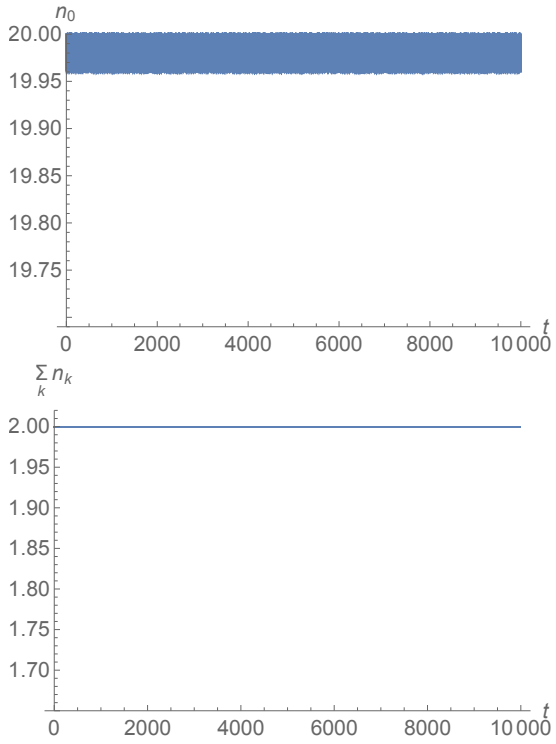

(a) $C_\mathrm{m} = 0$.

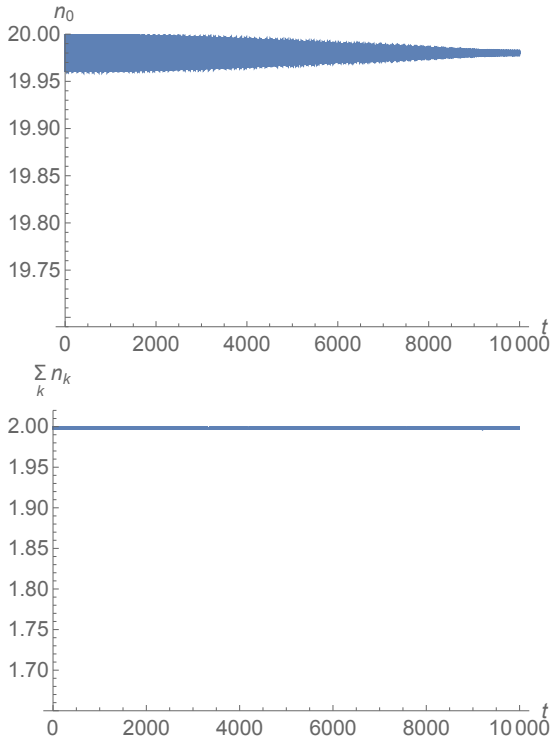

(b) $C_\mathrm{m} = 0.1$.

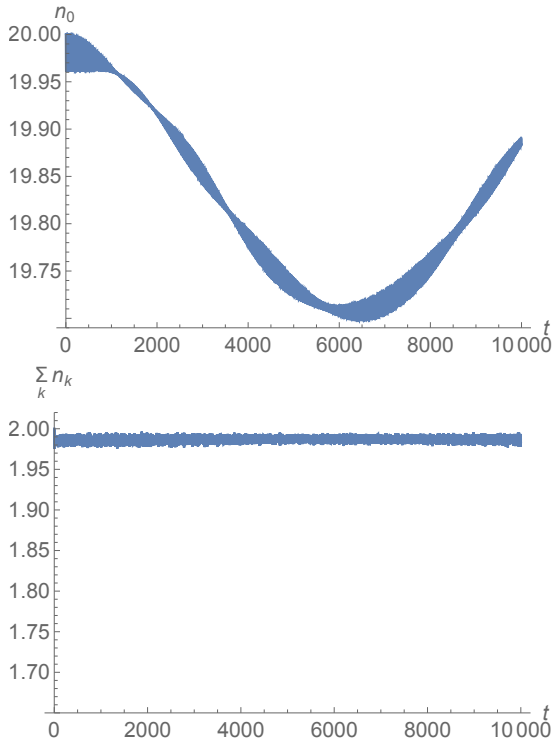

(c) $C_\mathrm{m} = 0.30055$.

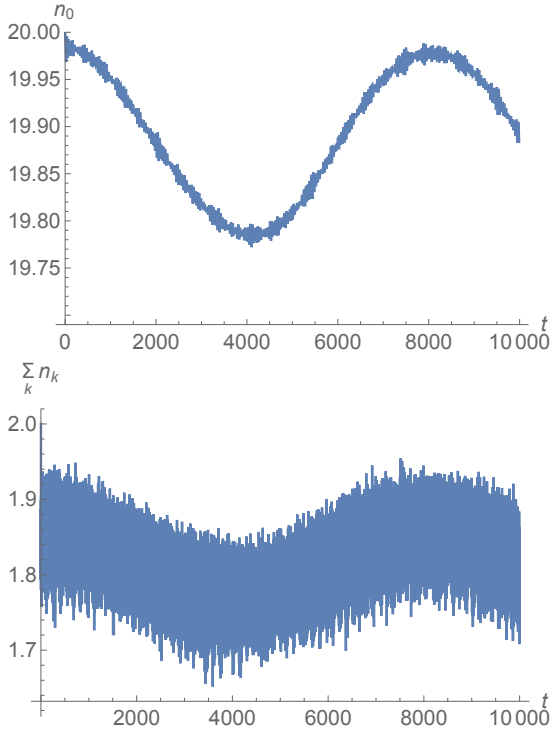

(d) $C_\mathrm{m} = 1.239$.

Figure 2.15: Time evolution of the initial state (2.114) for different values of C_m. n_0 is the expectation value of the occupation of the mode $\hat{a}_0$ and $\sum_k n_k$ that of the total occupation in the first critical sector. Time is plotted in units of $\epsilon_0^{-1}\hbar$.

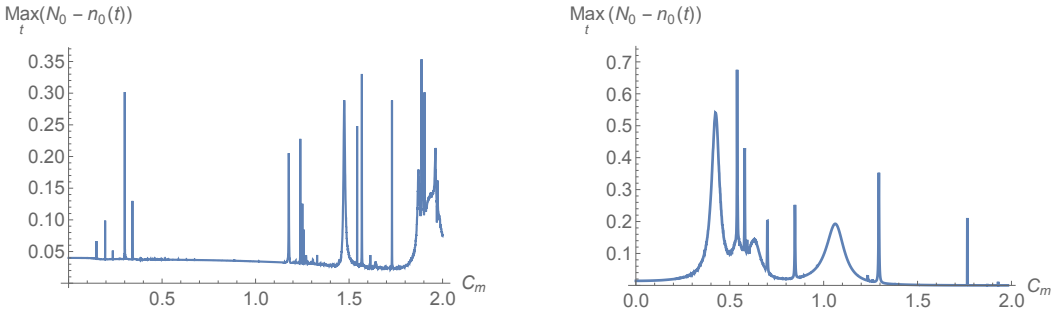

(a) $p = 1\,,\ C_0 = 0.01$ (b) $p = 2\,,\ C_0 = 0.0003$

Figure 2.16: Maximal amplitude of the expectation value of $\hat{n}_0$ for different values of C_{m}.

2.4.7 Parameter Scalings

After confirming that rewriting does indeed take place dynamically in the system (2.97), we shall continue to investigate how this behavior quantitatively depends on the parameters of the model. The dependence on the information capacity of the memory sector is of particular interest for us and will be discussed later in more detail. As a second observable beside the rewriting value we determine the rate Γ with which n_0 can transfer occupation to m_0. We define it as the ratio of the maximal amplitude and the timescale on which this maximal value is attained. This observable is especially motivated in light of the application to black hole evaporation, see section 3.2. At this point it can be interpreted as a general decay rate of a macroscopic system. In the following, we will only consider $p = 1$, since preliminary checks indicate no qualitative changes for higher p.

In order to determine how the rewriting values of C_m and the corresponding rates Γ scale with the parameter $X \in \{N_c, \epsilon_m, C_0, \Delta N_c, K\}$, the system has been time evolved with different fixed X, with the remaining parameters fixed at the values given in (2.115). For each X-value, the time evolutions have been done for many couplings $C_m \in [0, 1]$ (or a larger interval), where we used a sampling step of $\delta C_m = 10^{-3}$ or smaller.

We define as a rewriting values the coupling prefactor C_m for which the amplitude of n_0 exceeds the one in absence of inter memory sector coupling,i.e. the case of $C_m = 0$ by 20%. In case rewriting values cannot be distinguished with regard to our sampling rate, i.e. they appear as a continuum, we only consider the one with the highest value of Γ. Since the rate is very sensitive to the coupling strength, we perform time evolutions with a smaller sampling step of $\delta C_m = 5 \times 10^{-5}$ to map the rewriting value more accurately. Finally, we select the point with the highest rate. This choice is again motivated by our application to black hole evaporation later on.

The scalings for the rewriting values C_m and the decay rate Γ are as follows:

1. N_c scaling:
   To distinguish the effect of this parameter from the distance between the two memory sectors, we simultaneously vary ΔN_c such that $N_c/\Delta N_c$ stays fixed. The dependence on the critical occupation N_c,i.e. the occupation number at which the first memory sector becomes gapless, is illustrated in Fig. 2.17. The data points from simulations are given in blue. To extract the scaling of the rewriting values

we fit a function of the form $f_C(N_c) = a(\frac{N_c}{22})^{-b}$ to the data. The function parameters are fitted to $a \approx 0.275$ and $b \approx 0.911$. For the rate Γ we chose the function $f_\Gamma(N_c) = A(\frac{N_c}{22})^{-B}$, with the fit result $A \approx 4.46 \times 10^{-5}$ and $B \approx 1.14$. These fit functions are plotted in orange in Fig. 2.17. Therefore, the scaling with regard to N_c is approximately given by

$$C_\mathrm{m} \sim N_c^{-1}\,, \qquad \Gamma \sim N_c^{-1}\,. \tag{2.117}$$

2. ϵ_m scaling:
To determine how C_m and Γ scale when varying the free gap ϵ_m we plot the numerical data in Fig. 2.18. We fit a function of the form $f_C(\epsilon_m) = a\epsilon_m$, with the fit result $a \approx 0.300$. According to the data Fig. 2.18b the rate Γ is in good approximation independent from the value of the free gaps. The free gap of the memory modes ϵ_m scaling is:
$$C_\mathrm{m} \sim \epsilon_m^1\,, \qquad \Gamma \sim \epsilon_m^0 \text{ (independent)}\,. \tag{2.118}$$

3. C_0 scaling:
The data used to determine the scaling with C_0 is illustrated in Fig. 2.19. Within our precision and purpose, we observe no dependence of the rewriting values on the coupling between $\hat{a}_0$ and $\hat{b}_0$. It is negligible compared to the scaling with the other parameters. To determine the scaling for the decay rate we fit $f_\Gamma(C_0) = AC_0^B$ to the data. The fit results in $A \approx 2.85 \times 10^{-2}$ and $B \approx 1.38$. The scaling with the C_0 coupling is given by

$$C_\mathrm{m} \sim C_0^0 \text{ (independent)}\,, \qquad \Gamma \sim C_0^{1.4}\,. \tag{2.119}$$

4. ΔN_c scaling:
The dependence of the occupation number distance between the two memory sectors ΔN_c is illustrated in Fig. 2.20. The abundance of rewriting values complicates determining the actual scaling. For this reason we select data points for which a scaling is apparent. For the function $f_C(\Delta N_c) = a(\frac{\Delta N_c}{12})^b$, this fit indicates $a \approx 0.300$ and $b \approx 0.207$. Another scaling behavior can be extracted with $b \approx -0.130$. The rate Γ is determined by using the fit function $f_\Gamma(\Delta N_c) = A(1 - B\frac{\Delta N_c}{20})$. The fit parameters are estimated to $A \approx 1.38 \times 10^{-4}$ and $B \approx 1.07$. The ΔN_c scaling is observed to be

$$C_\mathrm{m} \sim (\Delta N_c/N_c)^{0.2}\,, \qquad \Gamma \sim (1 - \Delta N_c/N_c)\,. \tag{2.120}$$

5. K and K' scaling:
Next we shall study the scaling with regard to the amount of memory modes K and K'. Unfortunately, due to limited numerical resources we can only study three values, namely $K = K' = 4, 6, 8$. In the following we assume that the first sector is initially half filled, so $N_m = K/2$. The motivation for this is twofold. First, this corresponds to be the most probable state in the limit of large macroscopic systems and assuming that the cases $n_k = 0$ and $n_k = 1$ are equally likely. This is again

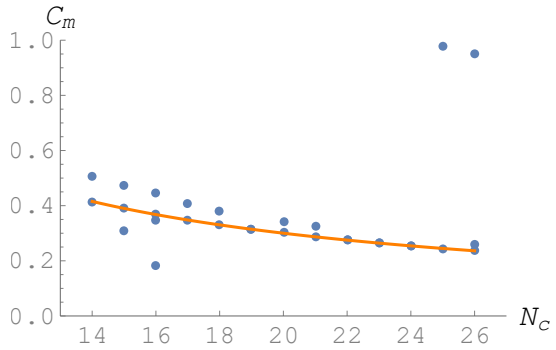

(a) Rewriting values of C_{m}.

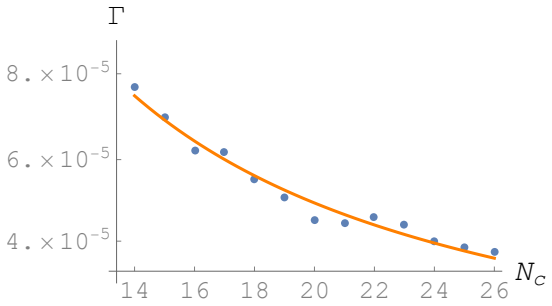

(b) Rates Γ at those rewriting values.

Figure 2.17: Data and fits for the rewriting values of C_m and the rates Γ as function of N_c. ΔN_c has been varied to keep $N_c/\Delta N_c$ fixed.

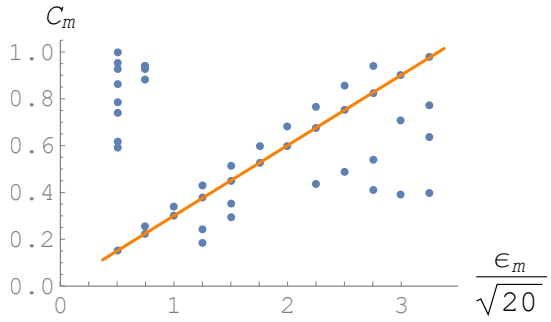

(a) Rewriting values of C_{m}.

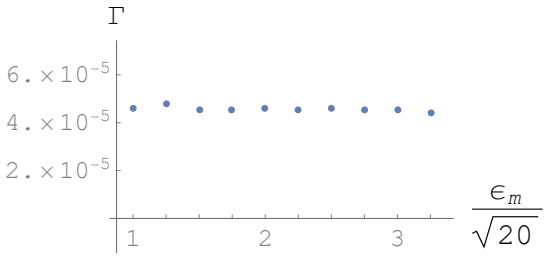

(b) Rates Γ at those rewriting values.

Figure 2.18: Data and fit for the rewriting values of C_m and the rates Γ as function of ϵ_m.

important for applying these results to gravity. On the other hand, it dampens the effect of varying N_m since the ratio K/N_m remains constant when varying K.

The numerical results are displayed in Fig. 2.21. We parameterize the rewriting values and rate as

$$C_{\mathrm{m}} \sim K^{\beta_C}\,, \qquad \Gamma \sim K^{\beta_\Gamma}\,. \tag{2.121}$$

Note that because we only have access to limited data points we cannot make precise statements here and the correct values for β_C and β_Γ might differ significantly. To emphasize this we plot the fit function in dashed lines. The rough estimate for the parameters are

$$\beta_C \approx 1\,, \qquad \beta_\Gamma \approx -1\,. \tag{2.122}$$

2.4.8 Efficiency of Rewriting - Numerical Results

It is apparent from the real time plots 2.15c and 2.15d that the memory burden can actually (partially) overcome by transferring occupation from the first to the second memory sector. However, there is still large backreaction to the time evolution of the *master mode*

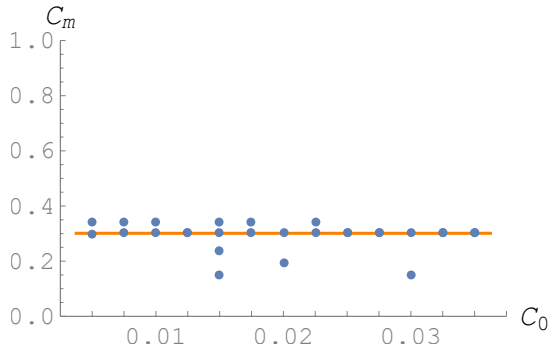

(a) Rewriting values of C_{m}.

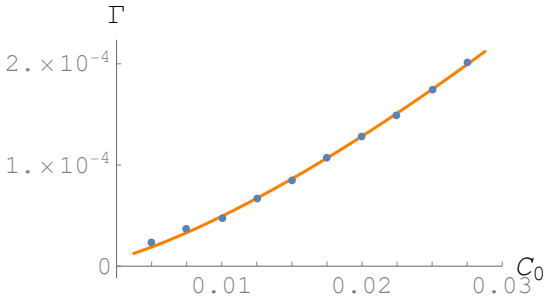

(b) Rates Γ at those rewriting values.

Figure 2.19: Data and fits for the rewriting values of C_m and the rates Γ as function of C_0.

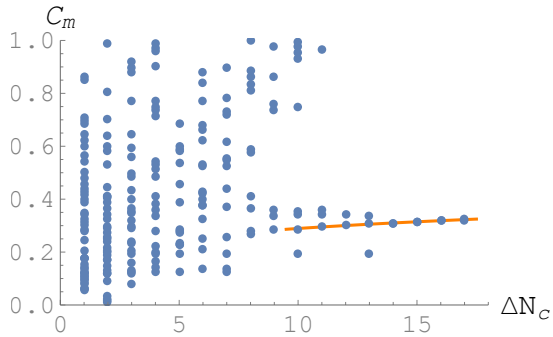

(a) Rewriting values of C_{m}.

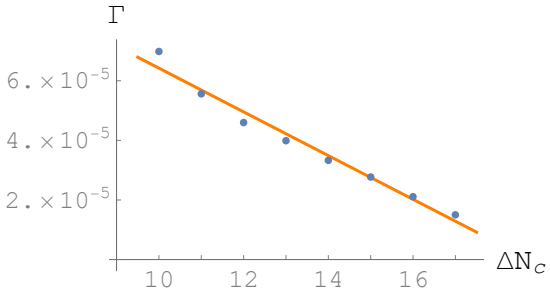

(b) Rates Γ at those rewriting values.

Figure 2.20: Data and fits for the rewriting values of C_m and the rates Γ as function of ΔN_c.

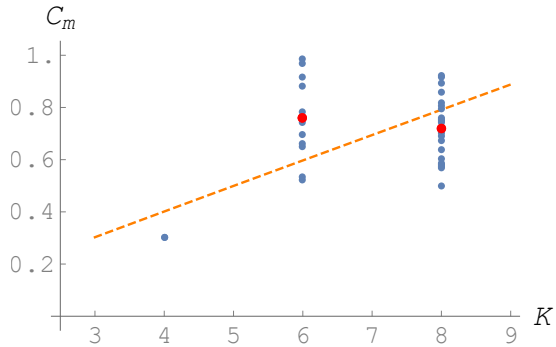

(a) Rewriting values of C_{m}.

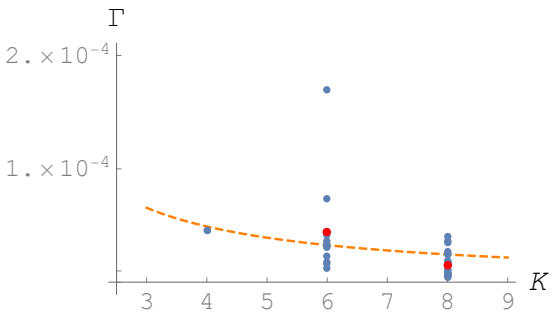

(b) Rates Γ at those rewriting values.

Figure 2.21: Data and fits for the rewriting values of C_m and the rates Γ as function of K. The orange curves correspond to the fit of the mean values (red squares) with a function given by Eq. 2.121 with parameters 2.122. The fit is plotted in dashed lines to emphasize the large statistical uncertainty.

in form of a severe slow down compared to the free oscillation (with a time scale set by C_0) in case of absence of memory burden. In the following we shall investigate if rewriting is indeed a viable option to alleviate memory burden in larger systems and how much the decay is slowed down with increasing number of memory modes. Unfortunately, due to limited available data we can't extract a reliable scaling when varying K. However, we can at least try to constrain rewriting, i.e. give a lower bound on C_m and an upper bound on Γ. To this end, we calculate the mean value of C_m for the 11 data points at $K = 6$. In order to obtain a maximally conservative bound, we moreover choose among the results for $K = 8$ the 11 data points with the lowest values of C_m and compute their mean. Performing a fit with the two resulting mean values, we get

$$\beta_C \gtrsim -0.7\,. \tag{2.123}$$

We have not included the value at $K = 4$ since doing so would increase β_C. For the rate Γ we will adapt a similar procedure and try to be as conservative as possible. Equivalent to the rewriting values we average over the 11 data points at $K = 6$. At $K = 8$ we choose the 11 data points with the highest rate and compute their mean. Performing a fit over the value at $K = 4$ and those two obtained as described above we obtain

$$\beta_\Gamma \lesssim -0.7\,. \tag{2.124}$$

Note that we have not excluded the value at $K = 4$, in this case since thous would decrease β_Γ. As with the fit value in Eq. (2.121) the statistical significance of these results is far too low to make any reliable statement, so the true values might not respect the bounds (2.123) and (2.124). So, although we can not give reliable numbers, we observe clear indications that rewriting becomes more difficult for larger systems.

2.4.9 Efficiency of Rewriting - Analytic Considerations

To increase the credibility of the numerical result from the last section we shall provide analytical estimates on the process of rewriting in the following. To simplify computation we specialize to a system with $K = K'$ and assume each set of memory modes to be diagonal and also come with equal energy gaps. Therefore we set $\tilde{C}_{k,l} = \tilde{C}_{k',l'} = 0$ and $\epsilon_k = \epsilon_{k'} = \sqrt{N_c}\epsilon_0$. Then, without any loss of generality, the matrix $C_{k,k'}$ can be set diagonal, since we can always achieve this with a unitary transformation that leaves the physics unchanged. Our prototype system (2.97) then simplifies to

$$\begin{aligned}\hat{H} = {} & \epsilon_0\hat{n}_0 + \epsilon_0\hat{m}_0 + C_0\left(\hat{a}_0^\dagger\hat{b}_0 + \hat{b}_0^\dagger\hat{a}_0\right) \\ & + \mathcal{E}\sum_k \hat{n}_k + \mathcal{E}'\sum_k \hat{n}'_k + \sum_k C_{k,k}\left(\hat{a}_k^\dagger\hat{a}'_k + \text{h.c.}\right)\,,\end{aligned} \tag{2.125}$$

where the operators for the effective gaps for the first and second memory sector are given by

$$\mathcal{E} \equiv \sqrt{N_c}\left(1 - \frac{\hat{n}_0}{N_c}\right)\epsilon_0\,, \quad \text{and} \quad \mathcal{E}' \equiv \sqrt{N_c}\left(1 - \frac{\hat{n}_0}{N_c - \Delta N_c}\right)\epsilon_0\,, \tag{2.126}$$

respectively. Again, we shall be interested in initial states of the form (2.101). For this state the master mode has a critical occupation and the effective gaps are given by

$$\mathcal{E} = 0\,, \qquad \mathcal{E}' \simeq -\frac{\Delta N_c}{\sqrt{N_c}}\epsilon_0 < 0\,. \tag{2.127}$$

Since the second gap is negative, there exist states with much lower energy than the initial one (2.101). A particular extreme example would be

$$|\text{low}\rangle = |\underbrace{N_c}_{n_0}, \underbrace{0}_{m_0}, 0, \ldots 0, \underbrace{n_1}_{n'_1}, \ldots, \underbrace{n_K}_{n'_K}\rangle\ , \tag{2.128}$$

where all information is transferred from the first to the second sector while keeping the occupation in the master mode constant. The macroscopic energy difference between the initial state (2.101) and (2.128) is

$$\langle\text{low}|\,\hat{H}\,|\text{low}\rangle - \langle\text{in}|\,\hat{H}\,|\text{in}\rangle = \mathcal{E}'\sum_k n_k \sim \Delta N_c \mu\,, \tag{2.129}$$

where we wrote the energy difference in terms of the memory burden

$$\mu = -\epsilon_0 \sum_k \frac{n_k}{\sqrt{N_c}}. \tag{2.130}$$

Since μ is negative, the energy difference (2.129) is negative as well. To avoid confusion we stress that all considered systems including (2.125) is energy conserving, so a transition from (2.101) to (2.128) is energetically forbidden. The important point here is that deforming $|\text{in}\rangle$ in the direction of $|\text{low}\rangle$, i.e. transferring occupation from $\hat{a}_k$ to $\hat{a}'_{k'}$ without altering the value of n_0, results in a negative energy balance. On the other hand of course, there are states with much higher energy. For example:

$$|\text{high}\rangle = |\underbrace{N_c - \Delta N_c}_{n_0}, \underbrace{\Delta N_c}_{m_0}, n_1, \ldots, n_k, \underbrace{0}_{n'_1}, \ldots, \underbrace{0}_{n'_{k'}}\rangle\ . \tag{2.131}$$

For this specific state the effective gaps (2.126) are

$$\mathcal{E} \simeq \frac{\Delta N_c}{\sqrt{N_c}}\epsilon_0 > 0\,, \qquad \mathcal{E}' = 0\,. \tag{2.132}$$

Therefore, the energy difference between the initial state and $|\text{high}\rangle$ is

$$\langle\text{high}|\,\hat{H}\,|\text{high}\rangle - \langle\text{in}|\,\hat{H}\,|\text{in}\rangle = \mathcal{E}\sum_k n_k \sim \epsilon_0 \frac{\Delta N_c}{\sqrt{N_c}}\sum_k n_k\,, \tag{2.133}$$

which is a positive number. So by reducing the occupation of the master mode without offloading the memory burden, we create an energy imbalance in positive direction. It is then clear that by simultaneously deforming the initial state in both $|\text{low}\rangle$ and $|\text{high}\rangle$ direction, such that the exchange of the occupation number between the sets n_k and $n'_{k'}$ is balanced by the exchange between n_0 and m_0, we obtain intermediate states that are

nearly degenerate with $|\text{in}\rangle$ state. Therefore, it seems possible that rewriting is a valid option to overcome memory burden [2], [74]. However, this is in contrast to the numerical results in section 2.4.8. There we found that although it is possible to deviate from the critical configuration by offloading information, the backreaction due to the burden is still strong, thus resulting in a suppressed amplitude and severely diminished rate. The reason for this can be easily traced back to the following. To maintain the energy balance the trajectory in state space requires a synchronized evolution of both the master mode, as well as the memory sectors. These sets have to produce opposite contributions to the energy budget such that the net difference is zero. However, each of those two evolutions has a highly suppressed amplitude due to the huge energy splitting. This breaks the process and is the reason why the system cannot evolve efficiently. To illustrate this let us consider the early time evolution of the system (2.125) in the initial state (2.114). Near $t = 0$ the system can be described as a set of coupled 2×2-problems of the form

$$\hat{H} = \sum_k \begin{matrix} \\ \hat{a}_k^\dagger \\ \hat{a}_k^{\prime\dagger} \end{matrix} \begin{matrix} \begin{matrix} \hat{a}_k & \hat{a}_k^{\prime} \end{matrix} \\ \begin{pmatrix} 0 & C_{k,k} \\ C_{k,k} & \mathcal{E}' \end{pmatrix} \end{matrix} + \begin{matrix} \\ \hat{a}_0^\dagger \\ \hat{b}_0^\dagger \end{matrix} \begin{matrix} \begin{matrix} \hat{a}_0 & \hat{b}_0 \end{matrix} \\ \begin{pmatrix} \epsilon_0 + \mu & C_0 \\ C_0 & \epsilon_0 \end{pmatrix} \end{matrix} . \tag{2.134}$$

The subsystems of modes with index 0 and those with k and k' respectively are coupled via the occupation dependency of the effective gap $\mathcal{E}'$ and the memory burden μ. This interdependence on each other makes this system difficult to solve. However, since our goal is to only obtain a qualitative picture on the behavior for early times, we can solve this system iteratively. In this zero order approximation we evolve those two subsystems independently by holding $\mathcal{E}'$ and μ constant for each iteration steps. The $(\hat{a}_0, \hat{\hat{b}}_0)$ and $(\hat{a}_k, \hat{a}'_{k'})$ subsystems are coupled via $\mathcal{E}'$ and μ, which depend on n_0 and $\sum_k n_k$ respectively. To extract the qualitative behavior for early times we solve the system (2.134) iteratively by succeedingly holding one subsystem constant. Therefore, μ and $\mathcal{E}'$ can be treated as constant for each iteration in this zeroth order approximation. We then evolve the decoupled systems in the first order by taking into account the variations of the occupation numbers obtained in the zeroth order. To leading order we have

$$\delta n_0 \sim -N_c \frac{C_0^2}{\mu^2} \quad \text{and} \quad \delta n_k \sim -\frac{C_{k,k}^2}{\mathcal{E}'^2} . \tag{2.135}$$

Since the variation of $\mathcal{E}'$ and μ are of higher order and extremely small, their variation is negligible in the next iteration. Therefore, we can assume within one timestep that $K = N_c = \sum_k n_k$. Furthermore, we have to take into account the bound $C_0 \lesssim \epsilon_0/\sqrt{N_c}$, which shall be of special importance in the black hole case (see section 3.2), as well as the condition (2.105), which ensures that gaplessness is not disturbed too much. This yields

$$\frac{C_{k,k}^2}{\mathcal{E}'} \lesssim \frac{\epsilon_0}{\sqrt{N_c}} . \tag{2.136}$$

The variation of for the effective gaps and memory burden are given by

$$\frac{\delta\mu}{\mu} \lesssim \frac{\epsilon_0}{\sqrt{N_c}\mathcal{E}'} \quad \text{and} \quad \frac{\delta\mathcal{E}'}{\mathcal{E}'} \sim \frac{1}{\Delta N_c N_c} . \tag{2.137}$$

Remembering the condition on the effective gaps of the second sector at the beginning of evolution, see Eq. (2.103) or (2.104), we get a lower bound on $|\mathcal{E}'|$. To be as less restrictive as possible we choose the softer bound (2.104). This is already sufficient to conclude that the iteration series rapidly converges. We see that the time evolution is such that the system is essentially trapped in the initial state. As a side remark we note that by assuming an equal distribution of plus and minus signs in the interaction terms, (2.136) acquires an additional factor $1/\sqrt{N_c}$.

2.4.10 Role of Number Non-Conservation

Up until now we only considered systems that exhibit total particle number conserving interaction. We shall discuss that this assumption is not to restrictive. In the following we see why particle conservation is by no means the reason for the inefficiency of rewriting. For the sake of clarity, let us consider the subsystems $(\hat{a}_0, \hat{b}_0)$ and $(\hat{a}_k, \hat{a}'_{k'})$ again independently.

Number non-conserving decay of the master mode

We start with considering a non number conserving interaction between the master mode $\hat{a}_0$ and the external mode $\hat{b}_0$. For simplicity we neglect the dynamics of the memory sector and assume a constant memory burden μ. This system is then described by the Hamiltonian

$$\hat{H} = (\epsilon_0 + \mu)\hat{a}_0^\dagger \hat{a}_0 \; + \epsilon_0 \hat{b}_0^\dagger \hat{b}_0 + C_0(\hat{a}_0 \hat{b}_0 + \hat{a}_0^\dagger \hat{b}_0^\dagger)\,, \tag{2.138}$$

where we have taken the parameter C_0 to be real and of the same strength as in the number-conserving version to make a comparison between the two cases possible. Since our most interesting application of the memory burden effect will be black hole evaporation we shall assume $C_0 \sim \epsilon_0/N_c$. This is motivated by the fact that in the black hole picture this corresponds to half-decay time of $t \sim N_c/\epsilon_0$ in units of the energy of the Hawking quanta. This imitates the scaling of the black hole lifetime at the level of our toy model. As discussed in section 2.2, a system of the form (2.138) can be brought to diagonal form by a Bogoliubov transformation:

$$\hat{a}_0 = u\hat{\alpha} - v\hat{\beta}^\dagger\,, \qquad \hat{b}_0 = u\hat{\beta} - v\hat{\alpha}^\dagger\,, \tag{2.139}$$

where $\hat{\alpha}$ and $\hat{\beta}$ are the eigenmodes and

$$v^2 = \frac{1}{2}\left(\frac{1}{\sqrt{1 - \frac{4C_0^2}{(2\epsilon_0+\mu)^2}}} - 1\right), \qquad u^2 = \frac{1}{2}\left(\frac{1}{\sqrt{1 - \frac{4C_0^2}{(2\epsilon_0+\mu)^2}}} + 1\right). \tag{2.140}$$

Employing the black hole parameters again the full memory burden $\mu \sim -\epsilon_0\sqrt{N_n}$. Taking into account that $C_0 \sim \epsilon_0/N_c$, Eq. (2.140) gives,

$$v^2 \simeq \frac{C_0^2}{\mu^2} \sim \frac{1}{N_c^3}\,, \quad u^2 = 1 + \mathcal{O}(1/N_c^3)\,. \tag{2.141}$$

We can read off that the depletion coefficient v^2 is miniscule due to an extra $1/N_c$ suppression due to the memory burden factor ϵ_0/μ. This is exactly the same suppression that we also found in the number conserving case, see Eq. (2.88).
Another way to see that number violating interaction is no shortcut to get rid of memory burden is by applying the Bogoliubov approximation in case for a macroscopically occupied master mode. In this case we can replace operators of the $\hat{a}_0$ mode by their respective expectation values again, namely $\hat{a}_0 \to \sqrt{N_c}$ and $\hat{a}_0^\dagger \to \sqrt{N_c}$. The Hamiltonian (2.138) then becomes

$$\hat{H} = \epsilon_0 \hat{b}_0^\dagger \hat{b}_0 + C_0 \sqrt{N_c}(\hat{b}_0^\dagger + \hat{b}_0)\,, \tag{2.142}$$

where we discarded the constant and terms that are smaller than $1/\sqrt{N_c}$. This is self-consistent as long as the departure of $\hat{a}_0$ from $\sqrt{N_c}$ is small. Using the canonical transformation

$$\hat{b}_0 = \hat{\beta} - C_0 \sqrt{N_c}/\epsilon_0\,, \tag{2.143}$$

the Hamiltonian (2.142) can be diagonalized. Furthermore, the occupation of the $\hat{b}_0$ mode in the β vacuum can be easily computed:

$$\langle \hat{b}_0^\dagger \hat{b}_0 \rangle = \frac{C_0^2 N_c}{\epsilon_0^2}\,. \tag{2.144}$$

Thus, depletion is still suppressed by C_0. It is clear that as long as the m_0 is small and the inverse processes that increase the occupation number of $\hat{a}_0$ are not effective, the nature of the interaction if not important. Regardless of whether the mixing is number conserving or not, any deviation from the critical occupation is severely restricted. Note as well that higher order decay processes also do not allow for the memory burden effect to be alleviated efficiently. Terms of the form $\hat{a}_0 \hat{b}_0^l$, converting a single $\hat{a}_0$ quanta in l $\hat{b}_0$ ones are negligible, since each extra $\hat{b}_0$ operator brings an additional factor of $1/\sqrt{N_c}$ in the interaction vertex. Thus each of these terms scales as $\epsilon_0/N_c^{l/2}$.

Number non-conserving decay of memory modes

Next we shall show that our reasoning still hold true, when we allow reducing occupation numbers in the memory sector via non-conserving interactions. Note that if we drop the requirement of particle number conservation, it is in principle possible that a tachyonic instability emerges in case that one of the effective gaps becomes negative. This is especially the case if $p = 1$, see Eq. (2.92), as it was assumed in the previous sections. In the following we shall assume that gaps are always positive, so the system is stable and to avoid mixing the notion of instability with the alleviation of memory burden. This imposes a constraint on the structure of the Hamiltonian, which we will take into account in the following.

Similar to (2.138) let us consider a non-number conserving mixing in the memory sector

$$\hat{H} = \mathcal{E}_k \hat{n}_k + \mathcal{E}_{k'} \hat{n}'_{k'} + + C_{k,k'} \left(\hat{a}_k \hat{a}'_{k'} + \text{h.c.}\right)\,. \tag{2.145}$$

Again, we only consider one-to-one mode coupling to simplify calculations and make our illustration more clear. Neglecting for a moment the dynamics of the energy gaps reduces the system to a set of independent 2×2 problem. The exact form of the energy gaps $\mathcal{E}_k$ and $\mathcal{E}_{k'}$ is not important for our reasoning. The only requirement (besides positivity) we shall assume in the following is that they alternatively become zero for two specific and macroscopically distinct values of the occupation number of the master mode. Therefore we require

$$\begin{aligned} &\mathcal{E}_k = 0\,, \qquad \mathcal{E}_{k'} \gg \epsilon_0, \qquad \text{for } n_0 = N_c, \\ &\mathcal{E}_{k'} = 0\,, \qquad \mathcal{E}_k \gg \epsilon_0, \qquad \text{for } n_0 = N_c - \Delta N_c. \end{aligned} \tag{2.146}$$

For example, we can choose

$$\mathcal{E}_k \equiv \left(1 - \frac{\hat{n}_0}{N_c}\right) \epsilon_k\,, \tag{2.147}$$

as before, and for $\mathcal{E}_{k'}$ assume one of many possible shapes, e.g.,

$$\mathcal{E}_{k'} \equiv \left(1 - \frac{\hat{n}_0}{N_c - \Delta N_c}\right)^2 \epsilon_{k'} \quad \text{or} \qquad \mathcal{E}_{k'} \equiv \left(\frac{\hat{n}_0}{N_c - \Delta N_c} - 1\right) \epsilon_{k'}\,. \tag{2.148}$$

Even a gap function such as $\mathcal{E}_{k'} \equiv \left(1 - \frac{N_c - \Delta N_c}{\hat{n}_0}\right) \epsilon_{k'}$ for example would be admissible, since we are not restricted by renormalizability and only interested in the regime of $n_0 \gg 1$ in this context. Let us reiterate the point that we want to treat the number conserving and non-conserving case on equal footing. Therefore, we choose the coupling strength to be of similar order. Specifically, we require that it is small enough to not disturb gaplessness leading to condition (2.136). Now, let us recall that the reason why the depletion of the gapless memory modes in the particle number-conserving case (2.97) was not efficient, is:

- Relatively large level-splitting: $\Delta\mathcal{E} = \mathcal{E}_{k'} - \mathcal{E}_k$
- Suppressed mixing coefficient $C_{k,k'}$.

As long as these conditions are maintained, the behavior of the system does not change significantly irregardless of the nature of interaction. Equivalent to solving the system (2.138) we can also use a Bogoliubov transformation,

$$\hat{a}_k = u\hat{\alpha}_k - v\hat{\beta}^\dagger_{k'}\,, \qquad \hat{a}'_{k'} = u\hat{\beta}_{k'} - v\hat{\alpha}^\dagger_k\,, \tag{2.149}$$

with

$$u^2 = 1 + v^2\,,\ v^2 = \frac{1}{2}\left(\frac{1}{\sqrt{1 - \frac{4C^2_{k,k'}}{(\mathcal{E}_k + \mathcal{E}_{k'})^2}}} - 1\right)\,. \tag{2.150}$$

Next, taking into account Eqs. (2.136) and (2.146), we obtain for the first critical occupation $n_0 = N_c$

$$v^2 \sim \frac{C^2_{k,k'}}{(\mathcal{E}_{k'})^2} \ll \frac{\epsilon_0}{\sqrt{N}\mathcal{E}_{k'}}\,, \qquad u^2 \simeq 1\,. \tag{2.151}$$

Again we end up with a highly suppressed rate. This rate is negligible and of no help for alleviating the memory burden on any reasonable timescale. Let us conclude this discussion by noting that equivalent to the previous case, higher order operators cannot improve the situation due to extra suppression by powers of $1/N_c$.

As we have seen in both subsystems, number non-conserving mixing cannot help to get rid of memory burden more effectively than number conserving interactions. It is important to be aware of the fact that memory burden is a relative effect. This phenomenon results in a delay of the otherwise unperturbed time evolution due to the backreaction of the stored quantum information. It is therefore an effect which is intrinsically quantum. Due to its relative nature one has to compare the time evolution of both with and without quantum information and corresponding memory burden in order to quantify the effect.

Above we have considered a specific example which we have normalized such that the system looses half its constituents in case of absence of memory burden on a timescale set by N_c. Note that we have measured time in units of the elementary gap ϵ_0. This choice is motivated by black hole physics to which we shall apply these results in section 3. At this point for understanding memory burden in general the precise normalization is not important. The chosen half-decay time N_c fixes the interaction strength of the coupling between $\hat{a}_0$ and $\hat{b}_0$, which is responsible for the transfer of occupation number away from the master mode. Within our frame it is also responsible for the macroscopic or classical evolution of the system. Let us now turn to the analogue system with a full memory sector such that the memory burden is maximal. First let us assume that the system exhibits only particle number conservation interaction. In this case we saw both numerically in section 2.4.5 and analytically in section 2.4.9 that memory burden sets in at the latest after half life time, the time scale after the master mode has lost of order half its constituents. Whenever the stored quantum information starts backreacting, the leakage of master mode occupation to the environment is stopped and the system gets stabilized. In this subsection we studied, if the assumption of particle number conserving interaction is the cause for the inevitability of avoiding memory burden. The answer to that question is negative since, regardless of the nature of interaction, the requirement that gaplessness needs to be maintained severely restricts the coupling strength among the memory modes and also to possible external fields. This restriction is enough to prevent any efficient offloading of the information out of the memory sector, which in turn makes memory burden impossible to avoid on long enough timescales.

The fact that it makes no difference in regard to offloading whether we assume/use a number conserving or a number non-conserving system, can also be seen from a different perspective. The initial state is critical and the memory modes carry at least a typical information load whereas the environment and the second memory sector are empty due to their large free gaps. We are interested in the possibility to avoid the burden by offloading particles off the $\hat{a}_k$ modes by coupling them to some other modes. This interaction can either be number conserving or not. The only difference is the number of particles that would be created by annihilating one quantum of $\hat{a}_k$. However, a critical observation is that within the allowed range of values for the coupling strengths the other sectors never get populated significantly on any reasonable timescale. This implies that on average the inverse process can not play any role whatsoever in the dynamics. Therefore, the total

number conservation is irrelevant for the phenomenon of memory burden. So it makes no difference for an observer of the $\hat{a}_k$-sector which kind of interaction is responsible for the decay. It is simply not possible to determine the kind of interaction, since the inverse process. which would allow do differentiate the conserving from the non-conserving one, is not observable.

2.5 Summary

Before we continue and apply all the concepts discussed above to gravitational systems and quantum neural networks we shall briefly summaries our findings. In this chapter we started section 2.1 by introducing the concept of systems of enhanced memory capacity. These are systems that exhibit critical configurations around which an abundance of (nearly) gapless degrees of freedom emerge. This is equivalent to a macroscopic state with an enhanced microstate entropy. We discussed a dynamic mechanism that ensures the existence of such a special state in the spectrum. This mechanism, which we call *assisted gaplessness*, relies on a weakly attractive interaction between a large set of modes and a macroscopically occupied *master mode*. Due to the special signature of the coupling increasing the occupation number of the master mode *assists* the other modes in lowering their effective gap until a critical occupation is reached at which they become gapless.

Next, we introduced the C-number method, as a robust procedure to find gapless modes in a system that exhibits large occupations and a weakly attractive interaction among at least some modes in section 2.2. If the energy landscape is non trivial, this method simplifies the task of finding flat directions corresponding to gapless degrees of freedom compared to the computationally intense task of full diagonalization. We applied this method to a 3-mode prototype system and confirmed the existence of gapless modes via their slow time evolution.

Although such states of enhanced memory capacity seemed to be extremely special and selectively prepared at first glance, we confirmed that system exhibiting those state actually evolve dynamically towards them. Provided that external constraints like energy or momentum conservation do not prohibit it, the system will move towards a state at which an enlarged portion of the Hilbert space opens up due to the emergence of an abundance of microstates. In section 2.3 we quantified the attraction with the proportion of critical Hilbert space in relation to whole Hilbert space.

In section 2.4 we discussed a very general feature of states of enhanced memory capacity. They are subject to the universal phenomenon of *memory burden* that resists any deformation from the critical configuration. Since the *memory modes*, which we have denoted by $\hat{a}_k$, are gapless due to a specific occupation of the *master mode*, any deviation from this critical number would reintroduce a gap for the memory modes. This creates a force that basically ties the system to its initial critical state. Next we analyzed if this drastic effect on the evolution can be avoided by alleviating or removing the memory burden. Since a direct offloading to generic degrees of freedom is not efficient enough due to a large level splitting, we studied the offloading of information stored in memory modes $\hat{a}_k$ to another sector $\hat{a}'_{k'}$ which is also subject to assisted gaplessness and therefore approximately gapless. We call this process rewriting. However, although this mechanism

is indeed suitable for reducing the memory load by transferring occupation, our results indicate that it is still not nearly efficient to avoid backreaction altogether. During rewriting we observed a severe slow down of evolution compared to the free case in the absence of a memory load.

Chapter 3

Application to Gravity and Neural Networks

This chapter is devoted to the study of quantum informational properties of black holes and de Sitter spacetime. We focus on the enormous Bekenstein and Gibbons Hawking entropy of black holes and de Sitter respectively and discuss possible implications of this high memory capacity to the evolution of these gravitational systems. Furthermore, we also apply our findings on systems that exhibit states of enhanced memory capacity to quantum neural networks.

As we have pointed out in the introduction in section 1.4 and 1.3, de Sitter spacetime, as well as black holes, saturate the Bekenstein bound. This means they are primary examples for systems of enhanced microstate entropy. We shall therefore apply the concept of assisted gaplessness, as well as memory burden, to those particular systems. Moreover, we shall see that this also applies to certain quantum neural networks as well.

In the first section 3.1 we only assume the well established fact that de Sitter exhibits an enhanced microstate degeneracy due to its Gibbons-Hawking entropy. Since de Sitter experiences loss of quanta during the process of Gibbons-Hawking evaporation, it is a natural assumption that the internal state changes and therefore moves away from the critical configuration. This leads to a memory burden effect.

In section 3.2 we study the effect of memory burden due to the large entropy of a black hole in combination with Hawking evaporation. Since the black hole mass is a continuous parameter it is imaginable that memory burden can be avoided with the help of rewriting. We shall see, however, that it is not efficient enough to maintain the semi-classical rate.

In section 3.3 we study the phenomenon of assisted gaplessness in (quantum) neural networks. We discuss a possible dictionary between neural networks consisting of neurons and their synaptic connections and a Hamiltonian consisting of quantum oscillatory modes and the interactions between them.

This chapter is based on paper [1], which is joint work with Gia Dvali and Sebastian Zell, as well as the papers [2] and [4], which is joint work with Gia Dvali, Lukas Eisemann and Sebastian Sell. The section 3.1 follows [2]. The section 3.2 follows [4]. The last section 3.3 is based on [1].

3.1 De Sitter Spacetime

We have discussed in the introduction 1.4 that de Sitter spacetime is a primary example for a system of enhanced memory capacity due its Gibbons-Hawking entropy which similar to a black hole saturates the Bekenstein bound [71]. Therefore, if this quantum informational property can be captured by the general mechanism discussed in section 2, de Sitter can not escape the effect of memory burden first introduced in [74] and which we thoroughly discussed in section 2.4. The information stored in the memory modes of de Sitter can literally be viewed as its primordial quantum memory.

3.1.1 Memory Burden of de Sitter

Let us now apply our findings on memory modes to the specific case of de Sitter spacetime. It is well established that it exhibits an enormous entropy [20] saturating natures absolute limit on the information capacity of a physical system. We shall denote this entropy by S. This means that de Sitter can be in $\sim e^S$ distinct microstates or equivalently that there are of order S nearly gapless degrees of freedom in the spectrum on top of this background. Following the multi-particle interpretation put forward in [24], we can adopt the premise that a mechanism similar to assisted gaplessness also exists in the scope of gravity and causes this enhanced microstate entropy. This means that a macroscopically occupied mode, which we here shall also refer to as $\hat{a}_0$ here, assumes a particular critical value N_c for which a large set of modes $\hat{a}_k$ with $k = 1, 2, \ldots, S$ becomes gapless. In the following we write their particle number operator with $\hat{n}_0$ and $\hat{n}_k$ respectively. We can write this similar to Eq. (2.5) in the form of a Hamiltonian depending on the effective gaps of the memory modes $\mathcal{E}_k = \mathcal{E}_k\left(\frac{n_0}{N_c}\right)$ and the occupation number of the individual memory modes. We write

$$\hat{H} = \sum_k \mathcal{E}_k \hat{n}_k \,. \tag{3.1}$$

Note that for simplicity we have set the gap of the $\hat{a}_0$ mode as $\epsilon_0 = 0$. The effective gaps are such that they collapse, whenever the critical occupation is attained, i.e. $n_0 \to N_c$. However, they are non-zero for generic occupation numbers of the $\hat{a}_0$ mode. In the critical configuration $n_0 = N_c$ the memory modes $\hat{a}_k$ become (approximately) gapless and can be excited at zero (very low) energy cost. Consequently, different patterns of the form

$$|pattern\rangle \equiv |n_1, n_2, ..., n_S\rangle \ . \tag{3.2}$$

become degenerate in energy and fit in an infinitesimal energy gap. The entirety of those states shall be called the memory space. All of the states are distinct from each other via their specific values n_k, therefore counting to the microstate entropy for a specific macrostate, which is characterized in this system by the macroscopic value of n_0. Assuming a cutoff d for the maximal occupation the number of different states is given by d^S. In particular, the number of states scales exponentially with the entropy S. The mechanism of assisted gaplessness is therefore sufficient to reproduce a microstate entropy that scales as S.

However, we have seen in section 2.4 that such a system inevitably experiences the effect of the burden of its memory. De Sitter has a large entropy, which means that

a large number of modes becomes gapless due to the critical value for n_0 through the mechanism of assisted gaplessness. Any deviation from this critical configuration would reintroduce an effective gaps for the memory modes of de Sitter. In this case the quantum information stored in a memory pattern would become very costly in energy. To prevent this, the quantum information backreacts on the decay and tries to tie the system to its initial critical state in the form of the memory burden effect. We suggest that because of the very general nature of this phenomenon, it must also be applicable to de Sitter. This provides a quantum clock in the form of a memory burden of a primordial pattern encoded in the memory modes of de Sitter. It is exactly those modes that account for its Gibbons-Hawking entropy. Due to the generality of our arguments and the universality of the phenomenon, which should apply to all systems that exhibit an enhanced microstate entropy, we actually do not require a precise microscopic understanding of these degrees of freedom. Furthermore, the classical evolution governed by Einstein's equation cannot affect the information stored in them, since they are intrinsically quantum. Therefore, the pattern cannot be erased by inflation and is only revealed after a long enough timescale due to cumulative quantum effects. Because memory burden is intrinsically quantum in nature, its effects can not be captured by any classical or semi-classical analysis. Therefore, any classical description breaks down after the point when the memory burden becomes unbearable. Our interpretation is that the memory overburden effect is a quantum information characteristic that accompanies the phenomenon of quantum breaking of de Sitter described in [24], [31], [34].

A very interesting aspect of these conclusions is that they provide a mechanism that potentially opens a new observational window into a pre-inflationary Universe. This would notably imply the possibility of catching a glimpse into the Universe's beginning, even before that last 60 e-foldings. This effect becomes more visible the closer the end of inflation is to its quantum break time, since the backreaction to the classical evolution due to the stored quantum information becomes increasingly stronger. This reversed situation is very intriguing, since pre-existing information usually gets readily washed out during the subsequent de Sitter phase. It would be an intriguing endeavor to search for these primordial imprints in cosmological observables.

3.1.2 Quantum Breaking of de Sitter

In the last section we discussed that a classical description of the time evolution of de Sitter cannot be accurate forever due to the memory burden effect. This fully agrees with the results in the composite picture of gravity proposed in [24]. As we have mentioned above, the quantum N-portrait of gravity interprets macroscopic extended spacetimes as a multi-graviton state not unlike a Bose-Einstein condensate. Already in [24] it has been shown that re-scattering processes among the constituents result in $\frac{1}{N}$-effects, which accumulate over time. This provides an intrinsic quantum clock which can be used to determine the actual duration of the de Sitter phase. This manifests as a decay or leakage process in this framework which results in a literal aging of de Sitter space time. This potentially leads to new types of observables that can probe the inflationary universe from a time long before the last 60 e-foldings. Possible quantum corrections arising in

this picture of widely used characteristics of inflation, like density perturbation or tilt, can be readily computed. For example, curvature perturbations produced at different epochs will differ. For details we refer to [24]. Note that these perturbations are independent from the variation of the Hubble parameter due to the standard slow-roll of the inflation field. These deviations are purely classical in origin. On top of that, a specific microscopic process in the form of quantum decay takes place. In other words, the backreaction of the accumulating $\frac{1}{N}$-effects leads to a breakdown of the de Sitter invariance in the same fashion as the evaporation of water from a finite volume tank violates the time-translation invariance. Even if the evaporation rate is constant and very small, over long enough timescales the water level in the tank will change which is an observable effect.

3.1.3 De Sitter and Inflation

After discussing the general idea we shall now try to make more quantitative statements. The two relevant quantities of de Sitter which will be important in the following are its Gibbons-Hawking entropy S and the Hubble scale H. These two values determine the free energy gap $\epsilon_0 \sim H$ as well as the entropy $N = S$. However, it is well established that, similar to a black hole, de Sitter evaporates. This means that after the time $t_Q = SH^{-1}$ a Hubble patch of size H^{-1} would emit a number of quanta N of order of its Gibbons-Hawking entropy S. The energy of a quantum in the Gibbons-Hawking radiation is typically of order $\epsilon_0 \sim H$. The total energy emitted is therefore of the same order as the total vacuum energy contained within the Hubble patch, which is equal to $E_{dS} \sim S\epsilon_0$. This simple estimate fully confirms the situation in [24], [31], [34]. There it was shown that in the multi-particle picture of de Sitter the time scale $t_Q = SH^{-1}$ is the same on which a coherent state description of the de Sitter Hubble patch loses of order half of its constituents. This is a strong indication that one can apply our general results of the previous section 2 to de Sitter spacetime by treating it as the special case $N = S$. With the established counting $S = N$, we know that this corresponds to order S nearly gapless degrees of freedom which we shall again denote by $\hat{a}_k$. At this stage, knowledge of the precious nature of these modes is not important and would require a precise microscopic theory of de Sitter. We shall see that for our purposes a general description is enough and we can already learn some valuable lessons from it. As an outlook, these modes should in principle be labeled by quantum numbers that correspond to symmetries in the classical limit. In order to have a level degeneracy N to account for the required entropy, the memory modes of de Sitter must belong to very high harmonics. We can use this to estimate the energy gaps of the memory modes: $\epsilon_k \sim \sqrt{N}\epsilon_0$. It is reassuring that this scaling also fully matches the holographic counting [76], [77] which yields the number of planckian qubits of order N. Using this we estimate the typical unactualized energy of a memory pattern encoded in a Hubble patch to $\epsilon_{pat} \sim N^{\frac{3}{2}}\epsilon_0 \sim E_{dS}\sqrt{N}$. This is an incredible result. This means that de Sitter spacetime is an extremely energy efficient storage device of quantum information. A pattern that, with naive counting, would exceed the energy of the entire de Sitter patch by a factor of $\sqrt{N}$ is stored with the same cost as the empty pattern. This statement is naturally completely equivalent to the observation that de Sitter exhibits an enormous microstate degeneracy, which is the origin of its

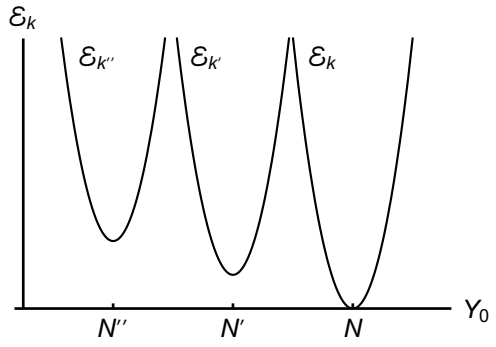

(a) For small m, the minima are narrow.

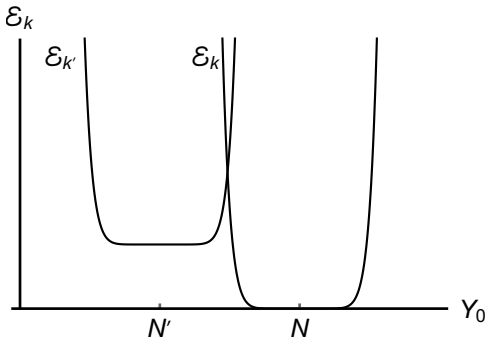

(b) For large m, the minima are wide.

Figure 3.1: Highly schematic plots (for even values of m) of the energy thresholds of the memory modes in a theory with cosmological constant. Only around a single value of Y_0, gapless modes emerge.

Gibbons-Hawking entropy. Note, that the only property, that we used so far, was the high entropy of the geometry. In particular, we have made no further assumption about its microscopic structure. We shall continue in this spirit and only add one additional assumption about its evaporation process. We add only one assumption that the loss of quanta implicates a deviation from the critical configuration in which all memory modes are exactly gapless. In other words, evaporation changes the internal structure in such a way that at least some modes acquire a gap to match the corresponding entropy of the partly evaporated de Sitter state, but then it is clear that this will result in a memory burden effect.

It is very important to note that for de Sitter, the critical occupation N_c is determined by the cosmological constant Λ. It therefore represents a *fixed parameter* of the theory. So even if the energy landscape of de Sitter exhibits more minima that can be used for efficient memory storage for other occupation numbers $n_0 = N_c' \neq N_c$, their energy must be an increasing function of $|N_c - N_c'|$. Let us illustrate this with the following Hamiltonian:

$$\hat{H} = \left(1 - \frac{\hat{n}_0}{N_c}\right)^m \sum_{k\neq 0} \epsilon_k \hat{n}_k \; + \tag{3.3}$$
$$+ \left(\left(1 - \frac{\hat{n}_0}{N_c'}\right)^m + \left(1 - \frac{\hat{n}_0}{N_c}\right)^l\right) \sum_{k'\neq 0} \epsilon_{k'}' \hat{n}_{k'}' \; + \; \ldots ,$$

where $l > 0$. The resulting energy landscape of this Hamiltonian is plotted in Fig. 3.1. Assuming that the two sets of modes $Y_{k'}'$ and Y_k can carry an identical pattern, i.e. $Y_{k'}' = Y_k$, their respective energy costs differ significantly. In a state with $n_0 = N_c'$ compared to a state with $n_0 = N_c$ the same pattern would require $E_{pat} = \left(1 - \frac{n_0}{N_c}\right)^l \epsilon_{pat}$ more energy. So even if we assume that de Sitter is able to copy the pattern from one set of memory modes into another, the memory burden will steadily increase. This completely matches our findings in section 2.4. Since we do not have a full theory of quantum gravity of de Sitter spacetime available, the exponents (3.3) m and l in Eq. remain free parameters.

We can, however, use the established semi-classical result that in the classical limit, which correspond in our picture to $N = N_c \to \infty$, only one macrostate of enhanced memory capacity has to emerge. This is a requirement to ensure that we can actually match a quantum state of the microscopic theory to the semi-classical description of de Sitter. Therefore, it is clear that the memory burden effect should set in at the latest after de Sitter lost of order 1 of its constituents,i.e. $\delta n_0 \sim N$. After this point memory burden is unavoidable and a strong backreaction will set it working against any further decay. Note that this upper bound after which quantum effects become important fully matches the quantum break-time discussed in [31]

The quantum breaking of de Sitter consequently results from two competing tendencies. On one hand, the system depletes by losing the constituent $\hat{n}_0$-mode into an external $\hat{b}_0$ mode in the form of Gibbons-Hawking radiation. This results into a deviation away from the critical configuration, for which the memory modes $n_{k\neq 0}$ become gapless and can therefore carry the enormous Gibbons-Hawking entropy. Consequently, the increasing energy gaps raise the energetic cost of the stored quantum pattern. On the other hand, it is impossible to offload this pattern into Gibbons-Hawking radiation due to the enormous level splitting between the critical modes $\hat{a}_k$ and their free counterparts $\hat{b}_k$, as discussed in section 2.4.1. The stored quantum information therefore backreacts on the evolution that renders Gibbons-Hawking emission more and more unfavorable. Thus, after a finite time the memory burden becomes unbearable and the emission stops.

It is likely that quantum breaking of de Sitter is a signal of a fundamental quantum inconsistency of theories with positive *constant* vacuum energy [24], [31], [34]. For alternative views we refer to other works e.g., [78]–[80]). Before we continue, we want to stress the fundamental importance if not confusing the quantum breaking phenomenon with a possible instability of the type suggested in [81], [82]. Quantum breaking [24], [31], [34] is not accompanied by any Lyapunov exponent, that could potentially provide a graceful exit from the problem and this is the very source of a possible inconsistency.

After analyzing the case of a fundamental de Sitter originating from a constant cosmological constant term in the theory we shall study de Sitter in case of inflation. For simplicity, we shall consider a slow-roll version of inflation (see e.g. [83] or [84]) sourced by a new scalar degree of freedom called the inflaton. The dynamics of this new field allow for a continuous change of the parameters and can potentially take the system out of the de Sitter phase before it quantum breaks. A microscopic description of this type of graceful exit was given in [24]. At this point we shall not speculate whether a sensible theory can allow de Sitter cosmologies, that extend beyond the quantum breaking point. This is still an debated question and out of the scope of this thesis. However, we can still make some important physical conclusions. Regardless of the details of the final state after de Sitter has experienced quantum breaking and the question if such a description is even possible in a consistent way, it is clear that within our Hubble patch, the inflaton found a graceful exit beforehand. This scenario seems very likely, since our semi-classical description of the late inflationary epoch shows no conflict with observations. We can therefore pursue the task of searching for observable imprints of the primordial quantum

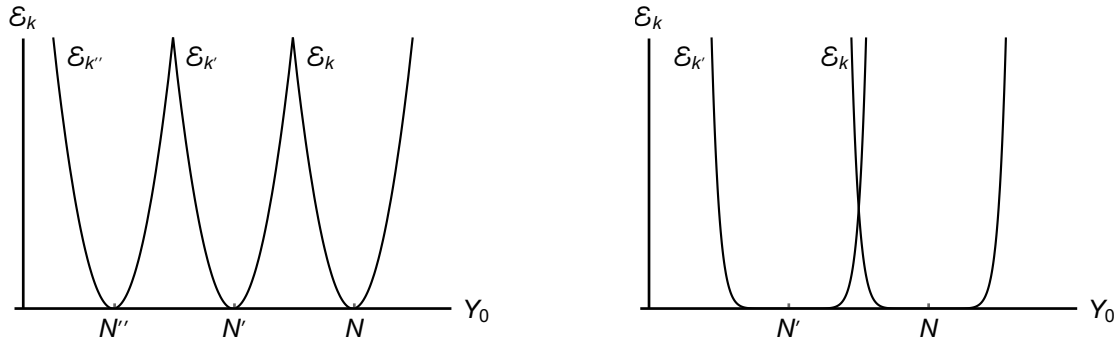

(a) Small m. (b) Large m.

Figure 3.2: Highly schematic plots (for even values of m) of the energy thresholds of the memory modes for the case of black holes. Multiple minima exist, corresponding to different possible black hole masses.

information, that leads to the memory burden. The observation and read-out of such a pattern becomes easier for a longer duration of inflation. This information can be interpreted as some kind of quantum hair. This memory pattern is stored in degrees of freedom, that were essentially gapless in the beginning. Therefore, it is not surprising that by quantum uncertainty a very long time is required for decoding a pattern, that is encoded in such a narrow energy gap.

De Sitter Versus Black Holes

As we have discussed multiple times, de Sitter spacetime and black holes share very similar quantum informational properties due to their enhanced microstate entropy. We shall discuss implications of this line of research to black holes extensively in the following section 3.2. However, here we already want to state the important question whether by a similar analogy the memory overburden could lead to an inconsistency for black holes. The answer is no [74]. Unlike the cosmological constant, the black hole mass is a parameter of the state and not the theory. This means that the theory contains many black hole states corresponding to different masses and correspondingly different entropies. To put it in a nutshell, the theory contains an entire family of states of enhanced memory capacity with different values of n_0. The corresponding energy landscape, analogue to Fig. 3.1, is plotted in Fig. 3.2.

An aspect, that was already suggested in [74] and will be discussed in greater detail in section 3.2, is that memory burden has important consequences in regard to the decay process of black holes due to Hawking evaporation. However, this does not lead to any inconsistency of the theory, since the black hole can move from a state with mass M to a state with mass M' during evaporation within the same theory, whereas de Sitter does not share this flexibility. Since the cosmological constant is a parameter of the theory and not the state, de Sitter is forever fixed to a single critical configuration set by Λ. In other words, for a fixed theory (and corresponding fixed cosmological constant) there is only a single de Sitter state.

3.2 Black Holes

As we have already discussed, black holes are nature's most efficient storage device of quantum information. Therefore, it makes sense to imagine that some of the previously discussed very general properties of systems of enhanced memory capacity should also apply to them. Specifically, we shall apply our findings on memory burden, as well as methods to alleviate the burden to black hole evolution and evaporation. Let us start with the well known fact, that the Bekenstein-Hawking entropy [7] depends on the mass M of the black hole

$$S = 4\pi G_N M^2 \,, \tag{3.4}$$

where G_N is Newton's constant. This already makes it clear that the number of gapless modes in the system has to scale with the mass, too. This has important implications in the case the black hole loosing mass due to evaporation, because then modes, that were previously gapless, have to acquire an energy gap in accordance with the reduced entropy. However, as we have iterated many times, this inevitably results in a memory burden as long as the initial state of the entropy carrying memory modes is typical, i.e. not empty. This memory burden tries to avoid any deviation from the critical configuration, ultimately back reacting to the semi-classical decay and resisting against the decrease of M. The generality of our arguments makes it hard to imagine how a black hole could avoid this fate and we conclude that similar to de Sitter spacetime a classical black hole has to quantum break at the latest when the memory burden becomes unbearable. As we have previously argued, we expect this effect to take place on a time scale not later than half-life time.

For more quantitative understanding and to judge, if rewriting can be a valid option in the black hole case, we shall adopt the model (2.97) and choose its parameters to mimic gravity as closely as possible. To find a concrete mapping between black hole characteristics and the parameter of our model, we shall again rely on a particular microscopic theory and employ again the black hole quantum N portrait [11] for this task. We want to reiterate that none of our results depend on the specifics of this particular theory and we shall only use it as a dictionary for our parameters.

To facilitate a precise mapping let us briefly state the connections of the N portrait and our many particle model (2.97). For more details we refer to our short review in section 1.5 or to the original paper [11]. In the N portrait a black hole represents a saturated bound state of soft gravitons at the critical point of a quantum phase transition. The role of the master mode $\hat{a}_0$ in our model can be identified with high wavelength gravitons which are constituting the background field responsible for the classical metric. Their characteristic wavelength is set by the Schwarzschild radius $r_g = 2G_N M$. Due to their naturally low gap they can he highly populated and, because of the attractive nature of gravitational interaction, assist other modes in becoming gapless. Without the background created by the low frequency modes those other modes would represent very high momentum modes with large free energy gaps and would therefore naturally not contribute to the microstate entropy of a black hole. While low momentum modes provide the classical background, these high momentum modes, which are rendered gapless due to the critical occupation of the former, are responsible for the Bekenstein-Hawking entropy (3.4).

Interpreting a black hole as a multi-particle bound state of soft gravitons, similar to a Bose-Einstein condensate, also allows for an easy incorporation and interpretation of Hawking evaporation [8]. In this picture the outgoing Hawking radiation is a result of quantum depletion process in which, similar to a condensate, the black hole loses constituents due to internal rescattering. Consequently, some of the particles of the master mode get converted into free quanta and the occupation number of the master mode decreases. The role of outgoing radiation is taken by $\hat{b}_0$ modes in our model. Of course, our model doesn't incorporate outgoing particles, since $\hat{a}_0$ and $\hat{b}_0$ can oscillate into each other. So our model can only capture a decay process, as long as the occupation in the $\hat{b}_0$ modes can be safely neglected. We expect that our mapping will therefore break down at the latest after $\hat{a}_0$ is getting populated again. There is a second reason why our model can't capture black hole evolution on long timescales. Classically, M is a free parameter of the system and black holes exist for all possible values of the mass. This means that for every M there exists a specific set of modes that become gapless to account for the entropy at this specific value. Furthermore, during decay this set of mode changes accordingly to the loosing mass. In contrast to that, our model only consists of two fixed sets of modes that become gapless for two distinct occupation values of the master mode. Setting up the correspondence initially for a certain mass M corresponding to a specific number of particles in the master mode $\hat{a}_0$, the mapping will only last as long as the deviation from the initial mass is not too big. Early times are incorporated with our second sector of memory modes, however, as soon as a third memory sector would become important our correspondence breaks down. Finally, our model does respect particle number conservation, gravity, on the other hand, does not. However, as we have discussed in section 2.4.10, this does not affect our conclusion, since the nature of interaction is not of importance for the attempt to alleviate memory burden.

In the following we present the specific mapping between our model parameters and characteristics of a classical Schwarzschild black hole:

- The elementary gap of a black hole is set by the inverse of its Schwarzschild radius r_g. Therefore we set the free gap of the master mode $\epsilon_0 = r_g^{-1}$. Since in our model this also determines the gap of the free counterpart $\hat{b}_0$, this also ensures that Hawking quanta correctly show the typical energy r_g^{-1}.

- To reproduce the correct entropy (3.4), we consider K memory modes in the first sector. According to Eq. (2.9) this leads to a microstate entropy of $S \simeq K$.

- As the initial occupation in the gapless memory sector we set $N_m = K/2$. In the limit of macroscopic black holes this corresponds to the most likely occupation number, since the number of patterns with different N_m is insignificant for $S \ll 1$.

- Due to its spherical symmetry we can label black hole states by the quantum numbers (l, m) of angular spherical harmonics. Assuming that excitations in radial modes are negligible, to account for the K modes that are necessary for the entropy S we have to occupy states at least until $l \sim \sqrt{K}$. This takes into account that the degeneracy of spherical harmonics scales as l for each level. Therefore, the highest modes have an energy that scales with $\sqrt{K}$. We set the free energy gap of the

memory modes to $\epsilon_k = \sqrt{K}\epsilon_0$. Note that in a black hole this would correspond to Planckian energy scales, $\epsilon_k \sim 1/\sqrt{G_N}$.

- Using only generic arguments about black hole properties, the exact value of the critical occupation N_c, remains a free parameter. We shall rely here on the N portrait which motivates the choice $N_c = S$. In this model the total energy of the black hole is then reproduced by $M = N_c\epsilon_0$.
- The coupling strengths C_0 and C_k remain undetermined and free parameters at this point. We shall, however, find consistency bounds below.

In summary, we can express all parameters of our model (2.97) in terms of the entropy and the Schwarzschild radius. For convenience we briefly reiterate the mapping in a concise manner:

$$\epsilon_0 = r_g^{-1}\,, \qquad N_c = S\,, \qquad K = S\,, \qquad N_m = S/2\,, \qquad \epsilon_k = \sqrt{S}r_g^{-1}\,. \tag{3.5}$$

Next we shall also cast the bounds on the coupling (2.108) and (2.111) to a form using black hole parameters. Gravitational interaction is universal, therefore all couplings have to be of the same order. Consequently, we use the stronger bound of those two and constrain the couplings with

$$C_{k,k'} \sim \tilde{C}_{k,l} \lesssim \frac{\epsilon_0}{S}\,. \tag{3.6}$$

Note that we used here again the assumption that the disturbance of the effective gaps scales with $\sqrt{N_m}$ rather than linearly in N_m, thus leading to softer constraints. In gravity this might not be the case and the real constraints may apply.
Since the gravitational interaction scales with energy, gravity also sets a bound on the coupling between $\hat{a}_0$ and $\hat{b}_0$ modes:

$$C_0 \lesssim \frac{\epsilon_0}{\sqrt{S}}\,. \tag{3.7}$$

Concluding we want to comment on additional shortcomings of our model. Since gravitational interaction is universal, our model should also contain couplings of the form $\hat{a}_k$ and $\hat{b}_k$ similar to the master mode and its free analogue. We have already concluded in section 2.4 that such an interaction is not efficient enough to avoid memory burden and here we shall argue why the reasoning is unchanged in the black hole case. Again, in real gravity the memory modes $\hat{a}_k$ with momentum label k, couple to their free counter part, which we shall denote with $\hat{b}_k$. However, those $\hat{b}_k$ are not subject to the effect of *assisted gaplessness*. Therefore, these (Planckian) modes satisfy the free dispersion relation and correspondingly have a huge energy gap. This setup can be described by the following Hamiltonian:

$$\hat{H}_{\text{higher}} = \sum_{k=1}^{K} \epsilon_k \hat{b}_k^\dagger \hat{b}_k + \sum_{k=1}^{K} C_k \left(\hat{a}_k^\dagger \hat{b}_k + \hat{b}_k^\dagger \hat{a}_k\right) + \sum_{k'=1}^{K'} C_{k'} \left(\hat{a}_{k'}'^\dagger \hat{b}_{k'} + \hat{b}_{k'}^\dagger \hat{a}_{k'}'\right)\,. \tag{3.8}$$

As before, we have $\epsilon_k = \sqrt{S}\epsilon_0$. Since we know the entropy of the black hole, we can now estimate bounds on the couplings C_k to ensure that the entropy-carrying modes $\hat{a}_k$ stay

sufficiently gapless. The corresponding coupling matrix, in case we start in the critical configuration $n_0 = N_c$, is

$$\begin{pmatrix} 0 & C_k \\ C_k & \epsilon_0\sqrt{S} \end{pmatrix} . \tag{3.9}$$

Still requiring that the effective gaps are not disturbed by more than $\epsilon_0/\sqrt{S}$, it follows that $C_k^2/(\epsilon_0\sqrt{S}) \lesssim \epsilon_0/\sqrt{S}$, i.e. $C_k \lesssim \epsilon_0$. Therefore, as we have stated previously, due to the enormous level splitting any transition between memory mode excitations and $\hat{b}_k$ modes is severely suppressed. Thus, the free modes stay unoccupied during the time of evolution. From a quantum informational point of view any leakage of the information stored in the memory modes to external free modes is highly suppressed. This mechanism was proposed in [74] as the microscopic explanation, why black holes at early stages of its evolution release energy, but almost not information. This fact is often considered as one of the mysteries of black hole physics. However, this setup offers a simple explanation to this well known fact: The large level splitting between the memory modes that are subject to assisted gaplessness and their free counterparts, combined with the bounds on the couplings to avoid losing gaplessness in the first place, prevents any efficient transfer of information.

Since it is apparent now that the $\hat{b}_k$ modes stay unoccupied, the fact that we did not include them in our numerical studies turns out to be of no importance.

3.2.1 Numerical Studies

We shall study our prototype system for memory burden and rewriting for the specific black hole parameters (3.5) numerically. As we have already discussed, the only free parameters remaining are the coupling of the master mode to the environment reservoir C_0, the overall coupling strength between the memory modes C_k and the distance between the two critical configurations ΔN_c and more specifically independent of the black hole entropy S. However, we can at least put bounds on these parameters. The specific black hole constraint (3.7) relates C_0 to S. Furthermore, the consistency requirement that the two memory sectors are sufficiently separated from each other (see the constraint (2.104)) and more specifically, the requirement that the separation of levels should not go to zero for large N_c, i.e. ΔN_c should not decrease with increasing N_c, leads to a bound for ΔN_c, namely

$$\Delta N_c \gg 1. \tag{3.10}$$

Using the observed scalings stated previously in section 2.4.5, namely Eqs. (2.117)-(2.119), for the coupling values, at which rewriting takes place, we get

$$C_{\mathrm{m}} \sim S^{-0.5+\beta_C}(\Delta N_c/S)^{0.2} \gtrsim S^{-0.7+\beta_C} , \tag{3.11}$$

as well as[1]

$$\Gamma \gtrsim S^{-1.7+\beta_\Gamma} . \tag{3.12}$$

[1]Since $\Delta N_c/S \to 0$, the rate Γ becomes independent from ΔN_c.

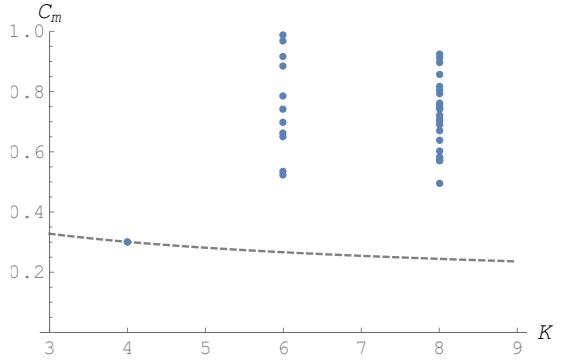

(a) Rewriting values of C_{m}

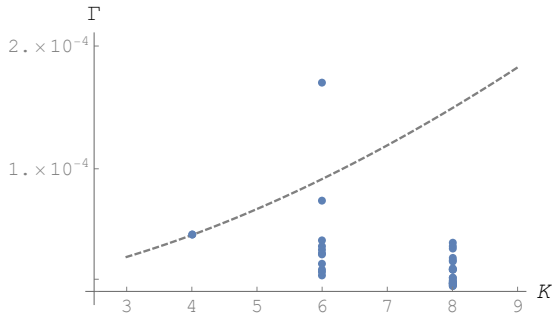

(b) Rates Γ at those rewriting values

Figure 3.3: Available data (blue dots) for the rewriting values of C_m and the rates Γ as function of $K = K'$, where we take $N_m = K/2$. The dashed gray curves are the constraints (3.13) and (3.14), that apply to a black hole. We see clear indications that for large black holes, rewriting is not fast enough to reproduce the semiclassical rate of evaporation.

Eq. (3.11) shows that in order to satisfy the constraint (3.6) on the S-dependence of C_m, the scaling of C_m with K would be constrained as

$$\beta_C \lesssim -0.3\,. \tag{3.13}$$

In a similar matter it follows from Eq. (3.12) that the requirement of reproducing the semiclassical rate, $\Gamma \sim 1$, leads to

$$\beta_\Gamma \gtrsim 1.7\,. \tag{3.14}$$

Next we investigate the compatibility of the numerical results for K-variation with the bounds in Eqs. (3.13) and (3.14). We compare the actual results for $K = 6, 8$ with the expectation for $K = 6, 8$ based on the result for $K = 4$ and a scaling saturating the bounds Eqs. (3.13) and (3.14). The resulting functions are plotted in Fig. 3.3. We observe that, although many more rewriting values exist at higher K, none of them satisfies both the constraints (3.13) and (3.14).[2]

To complement this analysis we shall also invoke a different approach. With the estimates for the rewriting values and their corresponding rates (2.123) and (2.124) in mind we can evaluate how the bounds (3.13) and (3.14) fit in this picture. However, one immediately realizes that even tough the exponent β_C might be small enough to fulfill the bound, β_Γ is vastly different. Moreover, the value is not only too small, but follows a completely different trend. We therefore conclude that even though rewriting is possible in this model, which suggests that rewriting might also be taking place in black holes, it is not efficient enough to avoid memory burden on long timescales. Thus, the semiclassical rate of particle creation, $\Gamma \sim 1$ is not sustainable and the semiclassical description breaks down, as soon as the memory burden effect sets in.

[2]In fact, none of them fulfills either condition, except for one data point at $K = 6$. It has a sufficiently high rate, but its coupling strength $C_m = 0.74$ is far too big to satisfy the bound (3.13).

In contrast to the behavior of our model (2.113) we expect the semiclassical description to be valid for newly formed macroscopical black holes. So at least at initial times the particle production according to Hawking's rate should be sustainable. Since our model incorporates immediate backreaction due to memory burden and rewriting is by no means efficient enough to keep up with the free rate, we observe an instant deviation. Therefore, our model can obviously not catch this early time behavior accurately and a real black hole has to realize an appropriate delay of the onset of memory burden. A possible mechanism to delay the memory burden effect was discussed in section 2.4 which entails making it a higher order process by choosing an appropriate exponent $p \gg 1$. With that however, it was not possible to get rid of the memory burden altogether, but only do delay it. The upper bound for such a delay is on the order of half-life time in case of a constant decay rate. The delay can be maintained at most until the master mode has lost on the order of half of its initial occupation, corresponding in the black hole N portrait to the order of half of its mass. Summarizing, a black hole first has to delay the memory burden to keep up with the semi-classical description, but after long enough timescale it will run into the memory burden effect and since rewriting is not an efficient enough process, experience a backreaction resulting in a break down of the semi-classical approximation.

After discussing the qualitative result that a black hole will experience memory burden and the break down of the semi-classical description at the latest after it has lost half of its mass we give a quantitative estimate on how strong the slowdown is, assuming that black hole evolution continues through a process of rewriting. Remember that in order to keep up with the semi-classical rate $\Gamma \sim 1$ during initial evolution, the coupling strength has to scale like $C_0 \sim 1/S$. Consequently, Eq. (3.12) gets modified to:

$$\Gamma \sim S^{-2.4+\beta_\Gamma} \,. \tag{3.15}$$

We emphasize again that due to numerical limitations we only have access to a small number of K values and can therefore not determine β_Γ accurately. So we pursue a less ambitious path and try to give a bound on it. There is little evidence from Eq. (2.124) that the rate increases with system size, so we conservatively estimate that $\beta_\Gamma < 0$. This gives us

$$\Gamma \lesssim \frac{1}{S^2} \,. \tag{3.16}$$

According to this analysis black hole evolution and evaporation has to drastically slow down at the latest after the black hole lost on the order of half ot its initial mass.

3.2.2 Metamorphosis

Although we could not give precise quantitative results, it is clear from the above discussion that the semi-classical approximation is not indefinitely valid. Moreover, at the latest after losing half of its mass, we expect a black hole to undergo a severe transition due to quantum backreactions. In the following, we shall discuss scenarios of black hole evolution after this point, that are consistent with above findings.

In the standard semi-classical treatment, the evaporation process of a black hole is presumed to be *self-similar*, i.e. it is assumed to be well described simply by a time-dependent mass $M(t)$, which in each moment in time determines the Schwarzschild radius

and the temperature as $r_g = 2G_N M(t)$ and $T = (8\pi G_N M(t))^{-1}$ respectively. Under the challenged assumption (see again section 1.3 for details) that Hawking's calculation can be applied to the finite mass case, black holes evaporate with a thermal emission spectrum, that shifts with the growing temperature, as the evaporation proceeds. Thus, the assumption is that a classical black hole evolves into a classical black hole of a lower mass with each quantum emission. Nevertheless, this estimate is widely accepted, despite the fact that there exist no self-consistent calculation on such timescales going beyond the semi-classical treatment. As we have already discussed in the introduction this assumption is inconsistent and can be easily challenged, since already corrections to thermality account for an order one deviation after a finite number of quanta have radiated away [19].

This immediately implies that it is unjustified to use the self-similar approximation over timescales comparable with black hole half-decay, $\tau \sim Sr_g$.

Indeed, without knowing the microscopic quantum theory, one can never be sure that the semi-classical approximation is not invalidated due to a build-up of quantum back-reaction over the span of many emissions.

This can be exactly traced in the microscopic theory of the quantum N-Portrait [11], [22]–[24]. In this picture quantum backreaction built up and become strong at the latest by the time a black hole loses of order of half of its mass. Consequently the semi-classical approximation breaks down and can no longer be used. In particular, the remaining black hole state is fully entangled after losing on the order of half of its constituents and therefore an intrinsically quantum without a classical analogue. Note, that self-similarity can only recovered in the semi-classical limit $N_c \to \infty$ [21], [85] corresponding to infinite mass.

The present study reveals a new microscopic meaning of the quantum backreaction. Namely, being states of maximal memory capacity, the black holes are expected to share the universal property of memory burden. Due to this phenomenon, the black hole evaporation rate must change drastically after losing half of its mass. What happens beyond this point can only be a subject to a guess work. However, given the tendency that the memory burden resist the quantum evaporation, the two possible outcomes are:

1. A partial stabilization by slowing down the evaporation.

2. Classical disintegration into some highly non-linear gravitational waves.

The second option becomes possible because after the breakdown of the semi-classical approximation, we cannot exclude any more that the the black hole exhibits a classical instability. Obviously, there could be a combination of the two options, where a prolonged period of slow evaporation transits into a classical instability. In the following, we shall focus on the first option as being the most interesting for the dark matter studies.

Thus, motivated from our analysis of the prototype model, we shall adopt that the increased lifetime due to the slowdown is

$$\tilde{\tau} \gtrsim r_g S^{1+k}\,, \tag{3.17}$$

where k indicates the power of additional entropy suppression of the decay rate as compared to the semiclassical rate, $\Gamma \sim r_g^{-1}$. Although the spectrum is no longer thermal,

we shall assume that the mean wavelength of quanta emitted during this stage is still on the order of the initial Schwarzschild radius $\sim r_g$, as long as the mass is still on the order of the initial mass. We must stress, however, that we cannot exclude that the black hole starts emitting much harder quanta after memory burden has set in. In particular, as the gap increases, the memory modes become easier-convertible into their free counterparts. This conversion is likely a part of the mechanism by which the information starts getting released after the black hole's half decay.

3.2.3 Small Primordial Black Holes as Dark Matter

The possible stabilization of black holes by the burden of memory could have interesting consequences for the proposal that primordial black holes (PBHs) constitute dark matter [86]–[89]. Of course, the full investigation of this parameter space requires more precise information about the behavior of black holes past their naive half life. Below, we first give a short qualitative discussion of how some of the bounds on primordial black holes change in this case. Subsequently, we provide a few quantitative considerations for one exemplary black hole mass.

There exist many different kinds of constraints on the possible abundance of PBHs (see [90], [91] for a review). However, the strength and/or the range of many of those constraints are based on the semiclassical approximation for BH evaporation, i.e. Hawking evaporation is assumed throughout the decay. Therefore, a slowdown due to the backreaction in form of memory burden, which sets in after the half-decay, affects the landscape of constraints quite dramatically.

If the validity of the semiclassical approximation is assumed throughout the whole decay process, all PBH with masses $M \lesssim M_* \equiv 5 \cdot 10^{14} g$ would have completely evaporated by the present epoch[91]. In contrast, such small PBHs can survive until today if evaporation slows down after half-decay. Thus, many of the constraints on the initial abundance of PBHs with masses $M \lesssim M_*$ are altered. In particular, a new window for PBHs as DM is opened up for some values of the mass below M_*.

For example, we can consider constraints from the galactic gamma-ray background, following [91]. Since the spectrum of photons observed due to PBHs clustering in the halo of our galaxy is dominated by their instantaneous emission, the range of the related constraints in the semiclassical picture applies to black holes with mass $M \gtrsim M_*$, with the strongest constraints coming from M close to M_* (since they would be in their final, high-energetic stage of evaporation today). On the one hand, a slowdown significantly alleviates the constraint around M_* since such black holes would now be in their second, slow phase of evaporation. On the other hand, because black holes with masses below M_* could survive until today, the galactic gamma-ray background would lead to new constraints on their abundance. At the same time, the fact that these black holes emit energetic quanta opens up a possibility to search for them via very high-energetic cosmic rays. Below we discuss this point in more detail.

As a different example, we consider constraints from BBN, as were studied in [92]. In the semiclassical picture, PBHs of mass smaller than about $M_N \equiv 10^{10}\,\mathrm{g}$ would have evaporated until then. Therefore, such black holes are typically considered to be uncon-

strained by BBN. In contrast, a slowdown would cause some PBHs with $M \lesssim M_N$ to still exist at that epoch. Therefore, BBN in principle leads to new constraints on such PBHs. However, the constraints are expected to be mild, since PBHs would already be in their second, slow phase of evaporation. On the other hand, the strong constraints on $M \sim M_N$ associated with the final stage of evaporation in the Hawking-picture is alleviated. Finally, the bound due to BBN on PBHs of masses $M \gg M_N$ is the same in the semiclassical and our picture because those black holes are in the early stages of evaporation during BBN.

In the following, we consider an exemplary scenario, in which small PBHs of mass below M_* appear to be able to constitute all of dark matter. It should be clear that we make no attempt to cover the whole spectrum of constraints or the whole range of masses, and content ourselves with rough estimates. We consider a monochromatic PBH mass spectrum with $M \sim 10^8 g$. Moreover, we need to specify how strong the slowdown is after half decay. Based on our numerical finding (3.16), we assume that the rate $\tilde{\Gamma}$ is suppressed by two powers of the entropy: $\tilde{\Gamma} \sim r_g^{-1}/S^2$. Correspondingly, we have $k = 2$ in Eq. (3.17), i.e. the lifetime $\tilde{\tau}$ is prolonged as $\tilde{\tau} \gtrsim S^2\tau$, where τ is the standard estimate based on extrapolation of Hawking's result. This leads to $\tilde{\tau} \gtrsim 10^{49}\,\mathrm{s}$ (see [93] for τ), which is longer than the age of the Universe by many orders of magnitude.

There are two kinds of constraints on the PBHs that we consider. Bounds of the first type are independent of the fact that the PBHs evaporate, i.e. they are identical to the ones for MACHOs of the same mass. We are not aware of relevant constraints for masses as low as $M \sim 10^8 g$ (see e.g. [93], [94]).[3] The second kind of bounds is due to the fact that, although with a suppressed rate, the PBHs still evaporate.

As explained above, the energy of emitted particles is expected to be around the initial black hole temperature, $T_{\mathrm{BH}} = M_p^2/(8\pi M) \sim 10^5\,\mathrm{GeV}$. Assuming that the galactic halo is dominated by the PBHs, the diffuse galactic photon flux due to the PBHs can be roughly estimated as

$$\Phi \sim n_{\mathrm{BH}}\, R\, \tilde{\Gamma} \sim 10^{-34}/(\mathrm{cm}^2\mathrm{s})\,, \tag{3.18}$$

where $R \sim 2 \cdot 10^{24}\,\mathrm{cm}$ is the typical radius of the Milky Way halo and n_{BH} is the galactic number density of PBHs. We can estimate the latter in terms of the mass of our galaxy $M_{\mathrm{MW}} \sim 2 \cdot 10^{42}\,\mathrm{kg}$ as $n_{\mathrm{BH}} \sim M_{\mathrm{MW}}/(MR^3)$. This corresponds to one particle hitting the surface of the earth approximately every 10^8 years. Clearly, it is impossible to observationally exclude such a low flux.[4] Moreover, one can wonder if the secondary flux, which predominantly comes from the decay of pions, can change the above conclusion. The answer is negative since the corresponding rate $\tilde{\Gamma}_S$ is only slightly higher than the one for primary emission, $\tilde{\Gamma}_S \sim 10\tilde{\Gamma}$ (see [92]).

Moreover, we can turn to constraints from the extragalactic gamma-ray background. Assuming that cold DM is dominated by PBHs of mass M, one can roughly estimate for

[3] Constraints would be similar to the ones on N-MACHOs [95].

[4] We are not aware of an observational lower bound on the diffuse galactic gamma-ray flux at photon energies $E_\gamma \sim 10^5\,\mathrm{GeV}$. For $E_\gamma \sim 10^3\,\mathrm{GeV}$, the observed flux is of order $10^{-10}/(\mathrm{cm}^2\mathrm{s})$ [96].

the flux due to secondary photons[5] (see [92]):

$$\Phi \sim \frac{\rho_{\rm DM}}{M}\tilde{\Gamma}\, t_0 \sim 10^{-31}/({\rm cm}^2{\rm s})\,, \tag{3.19}$$

where $\rho_{\rm DM} \sim 2 \cdot 10^{-30}\,{\rm g/cm}^3$ is the present energy density of dark matter in the Universe and $t_0 \sim 4 \cdot 10^{17}\,{\rm s}$ is the age of the Universe. Again, this flux is unobservably small.

Finally, the contribution from the considered PBHs to cosmic rays other than photons can be expected not to exceed significantly the photonic flux, in which case no bound would result from direct detection of other particles, either.

In conclusion, from the exemplary constraints considered above, the numerical example of PBHs of mass $M \sim 10^8 g$ passes an immediate test to be able to account for all DM. As stated above, a more complete analysis remains to be done.

We finish the section by making a general remark. The stabilized black holes can be detected via their emission but also via a direct encounter with earth, through gravitational or seismic disturbance. The latter possibility for standard PBH has been discussed in [98]. In the present context, the encounter becomes much more frequent and for certain masses the detection through a direct encounter could in principle become more probable than by emission spectrum.

3.3 Neural Networks

3.3.1 Mapping of Bosonic System on Neural Network

As one more application not necessarily connected gravity we shall discuss certain types of neural networks as systems of enhanced memory capacity.

This novel connection has first been suggested in [12], [13]. This section will be presented in two parts. The first one will introduce a general description of a quantum neural network by an effective Hamiltonian. After that we shall return back to our specific prototype system (2.50) and discuss its neural network representation. We shall make the identification on both a classical level, as well as a full quantum level. Note that this line of research is still in early states and requires more investigation. Before we start let us briefly review the basics of a neural network. A neural network is constituted of neurons and defined through the synaptic connections among them. Inspired from their biological analogue, these connections are usually only active and transmit information when a certain threshold of excitation is exceeded, a phenomenon often referred to as all-or-non law.

A spin-glass inspired realization of such a network, which is described by an energy function, is the Hopfield model [99]. One major advantage of this model is that it can be described in a physical language, i.e. a Hamiltonian. Since then there have been many proposals to extend the Hopfield network also to the quantum world. For an incomplete list see for example [100].

An alternative approach was proposed in [12], [13]. There the excitation level of each neuron was identified as the relevant degrees of freedom. Furthermore, these degrees

[5]The primary photons would effectively be screened by a cosmic gamma-ray horizon (see e.g. [97])

of freedom are described by an effective Hamiltonian. In this language the threshold excitations correspond to the energy gaps given by the kinetic term in the Hamiltonian. Furthermore, the synaptic connections are identified with the interaction terms grouping two or more neurons together. Consequently, the time evolution of such neural network is then generated by its effective Hamiltonian. This description has a major advantage over many other models of neural networks. Its description in terms of a Hamiltonian introduces the notion of energy and more specifically the energy cost of information storage to the system. Similar to the previous chapter this is the aspect we are most interested in. Therefore, we shall not study the learning process, let alone concrete algorithmic implementations of it, instead we shall merely focus on the energetics of information storage, recording and read-out.

The positive or negative sign of the interaction terms in the Hamiltonian translate to either a either excitatory or inhibitory synaptic connection in the neural network. This means that a certain value for the excitation of a given neuron k can either decrease or increase the probability of the excitation of another neuron j. On the physical side this of course has an energetic interpretation as a negative or positive sign translate positively or negatively respectively to the energy balance of the system.

In [12], [13] it was pointed out that a neural network with negative (and therefore attractive) interaction sign can exhibit the phenomenon of assisted gaplessness. This "gravity-like" interaction among neurons combined with certain high occupation numbers for some neurons lowers the excitation threshold for others. Therefore, these kind of networks can be considered systems of enhanced memory capacity. To illustrate that point let us consider again our simple prototype model for assisted gaplessness (2.5) and interpret it as an effective description of a quantum neural network. In this simple model all interactions come with a negative sign and are therefore attractive, or in the language of neural networks excitatory. This means that the excitation of one neuron lowers the threshold for another mode, because the synaptic connection energy of a set of interconnected neurons is negative.

To be specific, assuming that the free gap of a neuron, also denoted by ϵ is equal one, and the interaction among those is set by a strength α then the exciting a neuron to a level N, in general, lowers the threshold for the connected neurons by an amount of amount $\sim \alpha N$. This is a completely analogue effect to assisted gaplessness in a multi-particle quantum mechanical system as it was described above. Weak attractive/excitatory interaction in combination with high occupation/excitation of some modes/neurons assist other modes/neurons in becoming gapless. At the critical point the excitation threshold is lowered to zero up to an accuracy of order the coupling constant α. This has some important consequences because it results in a situation in which the effect of assisted gaplessness can become stronger for weaker coupling strength. Equivalent to the case of cold atoms lowering the coupling strength and while simultaneously increasing the excitation of a certain set of neurons such that their collective synaptic interaction αN remains constant, results in an state of enhanced memory capacity. Taking again the analogue limit of (2.17) makes the energy cost for storing a certain pattern more and more narrow and correspondingly the amount of possible stored patterns arbitrarily large. Note that in a similar fashion as for the multi-particle system we code information in the neural network

in the excitation numbers of its constituents. That these apparent similarities between a quantum neural network and a bosonic quantum field theory are in fact isomorphic has been shown in [13]. This isomorphism identifies the neural degrees of freedom with the momentum modes of a quantum field whereas the synaptic connections correspond to the interaction among different mode operators. Consequently, this identification allows to treat quantum neural networks on the same footing as a set of coupled harmonic oscillators from the perspective of enhanced memory capacity. This might also have intriguing experimental perspectives since it allows to simulate such a quantum neural network in a system of a cold Bose gas.

We can now use this mapping to represent our previously studied 3-mode system in section 2.2.3 as a neural network. Consequently we shall identify each momentum mode as a neuron and the interaction between different oscillatory modes as synaptic connections [6]. This neural network is visualized in Fig. 3.4.

Next, we shall make the connection even more explicit by writing the original Hamiltonian (2.50) in the language of a neural network. Therefore we case the Hamiltonian in following form

$$\hat{H} = \sum_{k=1}^{3} \epsilon_k \hat{a}_k^\dagger \hat{a}_k - \sum_{k,j=1}^{3} \hat{a}_k^\dagger \hat{\mathcal{W}}_{kj} \hat{a}_j \,, \tag{3.20}$$

where $\epsilon_k = \frac{1}{4}k^2$ is the threshold excitation energy of the k^{th} neuron and $\hat{\mathcal{W}}_{kj}$ is a Hermitian 3×3 operator valued matrix representing the synaptic connections. Its elements read:

$$\hat{\mathcal{W}}_{11} = \frac{3\alpha}{8} \hat{a}_1^\dagger \hat{a}_1 \,, \tag{3.21a}$$

$$\hat{\mathcal{W}}_{22} = \frac{3\alpha}{8} \hat{a}_2^\dagger \hat{a}_2 \,, \tag{3.21b}$$

$$\hat{\mathcal{W}}_{33} = \frac{3\alpha}{8} \hat{a}_3^\dagger \hat{a}_3 \,, \tag{3.21c}$$

$$\hat{\mathcal{W}}_{12} = \frac{\alpha}{8} \left(4\hat{a}_2^\dagger \hat{a}_1 + 2\hat{a}_1^\dagger \hat{a}_2 + \frac{4}{3} \hat{a}_2^\dagger \hat{a}_3 + \hat{a}_3^\dagger \hat{a}_2 \right) , \tag{3.21d}$$

$$\hat{\mathcal{W}}_{13} = \frac{\alpha}{8} \left(4\hat{a}_3^\dagger \hat{a}_1 + 2\hat{a}_1^\dagger \hat{a}_3 + \frac{4}{3} \hat{a}_2^\dagger \hat{a}_2 - 2\hat{a}_1^\dagger \hat{a}_1 \right) , \tag{3.21e}$$

$$\hat{\mathcal{W}}_{23} = \frac{\alpha}{8} \left(4\hat{a}_3^\dagger \hat{a}_2 + 2\hat{a}_2^\dagger \hat{a}_3 + \frac{4}{3} \hat{a}_1^\dagger \hat{a}_2 + \hat{a}_2^\dagger \hat{a}_1 \right) . \tag{3.21f}$$

After recasting the neural network in the form of an Hamiltonian we can directly apply our reasoning on systems of enhanced memory capacity to neural networks.

[6] Note that this simple three neuron system would not be useful for actual learning purposes nor as a storing device. As the system (2.50) was primary studied for its intrinsic quantum information storage properties this simple neural network only qualifies as a capacitor of information. This specifically means that it misses a coupling to the outside world to receive input data or retrieve it afterwards again. So we only consider the case which involves no input or output operations.

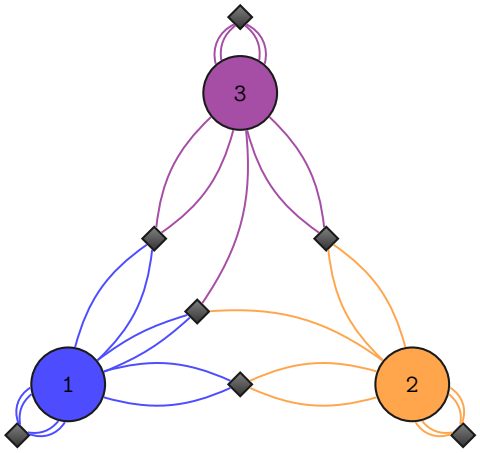

Figure 3.4: Representation of the Hamiltonian (2.50) as a neural network. The three neurons are displayed as circles and diamonds represent interaction terms. The number of lines to a diamond indicates how many mode operators of the corresponding neuron participate in the interaction.

3.3.2 Enhanced Memory Storage

For later comparison we shall first study the memory capacity in form of the energy cost of storing a specific pattern in the non critical case. So we shall first consider the case in which the total excitation of each neuron is well above the critical level, $N \ll \frac{1}{\alpha}$. Note that we again assume that the neurons are weakly coupled, $\alpha \ll 1$. In this case the negative contributions to the energy originating from the exitatory interaction is negligible. Therefore the free gaps are almost unaltered and consequently the energy cost for storing information is high. Again we shall quantize the lowering of energy cost by assisted gaplessness by the collective coupling $\lambda = \alpha N$. Note that in the regime of low excitation levels this is a small number, $N \ll \frac{1}{\alpha}$. Therefore the energy difference between tow patterns encoding information in the excitation numbers of the different neurons is large. Let $|N - n_2 - n_3, n_2, n_3\rangle$ and $|N - n_2' - n_3', n_2', n_3'\rangle$ be two distinct memory patterns. Then their difference in energy is mostly due to the free excitation cost given by the first term in (3.20). Since $\epsilon_k \gtrsim 1$ this is a large number and given by

$$\Delta E_{\lambda \ll 1} = \frac{1}{4}\left(3(n_2' - n_2) + 8(n_3' - n_3)\right) + \mathcal{O}(\lambda)\,. \tag{3.22}$$

Therefore, the set of different patterns range over a large energy interval. This means that the capacity of information storage for a fixed infinitesimal energy interval is very small and the neural network is not considered to be a system of enhanced memory capacity. For example, in order to rewrite a pattern stored in the number eigenstate $|N, 0, 0\rangle$ into $|N - 1, 1, 0\rangle$, we need to pay a energy fee $\Delta E \simeq \frac{3}{4}$, i.e, an external stimulus that is needed for the redial of information $|N, 0, 0\rangle \to |N - 1, 1, 0\rangle$ has to have an energy of order $\sim \frac{3}{4}$.

Next we shall consider the more interesting case in which we succeedingly increase the total excitation level N which is given by the sum of the individual neurons of the

network. By increasing N we simultaneously strengthen the collective synaptic connection λ and with that the contribution of the synaptic connection energy. Remember that this coupling is attractive so it helps lowering the overall energy of the system. By starting to excite a certain subset of neurons helps to gradually lower the excitation thresholds of the neighboring ones due to this negative synaptic connection. These thresholds are the smallest whenever the total excitation level N of all neurons reaches the critical value. Completely equivalent to the case of a Bose gas this critical point is given by

$$\lambda_{lm} = \alpha N. \tag{3.23}$$

For this special value a state of enhanced memory capacity emerges. This means that a a large subspace in pattern space opens up that is now energetically accessible to the system. We can estimate how the remaining energy gap scales as a number of total excitation. As it is apparent from the Bogoliubov analysis in previous chapters it is given by a inverse power law:

$$\Delta E_{\lambda=\lambda_{lm}} \sim \frac{1}{N^{\beta}}\,, \tag{3.24}$$

where β is a positive constant. This means that around the critical point we can make the gaps arbitrarily small by making again use of the double scaling limit (2.17). This results into an extremely efficient configuration to store quantum information encoded in the occupation or equivalently excitation level of the neurons in the network.

Up until now we have considered a quantum Hamiltonian consisting of operator valued quantum oscillators. Let us now move to classical neural networks. For this sake we shall use coherent states. By moving to a basis of coherent state we can replace operators in the Hamiltonian by their respective expectation value of this classical configuration. Note that the choice of coherent states as mediator of classicality is of course not unique. Consequently, this procedure yields a c-number valued energy function $H_{\text{bog}}(\vec{a}, \vec{a}^*)$ which describes the quantum network (3.20) in the classical analogue system.

Note that in a classical setting only the expectation values of occupation numbers for the different modes/neurons might be available. This pattern vector therefore naturally contains less information than the full quantum state. However, an external read-out or dial-in device might not be sensitive enough to resolve the full quantum picture of the storing device. For this reason the appropriate characteristics to code information has to be chosen. For example if the neural network is in a coherent state which can be described by three complex numbers $|a_1, a_2, a_3\rangle$ the read-out device might only be capable to resolve the absolute value of these number which of course contains less information compared to the full state. There might be the case the readout device is also capable of resolve also all phases. In this case the full quantum state of the network we can used as a pattern vector. To put it short, the coding scheme has of course be adjusted to the readout capabilities of the external connection.

Let us continue with a specific example for a code for a pattern vector in the system (3.20). First we consider the case in which the read-out device can resolve the full quantum state. Then we can take advantage of the previously introduced parametrization (2.51).

we write a memory pattern as

$$\begin{pmatrix} a_1 \\ a_2 \\ a_3 \end{pmatrix} = \sqrt{N} \begin{pmatrix} \sqrt{1-x}\cos(\theta) \\ \sqrt{x}e^{i\Delta_2} \\ \sqrt{1-x}\sin(\theta)e^{i\Delta_3} \end{pmatrix}, \tag{3.25}$$

where as before $0 \leq x \leq 1$. In contrast to that, in case the read-out device is not capable of catching the full quantum information encoded in a state vector we have to waive for example the information of the phases. For this purposes it would be equivalent to set $\Delta_2 = \Delta_3 = 0$ in the pattern vector (3.25). Let us again briefly review the mechanism of assisted gaplessness on the example of the specific neural network (3.20). First remember that we are working again in the Bogoliubov approximation of large occupation numbers, therefore we expect $1/N$ corrections to the following reasoning. In case of small collective synaptic connection $\lambda \ll 1$, the interaction term between different neurons is minuscule and the main contribution to the energy function comes from the free excitation thresholds resulting in an energy difference between different memory pattern given by (3.22). Keeping in mind that by counting different distinguishable microstate in the coherent state basis one has to be careful not to overcount only patterns that sufficiently differ in occupation numbers can be used for storing information. Because otherwise those memory patterns would share a too large overlap and could not be distinguished on a reasonable timescale. Therefore the energy difference for useful patterns is given by the threshold excitation energy, which are large in the current example, i.e. $\Delta E \gtrsim 1$. However, by bringing the quantum neural network into a critical configuration, this story changes dramatically. The closer the system gets to stationary inflection point in the Bogoliubov Hamiltonian $H_{\text{bog}}(\vec{a}, \vec{a}^*)$ of the neural network (3.20) the energy price one has to pay to redial the pattern vector becomes succeedingly more narrow, see Eq. (3.24). Therefore this gap can be made arbitrarily small by getting closer and closer to the critical value. This allows us to store information encoded in memory patterns (3.25) in an arbitrarily narrow energy gap. Note again the $1/N$ corrections in case of finite total excitation level. Let us repeat the steps to attain such a state in the language of a neural network. Again assuming a small synaptic interaction $\alpha \ll 1$ in the neural network (3.20). Gaplessness comes however not for free, therefore the first step is to "invest" in the network by increasing the total excitation level of the neural network to a total level of $N = \lambda_{lm}/\alpha \approx 1.8/\alpha$. Next, we have to shift the distribution of the excitation number N among the thee neurons such that their expectation values match the stationary inflection point in the Bogoliubov Hamiltonian approximation. This means one has to choose $\langle \hat{a}_2^\dagger \hat{a}_2 \rangle = x_{\text{inf}} N \approx 0.32N$, as well as $\langle \hat{a}_1^\dagger \hat{a}_1 \rangle = (1-x_{\text{inf}})\cos^2(\theta_{\text{inf}})N \approx 0.67N$ and $\langle \hat{a}_3^\dagger \hat{a}_3 \rangle = (1-x_{\text{inf}})\sin^2(\theta_{\text{inf}})N \approx 0.01N$. By preparing the neural network in this critical state collective nearly gapless excitations emerge and an increasing number of distinct patterns can be stored in a small energy gap, provided N is big enough. This procedure of course reproduces the findings visualized in Fig. 2.4b. Let us reiterate that this plot is technically only valid in the limit of infinite particle numbers $N \to \infty$ and corrections appear for finite values that scale as powers of $1/N$. This applies not only to the specific value of the gap but also to the exact location of the critical point in terms of the collective synaptic interaction λ_{lm}. We have quantified those finite size effects for a range of different N in Fig. 2.7.

As we have seen in section 2.2.3, a narrow energy gap directly leads to slow time evolution or equivalently an enhanced longevity of the specific state. We quantified this timescale t_{coh} as the duration on which the excitation levels, which determine a memory pattern change significantly. The time evolution for the corresponding Bose gas system is shown in Fig. 2.5. For states that are not critical this is illustrated in Fig. 2.5a and 2.5c. This timescale is short and approximately given by $t_{\text{coh}} \approx 1$ in energy units of the elementary gap. Opposed to that, in case the system is in a configuration of enhanced memory capacity the state gets long-lasting. This is shown in Fig. 2.5b where the coherence time is $t_{\text{coh}} \gg 1$. This timescale for different values of λ was studied in Fig. 2.6. In summary, if we prepare the system in a critical state, the time evolution significantly slows down compared to non critical configurations.

To conclude let us summarize the mechanism of applying assisted gaplessness to quantum neural networks. Since the synaptic connections are excitatory, at a certain critical value a flat direction appears in the energy landscape of the corresponding energy function. Moving along this flat direction at the stationary inflection point disturbs the systems without changing its energy balance. These perturbations can be used to store information energetically efficiently. At this point a large portion of pattern space opens up that are approximate degenerate in energy. At first glance, on would expect these states to mix and scramble the information on a very short timescale. Due to their gapless nature however, their time evolution is significantly slowed down. This allows us to distinguish them even after a long time scale since they evolve very slowly. Therefore, it is possible to store information and read it out again on a timescale shorter than the timescale of evolution.

Summarizing we can identify a system of oscillatory quantum modes, as they for example appear in a cold bosonic gas, with a quantum neural network in the way described in [13]. To illustrate this we mapped the truncated system (2.50) to the neural network described by Eq. (3.20). Although this network only consists of three neurons, the system already exhibits remarkably complex features, which it of course shares with its analogue system from which it was derived. Most interesting for our purposes this network also features the mechanism of assisted gaplessness and can therefore be brought into a state of enhanced memory capacity, in which it becomes an ideal storer of quantum information. This behavior also persists when taking the classical limit of the neural network by using coherent states. This dictionary might have exciting implications for simulating such quantum neural networks in experiments with cold bosons.

Chapter 4

Cosmic Attractor Solution to The Hierarchy Problem

The Hierarchy Problem is the question why the Higgs mass is so light in contrast to its sensitivity to any physics above the electroweak scale. One proposal to explain this puzzling hierarchy is the cosmic relaxation scenario of the Higgs vacuum expectation value by forward by Dvali and Vilenkin. In this chapter we shall numerically investigate this model.

First we briefly review core concepts of the cosmic attractor solution to the Hierarchy Problem suggested by G. Dvali and A. Vilenkin in section 4.1. After that we model the nucleation of branes as a random walk and simulate the relaxation process in section 4.2. In section 4.3 we compare our findings to the attractor behavior observed in states of enhanced memory capacity.

This chapter is based on the paper [3]. To large extent, this chapter is an ad verbatim reproduction of this publication.

4.1 Cosmic Higgs VEV Relaxation Mechanism

Before we start, we shall briefly review the Cosmic Attractor model introduced in [52] with further refinements in [53] and [41]. The proposed solution to the Hierarchy Problem relies on a high degeneracy of vacua around a certain hierarchically-small value of the Higgs VEV Φ_*. We call this special value point of *enhanced entropy* since it is in spirit very similar to states of enhanced memory capacity as it was discussed in chapter 2 and 3. It is dynamically reached via brane nucleations during inflationary cosmological evolution. An important assumption in this scenario is that inflation last eternally [101], [102]. This provides infinite time for the system to converge to the point *enhanced entropy* or attractor point. In such a scenario, it is therefore *natural* to find oneself in the vacuum with maximal entropy and corresponding Higgs VEVΦ_*.

Next, we shall introduce a model implementing these ideas. This can be achieved by coupling the Higgs to a massless three-form field which is sourced by a 2-brane with charge Q set by the Higgs field itself. Such a brane can for example be resolved in form of a domain wall of a heavy axion [52], [53]. However, for the following reasoning

the fundamental nature of the brane is not important. Every crossing of a 2-brane (or axionic domain wall) leads to a jump in the field strength F with the distance set by the corresponding charge on the brane. This is modeled in following equation:

$$\Delta F = Q(\Phi). \tag{4.1}$$

On the other hand, F is back-controlling the vacuum expectation value of the Higgs field via

$$\Phi^2 = \frac{1}{\lambda}\left(\frac{F^2}{M^2} - m^2\right), \tag{4.2}$$

where λ is a coupling constant, M is some cutoff and m incorporates all other contributions to the effective Higgs mass. Using Eq. (4.1) and (4.2) the change of the Higgs VEV for small values of Q when crossing a 2-brane is

$$\Phi\Delta\Phi = -\frac{F}{M^2\lambda}Q + \mathcal{O}(Q^2). \tag{4.3}$$

The final ingredient is the exact form of the dependence of Q on Φ. With the effective brane charge given by

$$Q(\Phi) = \pm\frac{(\Phi^N - \Phi_*^N)^K}{M^{NK-2}}, \tag{4.4}$$

where N and K are positive and integer valued parameters and the sign of the charge is not fixed, the difference in the Higgs VEV for neighboring vacua vanishes for $\Phi \to \Phi_*$. Correspondingly, the density of vacua diverges at that point. The result is a probability distribution for Φ with singular peak around Φ_*. This point is called an attractor since given infinite time Φ will inevitably move arbitrarily close to Φ_*.

For derivation of equations (4.1-4.4) and further details we refer to the original papers [41], [52], [53]. In the random walk model in the following sections the terms *brane nucleation* and *timestep* are used interchangeably. Furthermore, the variables Φ and λ are measured in units of the Planck mass M_P.

4.2 Numerical Simulation of the Higgs VEV Relaxation

4.2.1 Random Walk Model

Since we are solely interested in the efficiency of the attractor mechanism we neglect all contribution to the Higgs mass other than from F, so we set $m = 0$. With that the change of Φ simplifies to

$$\Delta\Phi = \frac{Q}{\lambda M^2} = \pm\frac{(\Phi^N - \Phi_*^N)^K}{\lambda M^{NK}}. \tag{4.5}$$

Sufficiently close to the attractor backreaction on the inflationary background can be ignored, therefore the probability of nucleating a brane or an anti-brane can be assumed to be equal. Correspondingly we assign to moving either in positive or negative direction the probability $P = 0.5$.

This allows us to abstract from the Hamiltonian time evolution and considerably simplify the dynamic description. Instead of solving the Schroedinger equation of the system we translate the problem to a stochastic process. Therefore, we will model the time evolution of Φ as a symmetric random walk. This is an extremely good approximation. Because brane nucleation is a non-perturbative process and rare, the nucleation of subsequent branes in the new vacuum is not sensitive to the original direction of nucleation. In other words, by the time that a given nucleation happens the walls of the bubble from the previous nucleation are exponentially far away and do not affect the succeeding nucleation direction.

Before we simulate the system we employ one additional simplification. Since we are neglecting any quantum corrections to the attractor point, which are suspected to move the VEV from zero to the observed small value, we set $\Phi_* = 0$ in the simulation. Moreover, we merge the coupling constant λ and the cutoff M into one parameter μ and keep the exponent of this parameter independent of $\nu \equiv NK$. The change $\Delta\Phi$ at each discrete timestep (or equivalently brane nucleation) is then given in compact form by

$$\Delta\Phi(\tilde{\Phi}, \mu, \nu) = \begin{cases} +\mu\tilde{\Phi}^{\nu}, & P = 0.5 \\ -\mu\tilde{\Phi}^{\nu}, & P = 0.5 \end{cases} \tag{4.6}$$

where P denotes the probability of the specific outcome and $\tilde{\Phi}$ is the current value of the variable Φ. For the remaining free parameters we assume $\mu \in (0, 1)$ and ν is an integer and greater than one.

With that the random walk can be defined iteratively by

$$\Phi_{i+1} = \Phi_i + \Delta\Phi(\Phi_i, \mu, \nu), \tag{4.7}$$

where i indexes the brane nucleations and Φ_i denotes the value of Φ after the ith brane has nucleated.

It is straightforward to generalize this model to multiple different charges on the brane. Since these are independent from each other, the sequence in Eq. (4.7) can be generalized to

$$\Phi_{i+1} = \Phi_i + \sum_{k=1}^{d} \Delta\Phi(\Phi_i, \mu_k, \nu_k), \tag{4.8}$$

for d distinct charges and possibly different and independent parameters ν_k and λ_k. So at every timestep the VEV of the Higgs is shifted by d different terms where again the sign of each contribution is equally likely due to the unfixed signs of the individual charges.

4.2.2 Simulations

The statistical model defined by Eq. (4.8) is in spite of its simple form difficult to analyze analytically. Therefore, we perform numerical simulations on a computer. Due to the statistical nature of the process, quantitative analyses can only be performed with a high number of realizations. The main focus in this section should lie on the question how the number of distinct brane charges d affects the convergence rate of the random walk.

All simulations in this section have been performed with an initial value of the Higgs VEV given by $\phi_0 = 0.1$. The two free parameters of the model were set to $\lambda = 0.5$ and $\nu = 3$, respectively and equal for all three-form fields. Every simulation was calculated for $n = 10^9$ steps. Random walks that diverged at some point were discarded from the analysis. This is justified since a Higgs particle with mass larger than the Planck mass would no longer be correspond to a elementary particle. Instead it would represent a (semi-)classical black hole as we discussed in section 1.8. For late times we plot illustrative random walks for $d = 1$ and $d = 10$ in Fig. 4.1. Matching the intuitive picture, both walks decrease on average as a function of the timestep i. Of course, the smaller Φ becomes, the slower becomes the rate in accordance with Eq. (4.6). Thus for the Higgs VEV to relax infinitely close to zero, infinite time would be required. However, this time requirement can be accounted for by eternal inflation [101], [102] as already explained in section 4.1.

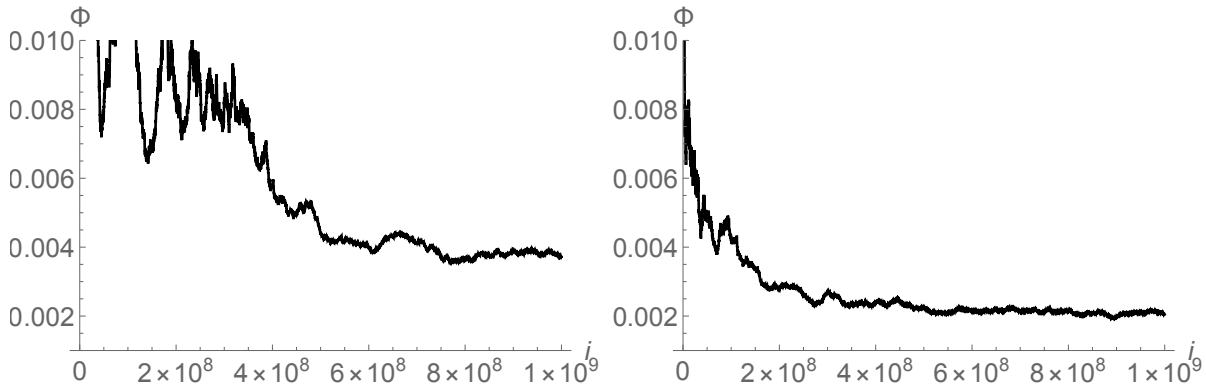

(a) $d = 1$ (b) $d = 10$

Figure 4.1: Exemplary realizations of the random walk defined in Eq. (4.8) for different number of brane charges. The parameters of the model are given by: $\mu = 0.5$, $\nu = 3$ and $\Phi_0 = 0.1$. The plot range has been set to emphasis late time behavior. In the plotted example the random walk with the higher number of charges converges faster.

Next, we analyze the dependence of the convergence rate of Φ on the number of charges d. For this purpose we average over the final value Φ_f after $n = 10^9$ steps for 100 runs for various $d \in [1, 100]$. If the run diverged at some point we reset and restarted it. The corresponding data is plotted in Fig. 4.2 in blue. In accordance with Fig. 4.1, we clearly observe an enhanced relaxation efficiency for higher d.

To obtain quantitative results we fit the data in Fig. 4.2 with a function of the form

$$f(x) = a \cdot x^b, \tag{4.9}$$

where a and b are fit parameters. The corresponding function is plotted in orange in Fig. 4.2. The fit parameters and their respective standard deviation are presented in table 4.1. The exponent matches, within statistical errors, the averaged exponent when fitting the values of Φ for individual runs. This completely matches the analytic intuition that increasing the brane nucleation channels is equivalent (up to a numerical factor) to the nucleation of more branes. The only difference that can be observed is at the beginning

when Φ is still large and when the attractor's pull is the strongest. Greater d results in larger jumps within n' steps in comparison with an equivalent run with $n'' = d \cdot n'$ steps and only one charge. For later times and small Φ, however, the difference between jump distances for neighboring values of Φ becomes negligible.

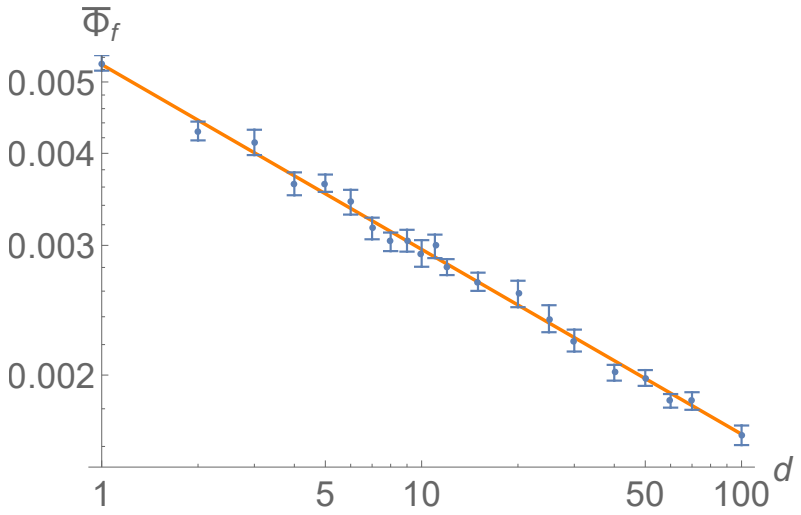

Figure 4.2: Average final value $\overline{\Phi}_f$ after $n = 10^9$ timesteps as a function of the number of charges d. For every point the average has been taken over 100 runs. For a fit function of the form $a \cdot x^b$ the parameters attain following values: $a = 0.0053$ and $b = -0.25$ with standard errors $\sigma_a = 5.3 \cdot 10^{-5}$ and $\sigma_b = 0.005$. The parameters of model (4.8) have been set to $\mu = 0.5$ and $\nu = 3$ with an initial value given by $\Phi_0 = 0.1$. The standard error is depicted as error bars around its mean value.

To map the parameter space at least partially we repeated the analysis also for $\nu \in \{2, 4\}$[1] The results of the random walks are presented in table 4.1. Matching our previous findings, we observe again that the inclusion of more brane charges is up to a numerical factor equivalent to additional nucleation of branes. We also checked for $\nu = 3$ that varying $\mu \in [0.05, 0.5]$ only results in a change of the prefactor a. We expect this behavior to hold also for smaller values of μ.

To summarize our findings, we observe a clear tendency that the system moves towards smaller and smaller values of Φ on long enough timescales on a large range of parameters. This fully matches the analytic consideration in the original papers [52], [53]. We extended previous work by including additional brane charges in the numerical simulation and, moreover, provided quantitative estimates for the relaxation rate in a simplified toy model.

[1]Within the considered number of steps the numerical value of $\Delta\Phi$ with $\nu \geq 5$ can not be resolved accurately enough with standard machine precision. However, this problem can of course in principle be solved with significant increase in computational complexity. However, we don't expect any significant deviation from our results for this parameter range.

ν	a	σ_a	b	σ_b	$\tilde{a}$	$\sigma_{\tilde{a}}$	$\tilde{b}$	$\sigma_{\tilde{b}}$
2	$4.8 \cdot 10^{-5}$	$1.1 \cdot 10^{-6}$	-0.48	0.014	0.05	0.02	-0.5	0.04
3	0.0053	$5.3 \cdot 10^{-5}$	-0.25	0.005	0.17	0.07	-0.25	0.06
4	0.026	$2 \cdot 10^{-4}$	-0.17	$2.7 \cdot 10^{-3}$	0.25	0.1	-0.16	0.04

Table 4.1: Fitting values for the evolution of Φ as a function of brane charges and number of nucleated branes. The values for the ladder are marked by a tilde. For both cases the fitting function is of the form $a \cdot x^b$. The obtained values have been obtained by averaging over 100 realizations of the random walk. The corresponding standard errors are denoted by σ.

4.3 Comparison to States of Enhanced Memory Capacity

It is very interesting to compare the attraction behavior of the relaxing Higgs VEV to zero with the attractiveness of states of enhanced memory capacity as discussed in section 2.3.

Let us briefly repeat the key observations in section 2.3. We observed that systems, which exhibit states with an abundance of gapless degrees of freedom tend to evolve towards such critical configurations. Assuming that access to these states (including the different microstates) is not restricted for example due to energy or particle number conservation we observed that a system which is prepared in a generic state will evolve towards the one, which occupies the largest portion of the available Hilbert space.

This behavior is very similar to the one observed in section 4.2. This is because the principle mechanism behind both phenomenon is very similar in nature. To illustrate this let us identify as a macrostate in the cosmological relaxation model states in which Φ differs by a macroscopic value $\delta\Phi$. We consider different states that fit within such a macroscopically distinguishable gap as its corresponding microstates. Since according to Eq. (4.6) the distance between two states diminish the closer Φ gets to zero, the amount of microstates per macrostate increases significantly for fixed $\delta\Phi$ towards smaller value of the VEV. In this sense, configurations with smaller value of Φ have a higher microstate entropy. With this identification we can apply our findings on the attractiveness of states of enhanced memory capacity to the random walk model (4.8). For those we know that, assuming no external factors prevent it, states of an enhanced microstate degeneracy are an attractor of dynamical evolution. Of course there are also fundamental differences between those two system. First, there is no notion of energy in the random walk model (4.8) since this system is not described by an Hamiltonian. Since in principle all values of Φ are allowed in the system we can imagine them having all the same energy in this picture. Another mayor difference is that the dynamics of the systems described in section 2 are defined in terms of a Schroedinger equation in contrast to the random walk model which is given as a stochastic iteration prescription. However, this description if of course only an approximation to the full quantum mechanical dynamics. Note that the study of

Schroedinger equation in terms of a random walk was already suggested in the 1940s, see e.g. [103] or for a more modern review [104] or [105].

Chapter 5

Summary

In this last chapter we shall summarize our findings and provide a view of some future directions in this line of research. First, we shall review our findings of each chapter separately. After that we try to draw an overall conclusion and give an outlook for promising future research projects.

5.1 Systems of Enhanced Microstate Entropy - General

In the first chapter, we introduced and studied systems of enhanced memory capacity. Although, we motivated this line of research with the quantum informational properties of black holes and de Sitter spacetime we were able to find such states also in nongravitational systems. This allowed us to put our findings in a wider context and study such systems in a more general setting. Moreover, such systems can also provide an alternative laboratory for shedding new light on basic principles of information storage and processing in black holes. This approach allows both to simulate black hole quantum information features as well as to generalize them to other contexts. The great advantage of many-body quantum systems is that they are much easier to control both in experiment and in theory.

In the scope of this chapter we introduced the notion of *assisted gaplessness*, which refers to a mechanism responsible for the emergence of nearly-gapless modes. The only prerequisites for it to occur is the presence of a weak and attractive interaction and the possibility of high occupation numbers. In this case, a certain occupation of some modes assists others in becoming gapless by lowering their respective energy thresholds. We demonstrated this mechanism on the example of a simple cold gas system.

Next, we proposed an analytic procedure for identifying states of enhanced microstate entropy in the theory. Since this method relies on large occupation numbers, which allows one to replace operators by c-numbers we call it the *c-number method*. This approach is a generalization of the procedure introduced in [10] and is closely related to the Gross-Pitaevskii equation. We demonstrated our method on a simple prototype system consisting of three quantum modes. Additionally, the *c-number method* emphasizes the generality of states of enhanced memory capacity in attractive bosonic systems.

Following that, we confirmed that such states are attractors of dynamical evolution in the sense that a general system exhibiting such states will evolve towards one of them assuming that they are dynamically accessible. Furthermore, we pointed out interesting implications of these results to the concept of classicalization, in which scattering amplitudes get unitarized by the production of a macroscopic objects like black holes.

Concluding, we introduced the phenomenon of *memory burden*. It is a measure for the backreaction of the stored quantum information that ties the system to the critical configuration and works against deviations that would reintroduce an energy gap for the memory modes. Following this, we discussed possible ways to alleviate the *memory burden* in order to avoid a strong backreaction. Although we discovered ways to delay the onset of memory burden we concluded that it can not be avoided as long as the information persists in the memory sector on a timescale after which the system has experienced a significant change. For a decaying system this can be identified to its half life. Offloading the information to the environment is not efficient enough due to an enormous level splitting between the memory modes and the corresponding free modes. The only possibility to alleviate the *memory burden* is to transfer the information from the memory modes to a another set of degrees of freedom, which is also subject to the mechanism of *assisted gaplessness*. In this process, the second sector becomes increasingly mode gapless while the original memory sector acquires a gap during evaporation. At some point their energy levels cross and a transfer of occupation numbers is energetically possible. We studied this process, which we call *rewriting*, in a specific prototype system numerically.

5.2 Systems of Enhanced Microstate Entropy - Application to Gravity

In section 3.1 we have applied the concept of *memory burden* to de Sitter spacetime. This lead to a qualitatively new mechanism by which primordial quantum information could have been carried through the entire inflationary epoch of the Universe's history. Due to its Gibbons-Hawking entropy, de Sitter shares the universal properties of systems of enhanced memory capacity. Since it additionally decays in form of Gibbons-Hawking evaporation it must be subjected to the universal phenomenon of *memory burden* typical for such systems [74]. Our point is that the primordial quantum information, which is carried by the gapless modes, cannot be erased by an inflationary time evolution. Instead, it leads to a memory burden that becomes stronger with time and eventually result in a deviation from the semi-classical evaporation rate after a finite amount of time. This gives a new physical source of quantum breaking of de Sitter complementing the studies of [24], [31], [34].

Obviously, inflation must have provided a graceful exit beforehand in our Hubble patch. However, the longer inflation lasted, the stronger becomes the imprint of the primordial quantum memory. This would lead to higher chances to find an observational evidence of the primordial memory pattern. Therefore, the most interesting cases are the inflationary scenarios that end maximally close to the quantum break-time. In this case the memory burden due to the quantum information stored in the memory modes

becomes close to unbearable and this will be imprinted in cosmological observables like the primordial spectrum of density perturbations. In this way, we could, at least in principle, read out the primordial quantum information of our Universe.

Furthermore, we investigated the memory burden effect in black hole evolution.

We can choose the parameters of our prototype model in such a way that it reproduces the information-theoretic properties of a black hole, in particular its entropy. In this case, we have concluded that as far as we can numerically access the system, rewriting happens significantly too slowly to match the semi-classical rate of particle production. This strongly indicates that evaporation has to slow down drastically whenever memory burden sets in. This is to be expected at the latest after the black hole has lost mass on the order of half its initial mass.

This could open up a new parameter space for primordial black holes as dark matter candidates. For sufficiently low masses, those black holes would evaporate on a timescale shorter than the age of the Universe, if Hawking's semi-classical calculations were valid throughout their lifetime. It is often assumed that this is the case, so that the corresponding mass ranges are considered as excluded.

In contrast, a significant slowdown of the rate of energy loss, as is displayed in Eq. (3.16) for example, allows the lifetimes of such PBHs to be much longer, so that they can still exist today. In this case, small PBHs become viable dark matter candidates. In a preliminary study, we have qualitatively discussed how some of the constraints change on a concrete example.

Finally, our analysis sheds more light on a quantum theory of black holes. It has been standard to assume that black hole evaporation is self-similar all the way until the black hole reaches the size of the cutoff scale. However, this extrapolation unjustly neglects the quantum backreaction that alters the state of a black hole. The lower bound on the strength of the back-reaction effect can be derived using solely the self-consistency of Hawking formula and is $\sim 1/S$ per each emission [19]. This fact already gives a strong warning sign that we cannot extrapolate the semi-classical result over timescales of order S emissions.

5.3 Electroweak Hierarchy Problem

In chapter 4 we studied numerically the model first introduced in [52], [53] which solves the Hierarchy Problem by cosmological relaxation of the Higgs mass towards the attractor vacuum during eternal inflation.

In this scenario the Higgs vacuum expectation value changes due to nucleation of branes. At the same time the Higgs VEV acts as a back-control parameter that directs the convergence of the relaxation progress. Such an attractor could in principle be realized in various different models each with its own specifics.

In this analysis, however, we only focused on universal key features of the Cosmic Attractor mechanism. For this we have modeled the Higgs VEV evolution as a random walk with each step mimicking a vacuum transition triggered by a brane nucleation. The observed convergence to $\Phi_* = 0$, which represents our attractor point, is in accordance with analytic considerations. Additionally, this matches the finding that states with an

enhanced number of microstates are attractor of dynamical evolution similar to the system studied in chapter 2. We then generalized this stochastic model to multiple different charges sourced by a 2-brane and studied the impact of their number on the relaxation rate of the Higgs VEV. We showed that a higher number of three-form fields leads to a faster convergence rate. That is less brane nucleation are necessary to relax the Higgs vacuum expectation value below a given value. This confirms the intuitive picture that adding brane charges is equivalent to an increase of brane nucleation channels.

5.4 Overall Conclusions

All in all, we have seen that collective quantum effects may play a very important role in gravity and high energy physics in general. We have shown that, on first sight mysterious, quantum informational properties of black holes and de Sitter can in fact be found in much easier many-body systems. This opens up the intriguing possibility of understanding black hole properties in terms of universal effects and furthermore also gives a potential for implementing black hole type mechanisms for information storage and quantum computing in a laboratory.

5.5 Outlook

There are many promising directions to continue the research summarized above. One interesting path would be to study the dynamics of the information encoded in the Bekenstein entropy itself. Black holes are not only extremely efficient storage device of quantum information, but it was furthermore suggested that they are also the fastest in processing information [106], [107]. Inspired by a concrete microscopic model as the quantum N-Portrait [11], using prototype models similar to those considered in this thesis could help to draw conclusions about the question if fast scrambling is realized in black holes.

The analogue systems considered in this thesis fully abstract from the geometry and primarily focus on the quantum informational properties of black holes. It would be very exciting to extend the analogies between those condensed matter models and gravitational black holes further by also including geometrical properties such as a horizon.

As a continuation of the study of quantum breaking in de Sitter in [31], it would be very interesting to extend this analysis to the Schwarzschild metric. In this way, one could study quantum breaking in black holes more closely. This would complement the study described in section 3.2, in which a quantum informational origin of quantum breaking was discussed.

Appendix A

Formulas

In this appendix we present the Bogoliubov Hamiltonian calculated in section 2.2.3. The first and second derivative of Bogoliubov Hamiltonian (2.54) for $\Delta_2 = \Delta_3 = 0$ are given by:

$$\begin{aligned}\frac{1}{N}\frac{\partial H_{\text{bog}}}{\partial x} &= \frac{1}{16}\Big[-16\lambda\sin(2\theta) - 2\lambda\sin(4\theta) + 16\cos(2\theta) - 9\lambda + 28\lambda x\sin(2\theta) \\ &\quad + 2\lambda x\sin(4\theta) + 3\lambda(x-1)\cos(4\theta) + 21\lambda x - 4\Big], \qquad \text{(A.1a)} \\ \frac{1}{N}\frac{\partial H_{\text{bog}}}{\partial \theta} &= \frac{1}{4}(x-1)\Big[-8\sin(2\theta) + \lambda(x-1)\cos(4\theta) \\ &\quad - \lambda\cos(2\theta)\Big(3(x-1)\sin(2\theta) - 7x + 1\Big)\Big], \qquad \text{(A.1b)}\end{aligned}$$

$$\begin{aligned}\frac{1}{N}\frac{\partial^2 H_{\text{bog}}}{\partial x^2} &= \frac{1}{16}\lambda\Big(28\sin(2\theta) + 2\sin(4\theta) + 3\cos(4\theta) + 21\Big), \qquad \text{(A.2a)} \\ \frac{1}{N}\frac{\partial^2 H_{\text{bog}}}{\partial x\,\partial \theta} &= \frac{1}{4}\Big(-8\sin(2\theta) + 2\lambda(7x-4)\cos(2\theta) \\ &\quad + \lambda(x-1)(2\cos(4\theta) - 3\sin(4\theta))\Big), \qquad \text{(A.2b)} \\ \frac{1}{N}\frac{\partial^2 H_{\text{bog}}}{\partial \theta^2} &= \frac{1}{2}(1-x)\Big(8\cos(2\theta) + \lambda\Big((7x-1)\sin(2\theta) + 2(x-1)\sin(4\theta) \\ &\quad + 3(x-1)\cos(4\theta)\Big)\Big). \qquad \text{(A.2c)}\end{aligned}$$

The second-order expansion of the full quantum Hamiltonian (2.50) around the point defined by the replacements (2.51) of macroscopic occupation for $\Delta_2 = \Delta_3 = 0$ is given by

$$H_{\text{quad}} = H^{(1)}_{\text{quad}} + \frac{1}{2}H^{(2)}_{\text{quad}}, \qquad \text{(A.3)}$$

where we neglected the constant zeroth order. The first and second order terms are

furthermore given by

$$\begin{aligned}
\frac{H^{(1)}_{\text{quad}}}{\sqrt{N}} = \frac{1}{8\sqrt{(1-x)\cos^2(\theta)}}\Bigg[\\
&+ 6\hat{a}_2\sqrt{x}\Big(3\lambda(1-x)^{3/2}\sin^3(\theta) + \lambda\sqrt{1-x}(4x-3)\sin(\theta) \\
&+ (\lambda(2x-1)+1)\sqrt{-(x-1)\cos^2(\theta)} + \lambda\tan^2(\theta)\Big((1-x)\cos^2(\theta)\Big)^{3/2}\Big) \\
&+ \hat{a}_3\Big(\lambda(x-1)^2\cos(4\theta) + \lambda(7x-1)(x-1)\cos(2\theta) \\
&+ \sqrt{4-4x}\sin(\theta)\sqrt{-(x-1)\cos^2(\theta)}(3\lambda(x-1)\cos(2\theta)+8)\Big)\Bigg] \\
&+ \text{h.c.}
\end{aligned} \tag{A.4}$$

$$\begin{aligned}
H^{(2)}_{\text{quad}} = \frac{1}{128\left((1-x)\cos^2(\theta)\right)^{3/2}}\Bigg[\\
&+ 16\hat{a}_2\hat{a}_2\lambda\Bigg(\sqrt{1-x}((23-16x)x-4)\sin(\theta) \\
&+ 4(4x-1)\left((1-x)\cos^2(\theta)\right)^{3/2} \\
&- (1-x)^{3/2}\sin^3(\theta)(2(x-1)\cos(2\theta)+21x-6)\Bigg) \\
&+ 16\hat{a}_2^\dagger\hat{a}_2\Bigg(2\sec^2(\theta)(\lambda(10x-1)+3)\Big((1-x)\cos^2(\theta)\Big)^{3/2} \\
&+ \sin(\theta)\Big(-14\lambda(1-x)^{5/2}\sin^4(\theta) - 7\lambda(1-x)^{3/2}(7x-4)\sin^2(\theta) \\
&- 6\lambda\tan^3(\theta)\sec(\theta)\left(-(x-1)\cos^2(\theta)\right)^{5/2} + \lambda\sqrt{1-x}((49-32x)x-14) \\
&- 2\tan(\theta)\sec(\theta)(\lambda(13x-4)+3)\Big((1-x)\cos^2(\theta)\Big)^{3/2}\Big)\Bigg) \\
&+ 16\hat{a}_2\hat{a}_3\lambda\sqrt{x}\Big((1-x)\cos^2(\theta)\Big)\Bigg(8(x-1)\cos(2\theta) + 3x\sec^2(\theta) \\
&+ 10\sqrt{1-x}\sin(\theta)\sqrt{-(x-1)\cos^2(\theta)} - x + 1\Bigg) \\
&+ 16\hat{a}_2\hat{a}_3^\dagger\lambda\sqrt{x}\Big((1-x)\cos^2(\theta)\Big)\Bigg(10(x-1)\cos(2\theta) + 3x\sec^2(\theta) \\
&+ 2\sqrt{1-x}\sin(\theta)\sqrt{-(x-1)\cos^2(\theta)} + x - 1\Bigg)
\end{aligned}$$

$$
\begin{aligned}
&+ \hat{a}_3\hat{a}_3\lambda(x-1)\Bigg(32\cos(2\theta)\sqrt{(1-x)\cos^2(\theta)} + 32x\sqrt{(1-x)\cos^2(\theta)} \\
&+ 32\cos(4\theta)\sec^2(\theta)\Big((1-x)\cos^2(\theta)\Big)^{3/2} \\
&- 6\sqrt{1-x}\sin(\theta)(4(3x-2)\cos(2\theta) + 3(x-1)\cos(4\theta) + 17x - 5)\Bigg) \\
&+ 16\hat{a}_3\hat{a}_3^\dagger\Big((1-x)\cos^2(\theta)\Big)\sec^2(\theta)\Bigg(2(\lambda(3x-1)+8)\sqrt{(1-x)\cos^2(\theta)} \\
&+ \sin(\theta)\Bigg(\sin(\theta)\Bigg(\lambda\sin(\theta)\Bigg(5(x-1)\sin(\theta)\Bigg(3\sqrt{1-x}\sin(\theta) \\
&+ 4\sqrt{(1-x)\cos^2(\theta)}\Bigg) + 9\sqrt{1-x}(3-4x)\Bigg) \\
&- 2(\lambda(13x-11)+8)\sqrt{(1-x)\cos^2(\theta)}\Bigg) + 12\lambda\sqrt{1-x}(2x-1)\Bigg)\Bigg) \\
&+ \text{h.c.}\,. \qquad \text{(A.5)}
\end{aligned}
$$

Appendix B

Numerical Methods

In this section we briefly review the numerical methods applied in computing the time evolution in chapters 2 and 3. This section is part of the work [6], which is in preparation for publication.

B.1 Krylov Subspace Methods

Given an initial state vector $v(0)$ and a hermitian Hamiltonian H, the state at any other point in time t can be computed as

$$v(t) = e^{-iHt} v(0)\,. \tag{B.1}$$

Of course, a plethora of approaches exist to exponentiate a matrix. But the special nature of the problem (B.1) – especially the fact that in the end knowledge of the full matrix e^{iHt} is not required – allows the use of techniques that are significantly more efficient than generic routines for matrix exponentiation. Particularly important are Krylov subspace methods, which were first used in 1986 for the purpose of numerical time evolution [108]. We shall briefly sketch them now, before we review them in more detail in section B.2.1.

The m-dimensional Krylov subspace $\mathcal{K}_m$ is defined as

$$\mathcal{K}_m := \text{span}\left\{v(0), Hv(0), \ldots, (H)^{m-1} v(0)\right\}\,, \tag{B.2}$$

where $m \ll d$. Typically, one has $m \lesssim 100$. The key idea is to project the large sparse matrix H (in our case the Hamiltonian) on the small subspace $\mathcal{K}_m$:

$$H_m := H|_{\mathcal{K}_m}\,, \tag{B.3}$$

and to effectively replace

$$e^{-iHt} \quad \to \quad e^{-iH_m t}\,. \tag{B.4}$$

The last step represents the crucial approximation. It introduces the error

$$\text{err}(t) := v(t) - \tilde{v}(t)\,. \tag{B.5}$$

where $v(t)$ is the exact result (computed using e^{-iHt}) and $\tilde{v}(t)$ represents the Krylov approximation (calculated using $e^{iH_m t}$). Once matrix exponentiation is restricted to the small subspace $\mathcal{K}_m$, it can be performed very fast using standard methods. In the full Hilbert space $\mathcal{H}$, only matrix-vector multiplications, as displayed in Eq. (B.2), need to be carried out. Thus, the effectiveness of Krylov subspace methods is due the fact that no matrix-matrix multiplication has to be performed in the large Hilbert space $\mathcal{H}$.

We can estimate how large the advantage of Krylov subspace methods is. Clearly, a necessary requirement for the feasibility of the calculation is that all intermediate results can be stored in (the memory of) a computer. It turns out the this condition, and not runtime, indeed is the limiting factor in many practical applications. If one uses standard matrix exponentiation, the biggest intermediate object is the matrix e^{iHt}, which unlike H is no longer sparse. So the required storage capacity scales as the number of entries, i.e. d^2. In contrast, the largest entities that are needed for the Krylov method are the basis elements of the Krylov space (B.2), so the required memory scales as md. In practice, this leads to a gain in Hilbert space size of more than two orders of magnitude.

The Krylov subspace (B.2) is specifically adapted to the initial state $v(0)$. Therefore, one can expect that for short enough times t, the error (B.5) is small whereas it grows large once the state $v(t)$ (as determined without any approximation) deviates sufficiently from $v(0)$. Thus, it becomes necessary to restart the procedure after a certain time interval, i.e. to take $\tilde{v}(t)$, computed by the Krylov method, as initial state for a new Krylov subspace. With such a time stepping procedure in place, it has become evident since the earliest numerical studies that in many circumstances the Krylov method works surprisingly well already for values of m as small as 10 (see e.g. [108]–[111]).

At the same time, these and subsequent investigations have lead to important conceptual progress in understand how these Krylov subspace techniques work. A possibly incomplete list of important studies includes [109]–[117], where it is important to mention that these publications have a wider scope in that they deal with the exponentiation of a generic spare matrix. In the works cited above, a particularly important object of study is to provide bounds on the error (B.5). In general, one can distinguish between *a priori* and *a posteriori* error bounds. The first ones can be evaluated without actually performing the Krylov technique while the second ones rely on the result of the Krylov method. Correspondingly, *a priori* error bounds tend to be more general (and in particular independent of the initial state $v(0)$ whereas *a posteriori* error bounds are often sharper.

However, both types of rigorous error bounds typically suffer from the problem that the function that bounds the error is difficult to evaluate in practice. Therefore, *a posteriori error estimates* have been introduced in [108], [110]. They play a twofold role in numerical implementations of Krylov subspace methods. First, they are used to determine the time interval after which restarting of the Krylov procedure becomes necessary. Secondly, they can be used to estimate the error of the final result. Obviously, using error estimates instead of error bounds leads to the problem that one can in general not be sure if the outcome of the Krylov method is indeed close to the true result.

As we have discussed, Krylov subspace methods represent an efficient approximation scheme for calculating the product of an exponentiated sparse matrix and a vector. Such

a problem appears in a wide range of context. In particular, it is relevant for computing time evolution in a generic quantum system, as displayed in Eq. (B.1). In this case, the sparse matrix iH, which is exponentiated, is anti-Hermitian. From the perspective of Krylov methods, this represents a special case, but in a physical context, this encompasses the most general quantum system.

In order to actually compute the result of time evolution in a given physical system, a numerical implementation of Krylov subspace methods is required. This crucial tool was provided by Sidje in 1998 when he published the software package Expokit [118].[1] Among other routines for matrix exponentation, this program provides Krylov subspace methods for generic sparse matrices. Since certain simplifcations occur for (anti-)Hermitian matrices, Expokit contain functions that are specific to this special case, which is extremely important for physical applications. In line with our previous discussions, Expokit does not employ a rigorous error bound, but it relies on a version of the error estimate proposed in [110].

The lack of a rigorous error bound represents a serious drawback for any practical application. If the problem at hand is such that one can compute the result by means of a different method, then one can of course check the validity of the error estimates. However, in such a case there is no need to employ Krylov subspace techniques in the first place. This is to say that Krylov approximation methods are only interesting if there is no other means of solving the problem. But then one does not have any means of making sure that the error estimates still yield viable results. Therefore, it is important to come up with a rigorous error bound that can be computed efficiently within a numerical implementation.

A posteriori error bound relies on the fact that the error (B.5) fulfills a simple differential equation. This was already noticed in early papers, in particular [116], [117], and was recently pointed out more clearly in [119]–[121]. Solving this equation is not an easy task, however, in the special case of an (anti-) Hermitian matrix the necessary computation can be significantly simplified. The key point is that the norm of e^{-iHt} is always 1. This trivial observation has important consequences. As e.g. explicitly shown in [122], this allows us to slightly modify existing Krylov methods in such a way that the approximate result $\tilde{v}(t)$ is endowed with a rigorous bound on the norm of the error (B.5). In fact, our algorithm can even adapt to yield a given desired bound on the error.

The second goal of the present work is to provide a numerical implementation of that approach. We call it *The TimeEvolver*. From the outset, we specialize to the case of an (anti-)Hermitian matrix. Consequently, our software package is considerably less general than Expokit. However, it is sufficient for the most general application of quantum mechanics, namely time evolving a generic physical system. In turn, we provide an open-access and based on free software implementation of the Krylov approximation with a rigorous error bound. In this way, one can be sure that the outcome of the numerical method is indeed as close as desired to the result of an exact time evolution.

[1] In particular, it is based on the theoretical investigations [109]–[112].

B.2 The Method

B.2.1 Krylov Subspace

Following [109]–[111], we shall review known Krylov subspace methods. The first step is to compute the Krylov subspace (B.2). This can be achieved using the Arnoldi algorithm (see e.g. [123] for a review), which simplifies because H is Hermitian. With the definition $v_1 := v(0)$, we calculate for $j = 1, \dots m$:

$$\begin{aligned} w_j =& Hv_j \,, && \text{(B.6a)} \\ h_{j,j} =& \langle w_j, v_j \rangle \,, && \text{(B.6b)} \\ \tilde{w}_j =& w_j - h_{j,j} v_j - (1 - \delta_{j,1}) h_{j-1,j} v_{j-1} \,, && \text{(B.6c)} \\ h_{j,j+1} =& h_{j+1,j} = \langle \tilde{w}_j, \tilde{w}_j \rangle \,, && \text{(B.6d)} \\ v_{j+1} =& \tilde{w}_j / h_{j+1,j} \,. && \text{(B.6e)} \end{aligned}$$

As discussed in the introduction, it is important to note that no matrix-matrix multiplications $H * H$ appear but only much cheaper matrix-vector multiplications $H * v_j$. Using the Arnoldi algorithm (B.6), we determine an orthogonal matrix $V_m := [v_1, \dots v_m]$ as well as the Hermitian Hessenberg matrix $(H_m)_{i,j} := h_{i,j}$. They fulfill

$$HV_m = V_m H_m + h_{m+1,m} v_{m+1} e_m^T \,, \tag{B.7}$$

where e_m is the unit vector with entry in the m^{th} component. This implies that

$$H_m = V_m^T H V_m \,, \tag{B.8}$$

i.e. H_m is the projection of H on the subspace $\mathcal{K}_m$, in line with Eq. (B.3). So far, all statements have been exact. Now we implement the approximation (B.4), which amounts to using H_m instead of the full H. Thus, the approximate result of time evolving $v(0)$ is

$$\tilde{v}(t) = V_m e^{-iH_m t} e_1 \,. \tag{B.9}$$

The key point is that unlike H, the Hessenberg matrix H_m is small. Therefore, any standard algorithm can be used to exponentiate it without significant computational cost.

B.2.2 Error Bound

Next we want to derive a bound on the error, $\mathrm{err}(t) := v(t) - \tilde{v}(t)$, i.e. the difference of $\tilde{v}(t)$ and the result $v(t)$ of an exact time evolution (see Eq. (B.5)). It is based on the well-known observation that $\mathrm{err}(t)$ fulfills a simple differential equation [116], [117], [119]–[121]. It can be derived by first noting that

$$\tilde{v}'(t) = -iV_m H_m e^{-iH_m t} e_1 = -iH\tilde{v}(t) + ih_{m+1,m} e_m^T e^{-iH_m t} e_1 v_{m+1} \,, \tag{B.10}$$

where we used (B.7) in the second step. Therefore, it follows that

$$\mathrm{err}'(t) = -iH\,\mathrm{err}(t) - ih_{m+1,m} e_m^T e^{-iH_m t} e_1 v_{m+1} \,. \tag{B.11}$$

For the initial condition $\mathrm{err}(0) = 0$, this differential equation is solved by

$$\mathrm{err}(t) = -ih_{m+1,m} \int_0^t e_m^T e^{-iH_m\tau} e_1 e^{-i(t-\tau)H} v_{m+1} \mathrm{d}\tau \,. \tag{B.12}$$

In order to find an upper bound on the norm $||\mathrm{err}(t)||$, one has to evaluate $||e^{-i(t-\tau)H}||$. For a generic, i.e. non-Hermitian, matrix H this is very hard since it involves the exponential of a large matrix. Calculating it is as difficult as the initial problem (B.1) we set out to solve. Thus, formula (B.12) makes evident the typical difficulty of rigorous error bounds: The bounding function on the r.h.s. contains quantities that cannot be computed efficiently.

Whereas we have not gone beyond the previous studies [116], [117], [119]–[121] so far, we want to point out now that significant simplifications occur in the case that H is Hermitian. Namely, the norm of $e^{-i(t-\tau)H}$ is 1 and this allows to explicitly bound Eq. (B.12). Of course, this remark is completely straightforward, and was already pointed out for example in [122]. Moreover, it is very interesting that the case of a Hermitian matrix H, which is of extraordinary relevance in physics, leads to such simplifications. Also taking into account that v_{m+1} is normalized, we obtain the error bound

$$||\mathrm{err}(t)|| \leq \int_0^t \mathrm{d}\tau \left| h_{m+1,m} e_m^T e^{-iH_m\tau} e_1 \right| \,. \tag{B.13}$$

The key point of this formula is that it only depends on quantities that are known in the Krylov algorithm or easy to determine: The element $h_{m+1,m}$ is already computed in the Arnoldi procedure and $e^{-iH_m\tau}e_1$ can be calculated without any significant computational cost since H_m is already known and – as already said – the time needed to exponentiate the small matrix H_m is negligible. So the only remaining task it to perform the integral in Eq. (B.13) numerically. As we shall show shortly, this poses no problem.

Formula (B.13) enables us to compute an upper bound on the error for a given Krylov space and a given time interval t. However, it can do even more. We can use it to find the optimal step size for a given desired accuracy, where as explained above the step size denotes the time after which the Krylov procedure is restarted, i.e. a new Krylov subspace is computed. The input data is the time t, at which we wish to evaluate $v(t)$, and an upper bound $\mathrm{err}_{\max}$ on the error. This determines an upper bound on the error rate $\mathrm{tol}_{\mathrm{rate}}$ as follows:

$$\mathrm{tol}_{\mathrm{rate}} = \frac{\mathrm{err}_{\max}}{t} \,. \tag{B.14}$$

Now we can evaluate the error formula (B.13) at different times. The optimal step size t_{step} is the largest time for which the resulting error rate is still below the desired bound:

$$t_{\mathrm{step}} = \max_{\tilde{t}} \frac{\mathrm{err}(\tilde{t})}{\tilde{t}} \leq \mathrm{tol}_{\mathrm{rate}} \,. \tag{B.15}$$

This allows us to use a minimal number of steps while still guaranteeing a rigorous a posteriori error bound.

Note that (B.15) is of course not the only way to evaluate (B.13). Another possibility is to approximate the exponential function via a series expansion, e.g. a Hermite interpolation. For details we refer to [124].

B.2.3 Pseudocode

We shall discuss more concretely our implementation of the algorithm sketched so far. It is displayed in pseudo-code 1 and consists of repeating three steps:

1. We perform the Arnoldi algorithm as shown in Eq. (B.6). This part is completely standard. The only aspect we have not gone into so far is the special situation of a "happy breakdown". Namely it can occur that the Krylov space $\mathcal{K}_m$, as defined in Eq. (B.2), has a dimension that is smaller than m. In this case, the result of orthonormalization, as displayed in line (B.6c), is zero for some value of j. If this happens, working in the Krylov subspace is no longer an approximation but yields an exact result. This means that our problem is solved and we can stop the algorithm. We shall not further discuss this special case.

2. We find the optimal step size according to Eq. (B.15). This requires evaluation of the integral in the error formula (B.13). As is well-known, one of the simplest methods for numerical integration is by Riemann sums. One discretizes time using a small substep s and approximates the integrand as step function by evaluating it at each discrete point in time. Subsequent integration of a sum of step functions is trivial. We slightly modify this scheme in that we do not initially know the end point of integration. This means that we evaluate the integral after each substep and then compare $\mathrm{err}(n_s s)/(n_s s)$ to tol_{rate}, where n_s is the number of substeps performed so far. If the first expression is smaller, we continue to the next substep. If it is bigger, we stop and determine the optimal step size as $t_{step} = (n_s - 1)s$. In order to ensure that error due to the finite step size in the numerical integration is sufficiently small, we demand that $n_s >$ N_SUBSTEPS_MIN, where N_SUBSTEPS_MIN is a given constant. If this is not the case, we restart step 2 with a smaller value of s.

3. Using the step size t_{step} determined above, we compute $v(t_{step})$ according to Eq. (B.9). Now we restart the Krylov procedure, i.e. we go back to step 1, where $v(t_{step})$ now is the initial vector for the next iteration of the algorithm.

It is important to point out that the fraction of runtime required for step 2 is small since computations are only performed in the small Krylov subspace of dimension m. Nevertheless, one can gain a slight improvement in performance by diagonalizing the Hessenberg matrix H_m at the beginning of step 2. If this is done once, no matrix exponential is needed any more to compute the integrand of (B.13) for different values of τ. We use this approach in our implementation.

The Krylov approximation (B.4) is not the only reason why our final result is not exact. Another source of inaccuracy is the finite precision of numerical computations. Its effect is the largest when a large number of numerical operations is applied consecutively (see e.g. [125]). Correspondingly, we expect the Arnoldi algorithm to be most important in the determination of the numerical error. Since in general d numbers are added in the computation of the components of v_i (see Eq. (B.6)), a conservative upper bound on the numerical error is given by

$$d\,\epsilon\,, \tag{B.16}$$

Input: Hamiltonian matrix H, inital vector v, time t, maximal error $err_{\max}$
Output: Approximation for $\exp(-iHt)v$
$A := -iH$; $t_{\text{now}} := 0$; $w := v$; $t_{\text{step}} = 0.1$; $tol_{\text{rate}} = err_{\max}/t$;
while $t_{now} < t$ **do**
  //Step 1: create Krylov space
  $v_1 := w$;
  for $j := 1 : m$ **do**
    $p := Av_j$;
    $M_{jj} := v_j p$; // M is different name for Hessenberg matrix H_m
    if *j=1* **then**
      $p := p - M_{jj}v_j$;
    else
      $p := p - M_{jj}v_j - M_{j-1,j}v_{j-1}$;
    end
    $no := ||p||_2$;
    if $no < tol_{rate}$ **then**
      // happy-breakdown
    end
    if $j \neq m$ **then**
      $M_{j,j+1} := -no$; $M_{j+1,j} := no$;
      $v_{j+1} := p/no$;
    else
      $h := no$;
    end
  end
  //Step 2: find optimal step size
  $s := 0.97\, t_{\text{step}}/\text{N\_SUBSTEPS\_MIN}$; $n_s := 0$;
  while $n_s < N\_SUBSTEPS\_MIN$ **do**
    $n_s := 0$;
    repeat
      $n_s := n_s + 1$; $t_{\text{step}} := n_s \cdot s$; $\omega := \exp(M \cdot t_{\text{step}}) \cdot e_1$;
      $err_{\text{rate}} := h||e_m^T \omega||$; $err_{\text{step}} := err_{\text{step}} + s \cdot err_{\text{rate}}$;
    until $err_{step} > tol_{rate} \cdot t_{step}$;
    $s := \min(s/2, s \cdot ((n_s + 1)/\text{MIN\_STEPS}))$;
  end
  //Step 3: perform step
  $w = V \cdot \omega$; $t_{\text{now}} := t_{\text{now}} + t_{\text{step}}$;
end

Algorithm 1: Krylov-Method

where ϵ is the machine precision. In order to ensure that the error of the final result is not dominated by the numerical one, we compare in each Krylov step the analytic error bound, err_{step}, to the estimate (B.16). If the latter is bigger, the program triggers a warning to alert the user that the analytic error bound may be spoiled by numerical imprecision.

Finally, we remark that the above algorithm can trivially be extended not only to compute the final vector but also to sample its values at intermediate points of time: In step 3, one can use the known matrices H_m and V_m to compute the vector at any t_s with $t_{\text{now}} \leq t_s \leq t_{\text{now}} + t_{\text{step}}$.

Bibliography

[1] G. Dvali, M. Michel, and S. Zell, "Finding Critical States of Enhanced Memory Capacity in Attractive Cold Bosons," *EPJ Quant. Technol.*, vol. 6, p. 1, 2019. DOI: 10.1140/epjqt/s40507-019-0071-1. arXiv: 1805.10292 [quant-ph].

[2] G. Dvali, L. Eisemann, M. Michel, and S. Zell, "Universe's Primordial Quantum Memories," *JCAP*, vol. 03, p. 010, 2019. DOI: 10.1088/1475-7516/2019/03/010. arXiv: 1812.08749 [hep-th].

[3] M. Michel, "Numerical study of a cosmological relaxation model of the Higgs boson mass," *Phys. Rev. D*, vol. 101, no. 11, p. 115 007, 2020. DOI: 10.1103/PhysRevD.101.115007. arXiv: 1910.10940 [hep-ph].

[4] G. Dvali, L. Eisemann, M. Michel, and S. Zell, "Black hole metamorphosis and stabilization by memory burden," *Phys. Rev. D*, vol. 102, no. 10, p. 103 523, 2020. DOI: 10.1103/PhysRevD.102.103523. arXiv: 2006.00011 [hep-th].

[5] ——, "Enhanced Memory States as Dynamical Attractors," *Work in progress*,

[6] M. Michel and S. Zell, "*Timeevolver*: a progam for time evolution with rigorous error bound," *Work in progress*,

[7] J. D. Bekenstein, "Black holes and entropy," *Phys. Rev. D*, vol. 7, pp. 2333–2346, 1973. DOI: 10.1103/PhysRevD.7.2333.

[8] S. W. Hawking, "Particle Creation by Black Holes," *Commun. Math. Phys.*, vol. 43, G. W. Gibbons and S. W. Hawking, Eds., pp. 199–220, 1975, [Erratum: Commun.Math.Phys. 46, 206 (1976)]. DOI: 10.1007/BF02345020.

[9] G. Dvali and C. Gomez, "Black Holes as Critical Point of Quantum Phase Transition," *Eur. Phys. J. C*, vol. 74, p. 2752, 2014. DOI: 10.1140/epjc/s10052-014-2752-3. arXiv: 1207.4059 [hep-th].

[10] G. Dvali, A. Franca, C. Gomez, and N. Wintergerst, "Nambu-Goldstone Effective Theory of Information at Quantum Criticality," *Phys. Rev. D*, vol. 92, no. 12, p. 125 002, 2015. DOI: 10.1103/PhysRevD.92.125002. arXiv: 1507.02948 [hep-th].

[11] G. Dvali and C. Gomez, "Black Hole's Quantum N-Portrait," *Fortsch. Phys.*, vol. 61, pp. 742–767, 2013. DOI: 10.1002/prop.201300001. arXiv: 1112.3359 [hep-th].

[12] G. Dvali, "Critically excited states with enhanced memory and pattern recognition capacities in quantum brain networks: Lesson from black holes," Nov. 2017. arXiv: 1711.09079 [quant-ph].

[13] ——, "Black Holes as Brains: Neural Networks with Area Law Entropy," *Fortsch. Phys.*, vol. 66, no. 4, p. 1 800 007, 2018. DOI: 10.1002/prop.201800007. arXiv: 1801.03918 [hep-th].

[14] G. Dvali and M. Panchenko, "Black Hole Type Quantum Computing in Critical Bose-Einstein Systems," Jul. 2015. arXiv: 1507.08952 [hep-th].

[15] ——, "Black Hole Based Quantum Computing in Labs and in the Sky," *Fortsch. Phys.*, vol. 64, pp. 569–580, 2016. DOI: 10.1002/prop.201600060. arXiv: 1601.01329 [hep-th].

[16] P. T. Chrusciel, J. Lopes Costa, and M. Heusler, "Stationary Black Holes: Uniqueness and Beyond," *Living Rev. Rel.*, vol. 15, p. 7, 2012. DOI: 10.12942/lrr-2012-7. arXiv: 1205.6112 [gr-qc].

[17] J. M. Bardeen, B. Carter, and S. W. Hawking, "The Four laws of black hole mechanics," *Commun. Math. Phys.*, vol. 31, pp. 161–170, 1973. DOI: 10.1007/BF01645742.

[18] D. N. Page, "Is black hole evaporation predictable?" *Phys. Rev. Lett.*, vol. 44, p. 301, 1980. DOI: 10.1103/PhysRevLett.44.301.

[19] G. Dvali, "Non-Thermal Corrections to Hawking Radiation Versus the Information Paradox," *Fortsch. Phys.*, vol. 64, pp. 106–108, 2016. DOI: 10.1002/prop.201500096. arXiv: 1509.04645 [hep-th].

[20] G. W. Gibbons and S. W. Hawking, "Cosmological Event Horizons, Thermodynamics, and Particle Creation," *Phys. Rev. D*, vol. 15, pp. 2738–2751, 1977. DOI: 10.1103/PhysRevD.15.2738.

[21] G. Dvali and C. Gomez, "Landau-Ginzburg limit of black hole's quantum portrait: Self-similarity and critical exponent," *Phys. Lett. B*, vol. 716, pp. 240–242, 2012. DOI: 10.1016/j.physletb.2012.08.019. arXiv: 1203.3372 [hep-th].

[22] ——, "Black Hole Macro-Quantumness," Dec. 2012. arXiv: 1212.0765 [hep-th].

[23] ——, "Black Hole's 1/N Hair," *Phys. Lett. B*, vol. 719, pp. 419–423, 2013. DOI: 10.1016/j.physletb.2013.01.020. arXiv: 1203.6575 [hep-th].

[24] ——, "Quantum Compositeness of Gravity: Black Holes, AdS and Inflation," *JCAP*, vol. 01, p. 023, 2014. DOI: 10.1088/1475-7516/2014/01/023. arXiv: 1312.4795 [hep-th].

[25] G. Dvali, C. Gomez, L. Gruending, and T. Rug, "Towards a Quantum Theory of Solitons," *Nucl. Phys. B*, vol. 901, pp. 338–353, 2015. DOI: 10.1016/j.nuclphysb.2015.10.017. arXiv: 1508.03074 [hep-th].

[26] P. Ehrenfest, "Bemerkung über die angenäherte Gültigkeit der klassischen Mechanik innerhalb der Quantenmechanik," *Zeitschrift fur Physik*, vol. 45, no. 7-8, pp. 455–457, Jul. 1927. DOI: 10.1007/BF01329203.

[27] V. L. Ginzburg and L. D. Landau, "On the Theory of superconductivity," *Zh. Eksp. Teor. Fiz.*, vol. 20, pp. 1064–1082, 1950.

[28] J. Bardeen, L. N. Cooper, and J. R. Schrieffer, "Theory of Superconductivity," *Physical Review*, vol. 108, no. 5, pp. 1175–1204, Dec. 1957. DOI: 10.1103/PhysRev.108.1175.

[29] A. Einstein, "Quantentheorie des einatomigen idealen gases. zweite abhandlung," in *Albert Einstein: Akademie Vorträge*. John Wiley & Sons, Ltd, 2005, pp. 245–257, ISBN: 9783527608959. DOI: https://doi.org/10.1002/3527608958.ch28.

[30] Bose, "Plancks Gesetz und Lichtquantenhypothese," *Zeitschrift fur Physik*, vol. 26, no. 1, pp. 178–181, Dec. 1924. DOI: 10.1007/BF01327326.

[31] G. Dvali, C. Gomez, and S. Zell, "Quantum Break-Time of de Sitter," *JCAP*, vol. 06, p. 028, 2017. DOI: 10.1088/1475-7516/2017/06/028. arXiv: 1701.08776 [hep-th].

[32] G. Dvali, D. Flassig, C. Gomez, A. Pritzel, and N. Wintergerst, "Scrambling in the Black Hole Portrait," *Phys. Rev. D*, vol. 88, no. 12, p. 124041, 2013. DOI: 10.1103/PhysRevD.88.124041. arXiv: 1307.3458 [hep-th].

[33] G. Dvali, C. Gomez, and S. Zell, "Quantum Breaking Bound on de Sitter and Swampland," *Fortsch. Phys.*, vol. 67, no. 1-2, p. 1800094, 2019. DOI: 10.1002/prop.201800094. arXiv: 1810.11002 [hep-th].

[34] G. Dvali and C. Gomez, "Quantum Exclusion of Positive Cosmological Constant?" *Annalen Phys.*, vol. 528, pp. 68–73, 2016. DOI: 10.1002/andp.201500216. arXiv: 1412.8077 [hep-th].

[35] G. Dvali and S. Zell, "Classicality and Quantum Break-Time for Cosmic Axions," *JCAP*, vol. 07, p. 064, 2018. DOI: 10.1088/1475-7516/2018/07/064. arXiv: 1710.00835 [hep-ph].

[36] G. Dvali, C. Gomez, and S. Zell, "A Proof of the Axion?," Nov. 2018. arXiv: 1811.03079 [hep-th].

[37] ——, "Discrete Symmetries Excluded by Quantum Breaking," Nov. 2018. arXiv: 1811.03077 [hep-th].

[38] M. D. Schwartz, *Quantum Field Theory and the Standard Model*. Cambridge University Press, Mar. 2014, ISBN: 978-1-107-03473-0, 978-1-107-03473-0.

[39] G. Dvali, "Strong Coupling and Classicalization," *Subnucl. Ser.*, vol. 53, A. Zichichi, Ed., pp. 189–200, 2017. DOI: 10.1142/9789813208292_0005. arXiv: 1607.07422 [hep-th].

[40] G. Senjanovi, "Natural Philosophy versus Philosophy of Naturalness," *Mod. Phys. Lett. A*, vol. 35, no. 18, p. 2030006, 2020. DOI: 10.1142/S0217732320300062. arXiv: 2001.10988 [hep-ph].

[41] G. Dvali, "Cosmological Relaxation of Higgs Mass Before and After LHC and Naturalness," Aug. 2019. arXiv: 1908.05984 [hep-ph].

[42] H. P. Nilles, "Supersymmetry, Supergravity and Particle Physics," *Phys. Rept.*, vol. 110, pp. 1–162, 1984. DOI: 10.1016/0370-1573(84)90008-5.

[43] J. L. Feng, "Naturalness and the Status of Supersymmetry," *Ann. Rev. Nucl. Part. Sci.*, vol. 63, pp. 351–382, 2013. DOI: 10.1146/annurev-nucl-102010-130447. arXiv: 1302.6587 [hep-ph].

[44] N. Arkani-Hamed, S. Dimopoulos, and G. R. Dvali, "The Hierarchy problem and new dimensions at a millimeter," *Phys. Lett. B*, vol. 429, pp. 263–272, 1998. DOI: 10.1016/S0370-2693(98)00466-3. arXiv: hep-ph/9803315.

[45] L. Randall and R. Sundrum, "A Large mass hierarchy from a small extra dimension," *Phys. Rev. Lett.*, vol. 83, pp. 3370–3373, 1999. DOI: 10.1103/PhysRevLett.83.3370. arXiv: hep-ph/9905221.

[46] G. Dvali, "Black Holes and Large N Species Solution to the Hierarchy Problem," *Fortsch. Phys.*, vol. 58, pp. 528–536, 2010. DOI: 10.1002/prop.201000009. arXiv: 0706.2050 [hep-th].

[47] G. Dvali and M. Redi, "Phenomenology of 10^{32} Dark Sectors," *Phys. Rev. D*, vol. 80, p. 055 001, 2009. DOI: 10.1103/PhysRevD.80.055001. arXiv: 0905.1709 [hep-ph].

[48] G. Dvali, I. Sawicki, and A. Vikman, "Dark Matter via Many Copies of the Standard Model," *JCAP*, vol. 08, p. 009, 2009. DOI: 10.1088/1475-7516/2009/08/009. arXiv: 0903.0660 [hep-th].

[49] N. Arkani-Hamed, T. Cohen, R. T. D'Agnolo, *et al.*, "Solving the Hierarchy Problem at Reheating with a Large Number of Degrees of Freedom," *Phys. Rev. Lett.*, vol. 117, no. 25, p. 251 801, 2016. DOI: 10.1103/PhysRevLett.117.251801. arXiv: 1607.06821 [hep-ph].

[50] S. Weinberg, "Implications of Dynamical Symmetry Breaking," *Phys. Rev. D*, vol. 13, pp. 974–996, 1976, [Addendum: Phys.Rev.D 19, 1277–1280 (1979)]. DOI: 10.1103/PhysRevD.19.1277.

[51] L. Susskind, "Dynamics of Spontaneous Symmetry Breaking in the Weinberg-Salam Theory," *Phys. Rev. D*, vol. 20, pp. 2619–2625, 1979. DOI: 10.1103/PhysRevD.20.2619.

[52] G. Dvali and A. Vilenkin, "Cosmic attractors and gauge hierarchy," *Phys. Rev. D*, vol. 70, p. 063 501, 2004. DOI: 10.1103/PhysRevD.70.063501. arXiv: hep-th/0304043.

[53] G. Dvali, "Large hierarchies from attractor vacua," *Phys. Rev. D*, vol. 74, p. 025 018, 2006. DOI: 10.1103/PhysRevD.74.025018. arXiv: hep-th/0410286.

[54] G. 't Hooft, "Naturalness, chiral symmetry, and spontaneous chiral symmetry breaking," *NATO Sci. Ser. B*, vol. 59, G. 't Hooft, C. Itzykson, A. Jaffe, *et al.*, Eds., pp. 135–157, 1980. DOI: 10.1007/978-1-4684-7571-5_9.

[55] S. Zell, "The quantum substructure of gravity," Ph.D. dissertation, Munich U., Jul. 2019. DOI: 10.5282/edoc.24429.

[56] M. Michel, "On Critical Phenomena in Attractive Bose Gases," M.S. thesis, Technische Universität München, 2017.

[57] C. Tsallis, "Diagonalization methods for the general bilinear hamiltonian of an assembly of bosons," *Journal of Mathematical Physics*, vol. 19, no. 1, pp. 277–286, 1978. DOI: 10.1063/1.523549.

[58] S. Sachdev, *Quantum Phase Transitions*, 2nd ed. Cambridge University Press, 2011. DOI: 10.1017/CBO9780511973765.

[59] E. P. Gross, "Structure of a quantized vortex in boson systems," *Nuovo Cimento (Italy) Divided into Nuovo Cimento A and Nuovo Cimento B*, vol. 10, 1961. DOI: 10.1007/BF02731494.

[60] L. P. Pitaevskii, "Vortex lines in an imperfect bose gas," *Sov. Phys.-JETP*, vol. 13, no. 2, p. 451, 1961.

[61] G. Dvali, "Area law microstate entropy from criticality and spherical symmetry," *Phys. Rev. D*, vol. 97, no. 10, p. 105 005, 2018. DOI: 10.1103/PhysRevD.97.105005. arXiv: 1712.02233 [hep-th].

[62] R. Kanamoto, H. Saito, and M. Ueda, "Quantum phase transition in one-dimensional bose-einstein condensates with attractive interactions," *Physical Review A*, vol. 67, no. 1, Jan. 2003, ISSN: 1094-1622. DOI: 10.1103/physreva.67.013608.

[63] D. Flassig, A. Pritzel, and N. Wintergerst, "Black holes and quantumness on macroscopic scales," *Phys. Rev. D*, vol. 87, no. 8, p. 084 007, 2013. DOI: 10.1103/PhysRevD.87.084007. arXiv: 1212.3344 [hep-th].

[64] M. Panchenko, "The Lieb-Liniger model at the critical point as toy model for Black Holes," Oct. 2015. arXiv: 1510.04535 [hep-th].

[65] E. H. Lieb and W. Liniger, "Exact analysis of an interacting bose gas. i. the general solution and the ground state," *Phys. Rev.*, vol. 130, pp. 1605–1616, 4 May 1963. DOI: 10.1103/PhysRev.130.1605.

[66] E. H. Lieb, "Exact analysis of an interacting bose gas. ii. the excitation spectrum," *Phys. Rev.*, vol. 130, pp. 1616–1624, 4 May 1963. DOI: 10.1103/PhysRev.130.1616.

[67] Y. Tikochinsky, "On the diagonalization of the general quadratic hamiltonian for coupled harmonic oscillators," *Journal of Mathematical Physics*, vol. 20, no. 3, pp. 406–408, 1979. DOI: 10.1063/1.524093.

[68] G. Dvali and C. Gomez, "Self-Completeness of Einstein Gravity," May 2010. arXiv: 1005.3497 [hep-th].

[69] G. Dvali, G. F. Giudice, C. Gomez, and A. Kehagias, "UV-Completion by Classicalization," *JHEP*, vol. 08, p. 108, 2011. DOI: 10.1007/JHEP08(2011)108. arXiv: 1010.1415 [hep-ph].

[70] G. Dvali, C. Gomez, and A. Kehagias, "Classicalization of Gravitons and Goldstones," *JHEP*, vol. 11, p. 070, 2011. DOI: 10.1007/JHEP11(2011)070. arXiv: 1103.5963 [hep-th].

[71] J. D. Bekenstein, "A Universal Upper Bound on the Entropy to Energy Ratio for Bounded Systems," *Phys. Rev. D*, vol. 23, p. 287, 1981. DOI: 10.1103/PhysRevD.23.287.

[72] G. Dvali, C. Gomez, R. S. Isermann, D. Lüst, and S. Stieberger, "Black hole formation and classicalization in ultra-Planckian 2→N scattering," *Nucl. Phys. B*, vol. 893, pp. 187–235, 2015. DOI: 10.1016/j.nuclphysb.2015.02.004. arXiv: 1409.7405 [hep-th].

[73] G. Dvali, "Classicalization Clearly: Quantum Transition into States of Maximal Memory Storage Capacity," Apr. 2018. arXiv: 1804.06154 [hep-th].

[74] ——, "A Microscopic Model of Holography: Survival by the Burden of Memory," Oct. 2018. arXiv: 1810.02336 [hep-th].

[75] T. Tao, *Topics in Random Matrix Theory*, ser. Graduate studies in mathematics. American Mathematical Soc., ISBN: 9780821885079.

[76] G. 't Hooft, "Dimensional reduction in quantum gravity," *Conf. Proc. C*, vol. 930308, pp. 284–296, 1993. arXiv: gr-qc/9310026.

[77] L. Susskind, "The World as a hologram," *J. Math. Phys.*, vol. 36, pp. 6377–6396, 1995. DOI: 10.1063/1.531249. arXiv: hep-th/9409089.

[78] T. Banks and W. Fischler, "An Upper bound on the number of e-foldings," Jul. 2003. arXiv: astro-ph/0307459.

[79] R. Bousso, B. Freivogel, and I.-S. Yang, "Eternal Inflation: The Inside Story," *Phys. Rev. D*, vol. 74, p. 103516, 2006. DOI: 10.1103/PhysRevD.74.103516. arXiv: hep-th/0606114.

[80] T. Banks and W. Fischler, "Holographic Inflation Revised," in *The Philosophy of Cosmology*, S. Saunders, J. Silk, J. D. Barrow, and K. Chamcham, Eds. 2017. DOI: 10.1017/9781316535783.013. arXiv: 1501.01686 [hep-th].

[81] A. M. Polyakov, "De Sitter space and eternity," *Nucl. Phys. B*, vol. 797, pp. 199–217, 2008. DOI: 10.1016/j.nuclphysb.2008.01.002. arXiv: 0709.2899 [hep-th].

[82] ——, "Infrared instability of the de Sitter space," Sep. 2012. arXiv: 1209.4135 [hep-th].

[83] A. D. Linde, *Particle physics and inflationary cosmology*. 1990, vol. 5. arXiv: hep-th/0503203.

[84] E. W. Kolb and M. S. Turner, *The Early Universe*. 1990, vol. 69, ISBN: 978-0-201-62674-2.

[85] V. F. Foit and N. Wintergerst, "Self-similar Evaporation and Collapse in the Quantum Portrait of Black Holes," *Phys. Rev. D*, vol. 92, no. 6, p. 064043, 2015. DOI: 10.1103/PhysRevD.92.064043. arXiv: 1504.04384 [hep-th].

[86] Y. B. Zeldovich and I. D. Novikov, "The hypothesis of coresretarded during expansion and the hot cosmological model," *Sov. Astron.*, vol. 10, p. 602, 1967.

[87] S. Hawking, "Gravitationally collapsed objects of very low mass," *Mon. Not. Roy. Astron. Soc.*, vol. 152, p. 75, 1971.

[88] B. J. Carr and S. W. Hawking, "Black holes in the early Universe," *Mon. Not. Roy. Astron. Soc.*, vol. 168, pp. 399–415, 1974.

[89] G. F. Chapline, "Cosmological effects of primordial black holes," *Nature*, vol. 253, no. 5489, pp. 251–252, 1975. DOI: 10.1038/253251a0.

[90] B. Carr, F. Kuhnel, and M. Sandstad, "Primordial Black Holes as Dark Matter," *Phys. Rev. D*, vol. 94, no. 8, p. 083 504, 2016. DOI: 10.1103/PhysRevD.94.083504. arXiv: 1607.06077 [astro-ph.CO].

[91] B. J. Carr, K. Kohri, Y. Sendouda, and J. Yokoyama, "Constraints on primordial black holes from the Galactic gamma-ray background," *Phys. Rev. D*, vol. 94, no. 4, p. 044 029, 2016. DOI: 10.1103/PhysRevD.94.044029. arXiv: 1604.05349 [astro-ph.CO].

[92] ——, "New cosmological constraints on primordial black holes," *Phys. Rev. D*, vol. 81, p. 104 019, 2010. DOI: 10.1103/PhysRevD.81.104019. arXiv: 0912.5297 [astro-ph.CO].

[93] B. Carr, K. Kohri, Y. Sendouda, and J. Yokoyama, "Constraints on Primordial Black Holes," Feb. 2020. arXiv: 2002.12778 [astro-ph.CO].

[94] C. Alcock *et al.*, "EROS and MACHO combined limits on planetary mass dark matter in the galactic halo," *Astrophys. J. Lett.*, vol. 499, p. L9, 1998. DOI: 10.1086/311355. arXiv: astro-ph/9803082.

[95] G. Dvali, E. Koutsangelas, and F. Kuhnel, "Compact Dark Matter Objects via N Dark Sectors," *Phys. Rev. D*, vol. 101, p. 083 533, 2020. DOI: 10.1103/PhysRevD.101.083533. arXiv: 1911.13281 [astro-ph.CO].

[96] M. Ackermann *et al.*, "The spectrum of isotropic diffuse gamma-ray emission between 100 MeV and 820 GeV," *Astrophys. J.*, vol. 799, p. 86, 2015. DOI: 10.1088/0004-637X/799/1/86. arXiv: 1410.3696 [astro-ph.HE].

[97] T. M. Kneiske, K. Mannheim, and D. H. Hartmann, "The Gamma-ray horizon," *AIP Conf. Proc.*, vol. 587, no. 1, S. Ritz, N. Gehrels, and C. R. Shrader, Eds., p. 358, 2001. DOI: 10.1063/1.1419430.

[98] Y. Luo, S. Hanasoge, J. Tromp, and F. Pretorius, "Detectable seismic consequences of the interaction of a primordial black hole with Earth," *Astrophys. J.*, vol. 751, p. 16, 2012. DOI: 10.1088/0004-637X/751/1/16. arXiv: 1203.3806 [astro-ph.CO].

[99] J. J. Hopfield, "Neural Networks and Physical Systems with Emergent Collective Computational Abilities," *Proceedings of the National Academy of Science*, vol. 79, no. 8, pp. 2554–2558, Apr. 1982. DOI: 10.1073/pnas.79.8.2554.

[100] P. Rebentrost, T. R. Bromley, C. Weedbrook, and S. Lloyd, "Quantum hopfield neural network," *Phys. Rev. A*, vol. 98, p. 042 308, 4 Oct. 2018. DOI: 10.1103/PhysRevA.98.042308.

[101] A. Vilenkin, "The Birth of Inflationary Universes," *Phys. Rev. D*, vol. 27, p. 2848, 1983. DOI: 10.1103/PhysRevD.27.2848.

[102] A. D. Linde, "Eternally Existing Selfreproducing Chaotic Inflationary Universe," *Phys. Lett. B*, vol. 175, pp. 395–400, 1986. DOI: 10.1016/0370-2693(86)90611-8.

[103] N. Metropolis and S. Ulam, "The monte carlo method," *Journal of the American Statistical Association*, vol. 44, no. 247, pp. 335–341, 1949, PMID: 18139350. DOI: 10.1080/01621459.1949.10483310.

[104] P. H. Acioli, "Review of quantum monte carlo methods and their applications," *Journal of Molecular Structure: THEOCHEM*, vol. 394, no. 2, pp. 75–85, 1997, Proceedings of the Eighth Brazilian Symposium of Theoretical Chemistry, ISSN: 0166-1280. DOI: https://doi.org/10.1016/S0166-1280(96)04821-X.

[105] A. B. McCoy, "Diffusion monte carlo approaches for investigating the structure and vibrational spectra of fluxional systems," *International Reviews in Physical Chemistry*, vol. 25, no. 1-2, pp. 77–107, 2006. DOI: 10.1080/01442350600679347.

[106] P. Hayden and J. Preskill, "Black holes as mirrors: Quantum information in random subsystems," *JHEP*, vol. 09, p. 120, 2007. DOI: 10.1088/1126-6708/2007/09/120. arXiv: 0708.4025 [hep-th].

[107] Y. Sekino and L. Susskind, "Fast Scramblers," *JHEP*, vol. 10, p. 065, 2008. DOI: 10.1088/1126-6708/2008/10/065. arXiv: 0808.2096 [hep-th].

[108] T. J. Park and J. C. Light, "Unitary quantum time evolution by iterative lanczos reduction," *The Journal of Chemical Physics*, vol. 85, no. 10, pp. 5870–5876, 1986. DOI: 10.1063/1.451548.

[109] E. Gallopoulos and Y. Saad, "On the parallel solution of parabolic equations," in *Proceedings of the 3rd International Conference on Supercomputing*, ser. ICS '89, Crete, Greece: Association for Computing Machinery, 1989, pp. 17–28, ISBN: 0897913094. DOI: 10.1145/318789.318793.

[110] Y. Saad, "Analysis of some krylov subspace approximations to the matrix exponential operator," *SIAM Journal on Numerical Analysis*, vol. 29, no. 1, pp. 209–228, 1992. DOI: 10.1137/0729014.

[111] E. Gallopoulos and Y. Saad, "Efficient solution of parabolic equations by krylov approximation methods," *SIAM Journal on Scientific and Statistical Computing*, vol. 13, no. 5, pp. 1236–1264, 1992. DOI: 10.1137/0913071.

[112] R. Sidje, "Parallel algorithms for large sparse matrix exponentials: Application to numerical transient analysis of markov processes," *PhD, Rennes*, 1994.

[113] V. Druskin and L. Knizhnerman, "Krylov subspace approximation of eigenpairs and matrix functions in exact and computer arithmetic," *Numerical Linear Algebra with Applications*, vol. 2, no. 3, pp. 205–217, 1995. DOI: https://doi.org/10.1002/nla.1680020303.

[114] D. Stewart and T. Leyk, "Error estimates for krylov subspace approximations of matrix exponentials," *Journal of Computational and Applied Mathematics*, vol. 72, no. 2, pp. 359–369, 1996, ISSN: 0377-0427. DOI: 10.1016/0377-0427(96)00006-4.

[115] M. Hochbruck and C. Lubich, "On krylov subspace approximations to the matrix exponential operator," *SIAM Journal on Numerical Analysis*, vol. 34, no. 5, pp. 1911–1925, 1997, ISSN: 00361429. DOI: 10.1137/S0036142995280572.

[116] E. Celledoni and I. Moret, "A krylov projection method for systems of odes," *Applied Numerical Mathematics*, vol. 24, no. 2, pp. 365–378, 1997, Second International Conference on the Numerical Solution of Volterra and Delay Equations, ISSN: 0168-9274. DOI: 10.1016/S0168-9274(97)00033-0.

[117] V. Druskin, A. Greenbaum, and L. Knizhnerman, "Using nonorthogonal lanczos vectors in the computation of matrix functions," *SIAM Journal on Scientific Computing*, vol. 19, no. 1, pp. 38–54, 1998. DOI: 10.1137/S1064827596303661.

[118] R. B. Sidje, "Expokit: A software package for computing matrix exponentials," *ACM Trans. Math. Softw.*, vol. 24, no. 1, pp. 130–156, Mar. 1998, ISSN: 0098-3500. DOI: 10.1145/285861.285868.

[119] M. A. Botchev, V. Grimm, and M. Hochbruck, "Residual, restarting, and richardson iteration for the matrix exponential," *SIAM Journal on Scientific Computing*, vol. 35, no. 3, A1376–A1397, 2013. DOI: 10.1137/110820191.

[120] Q. Ye, "Error bounds for the lanczos methods for approximating matrix exponentials," *SIAM Journal on Numerical Analysis*, vol. 51, no. 1, pp. 68–87, 2013. DOI: 10.1137/11085935X.

[121] Z. Jia and H. Lv, "A posteriori error estimates of krylov subspace approximations to matrix functions," *Numerical Algorithms*, vol. 69, no. 1, pp. 1–28, 2015. DOI: 10.1007/s11075-014-9878-0. arXiv: 1307.7219 [math.NA].

[122] H. Wang and Q. Ye, "Error bounds for the krylov subspace methods for computations of matrix exponentials," *SIAM Journal on Matrix Analysis and Applications*, vol. 38, no. 1, pp. 155–187, 2017. DOI: 10.1137/16M1063733. arXiv: 1603.07358 [math.NA].

[123] Y. Saad, *Iterative Methods for Sparse Linear Systems*, Second. Society for Industrial and Applied Mathematics, 2003. DOI: 10.1137/1.9780898718003.

[124] T. Jawecki, W. Auzinger, and O. Koch, "Computable upper error bounds for krylov approximations to matrix exponentials and associated φ-functions," *BIT Numerical Mathematics*, vol. 60, no. 1, pp. 157–197, Sep. 2019, ISSN: 1572-9125. DOI: 10.1007/s10543-019-00771-6. arXiv: 1809.03369 [math.NA].

[125] N. J. Higham, *Accuracy and Stability of Numerical Algorithms*, Second. Society for Industrial and Applied Mathematics, 2002. DOI: 10.1137/1.9780898718027.

Acknowledgments

I would like to extend my deep gratitude to Professor Gia Dvali for the opportunity to work with him and in his group. His deep insight in physics and his pursuit of an intuitive understanding have been an inspiring example. I am grateful for his support, guidance and opportunity to explorer new and exiting projects. My work with him motivated me to purse an academic career and continue as a postdoc in theoretical high energy physics.

I am thankful to Professor Goran Senjanović for agreeing to be the co-examiner of this thesis and for many interesting talks and discussions in our group, which greatly improved my knowledge on neutrino physics and my understanding on the Hierarchy Problem.

I am grateful to my collaborators Lukas Eisemann, Giorgos Karananas, Javier Rubio and Sebastian Zell, who strongly shaped my understanding of physics due to countless hours of fruitful discussions. I am thankful for the intense collaborations and great projects with them.

I would especially express my gratitude to Sebastian Zell for all his support and fruitful collaborations since I started in Gia Dvali's group.

I also thank Lukas Eisemann, Giorgos Karananas, Oleg Kaikov, Max Warkentin and Sebastian Zell for many stimulating conversations and making my time at the LMU truly enjoyable.

Moreover, I am thankful to Gia Dvali, Giorgos Karananas, Javier Rubio and Goran Senjanović for the help in finding my postdoc position.

It is a pleasure to thank the former and current postdocs and other students of the department, especially Lasha Berezhiani, Giordano Cintia, Lukas Eisemann, Manuel Ettengruber, Lena Funcke, Andrea Giugno, Andrea Giusti, Alexander Gußmann, Anna Jankowsky, Oleg Kaikov, Georgios Karananas, Emmanouil Koutsangelas, Andrei Kovtun, Florian Kühnel, Christoph Müller, Mischa Panchenko, Florian Pandler, Kaushik Roy, Otari Sakhelashvili, Dimitris Skliros, Juan Valbuena, Juan Valencia Villegas, Max Warkentin, Michael Zantedeschi and Sebastian Zell.

I am indebted to Gia Dvali and Nico Ewert for reading and improving large parts of this thesis.

I am thankful to Gabi Bodenmüller, Corinna Brunnlechner, Monika Goldammer, Frank Steffen and Herta Wiesbeck-Yonis for great administrative support.

Furthermore I knowledge the financial support and excellent research conditions provided by the International Max Planck Research Schools (IMPRS).

Last but not least I will be forever thankful to my family for their everlasting support.